



## 1.A Introduction and Definitions

*The engineers already involved in the production of unconventional plays will not need to read and will certainly skip this section. However other readers come from regions where the production of these plays is new or non-existent. Hence this little introduction...*

Hydrocarbons were generated in source rocks, where they stayed or migrated until they reached surface or were trapped by sealing rock barriers creating conventional reservoirs. Unconventional reservoirs are these source rocks where oil and/or gas remained in situ.

Knowledge of the presence of large amounts of hydrocarbons in these formations is not new. But they have a very low effective permeability and could not be produced because of technology limitations and prohibitive production costs.

Production has recently been made possible by creating multiple fractures along horizontal drains. This technique increases the order of magnitude of the contact area between the well and the formation, making the production economically viable.

Another way to introduce unconventional is to show the diagram below (Holditch), summarizing that the 'easy oil and gas' is coming to an end and unconventional formations represent a technological and economical challenge with the 'promise' of massive reserves.

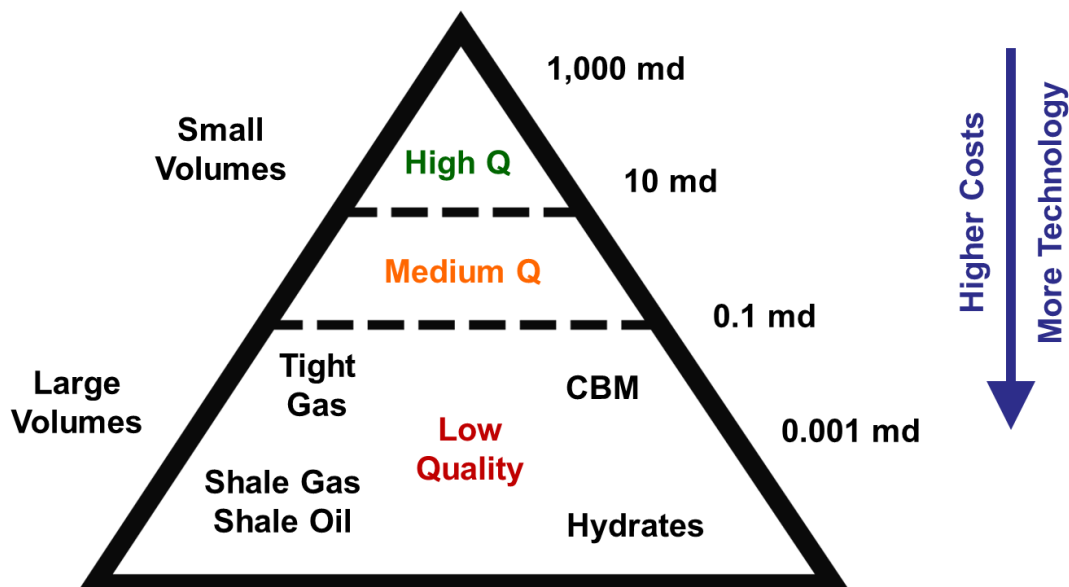


Fig. 1.A.1 – Resource triangle. (From Holditch, 2006)

It is the common understanding that the term 'unconventional' refers to shale gas, shale oil, coal seam gas, oil shale and methane hydrates. We will introduce all of them but in this chapter we will focus on shale oil and shale gas production.



Fig. 1.A.2 – North American shale plays. (From EIA, 2011)

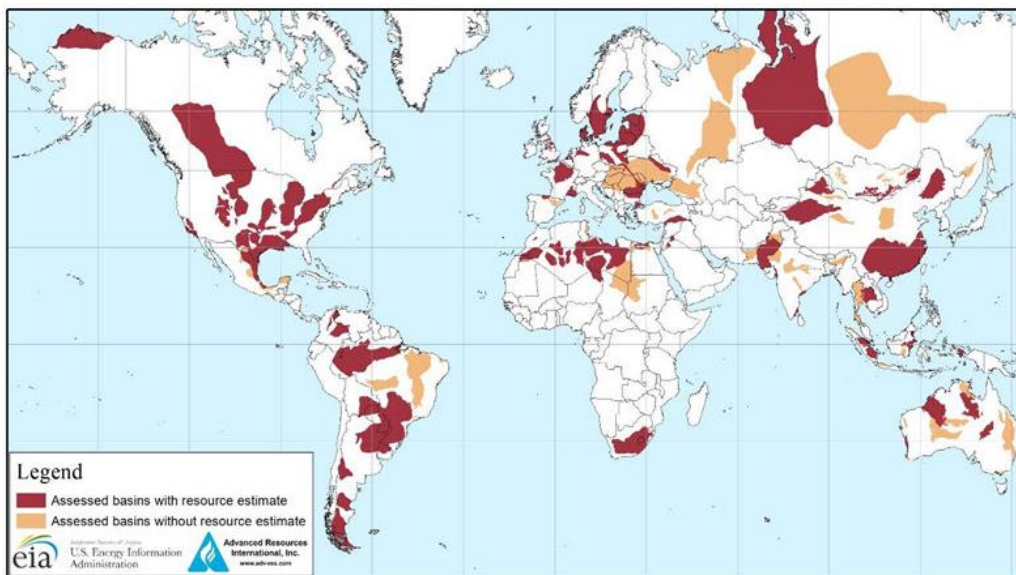


Fig. 1.A.3 – Global shale plays. (From EIA, 2011)

### 1.A.1 Shale gas

Shale gas is trapped within organic-rich sedimentary formations (usually 5-20% TOC) with a high proportion of fine-grained particles, such as shale (fissile), mudstone (non-fissile), siltstone, carbonates, and fine-grained sandstone interlaminated with shale or mudstone. Permeability in these source rocks typically range between  $1 \times 10^{-5}$  and  $1 \times 10^{-1}$  mD.

In 2013 the total technically recoverable shale resources was 7,300 trillion cubic feet, the main countries being China (1,100), Argentina (800), Algeria (700), the US (660), Canada (570), Mexico (540), Australia (440), South Africa (390), Russia (290) and Brazil (250) (From EIA, 2013). However the United States and Canada are by far the major shale gas producers.

According to the EIA (2012) the U.S. shale gas dry production was 25.7Bcf/d in 2012. Most of this production comes from nine formations, mainly from the Marcellus (West Virginia), the Haynesville (Louisiana) and the Barnett (Texas).

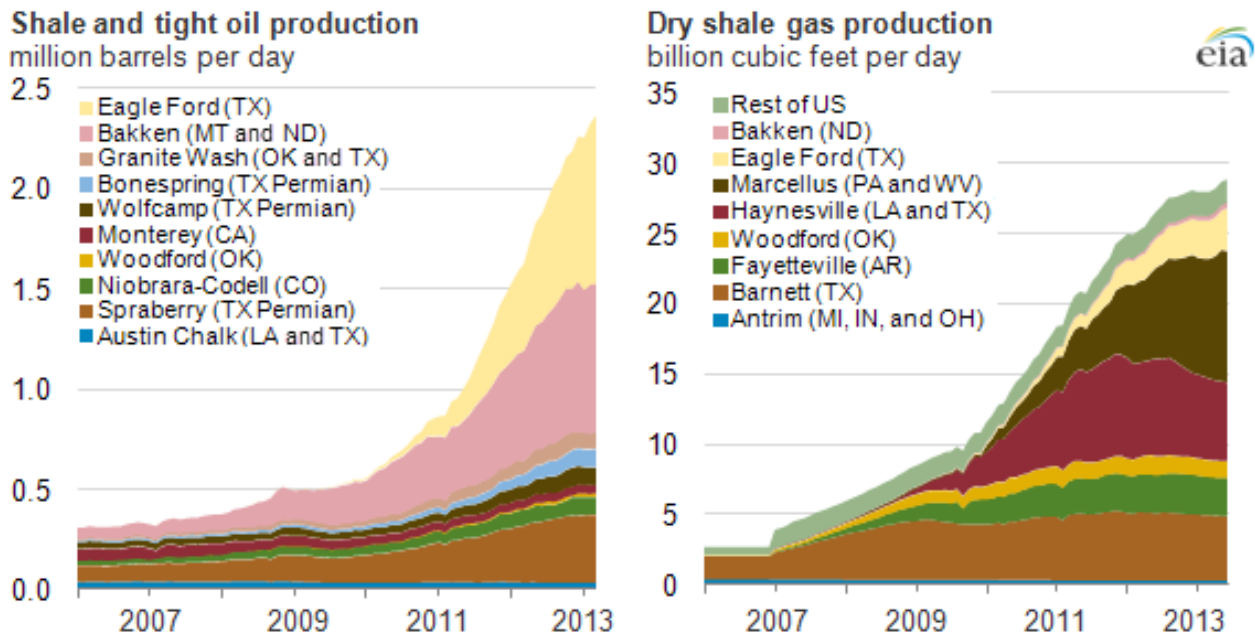


*Fig. 1.A.4 – US shale/tight oil and dry shale gas production.*  
(From IAEE/AEA meeting, January 4, 2014, Philadelphia, PA)

In Canada, the two main formations produced are the Horn River (British Columbia) and the Montney in the Western Canadian Sedimentary Basin (British Columbia and Alberta), with about 2.0 Bcf/d in 2012, (From IAEE/AEA meeting, January 4, 2014, Philadelphia, PA).

Although China was ranked as the largest holder of technically recoverable shale gas resources by the EIA, commercial production is still very limited and concentrated in Sichuan Basin. In Central and South America, operations are essentially located in Argentina and Mexico (exploration). In Europe, exploration operations are underway (Poland, Romania, Germany, U.K., Austria, Denmark) without any real commercial production yet.

## 1.A.2 Shale oil

During the sedimentation and burial processes the temperature and pressure increase in these organic rich shale rocks. Chemical reactions break the kerogen down into various forms of hydrocarbon. Heavy, liquid hydrocarbons are generated in a lower temperature and pressure range 'the oil window', followed by lighter hydrocarbons at higher temperature and pressure in 'the gas window'. The hydrocarbon content can hence vary depending on the maturation stage of the formation.

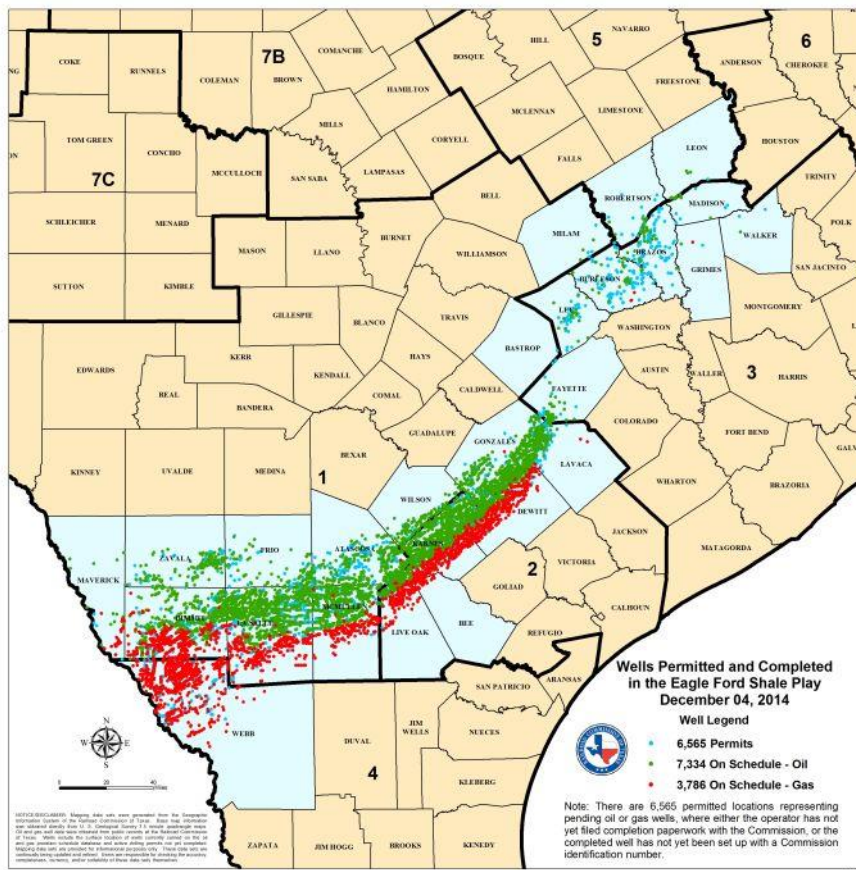


Fig. 1.A.5 – Eagle Ford shale play well permits and completions. (From TX RRC, 2014)

Initially, the production of shale plays was focused on gas windows, where the higher mobility enabled acceptable production despite the technical challenges. But technological advances in drilling and completion, as well as economic constraints (falling gas prices and relatively high oil prices) unlocked the production of source rock liquids. Hence production now tends to concentrate on the liquid-rich, condensate and oil windows.

In 2013 the total technically recoverable shale resources was 344 billion barrels, the main countries being Russia (75), the US (58), China (32), Argentina (27), Libya (26), Australia (18), Venezuela (13), Mexico (13), Pakistan (9) and Canada (9). (From EIA, 2013).

As for shale gas, the United States and Canada are so far the only major producers of shale oil. According to the EIA, the U.S. production of shale and tight oil averaged 3.22 MMbbl/d in 2013. Most of this production comes from two plays: the Eagle Ford (South Texas) and the Bakken Formation (North Dakota and Montana).

In Canada, the EIA estimated the shale and tight oil production to average 0.34 MMbbl/d in 2013, about 10% of the total Canadian crude oil production.

In Argentina, YPF is producing oil from the Vaca Muerta Shale in the Neuquén Basin. Exploration operations have also started in Australia, United Kingdom and China.

### 1.A.3 Coal seam gas (not covered in this chapter)

Coal Seam Gas, or CSG, was initially called Coalbed methane, or CBM, until the name became too unpopular and was changed. CSG refers to methane that is produced from coal beds.

It is generated during the conversion of plant material to coal through burial and heating (coalification). Most of the methane migrates to surface or into a reservoir rock, but a significant volume remains trapped within the coal itself. Hydraulic pressure, rather than a conventional pressure seal, is the major trapping force.

Two distinctive porosity systems characterize coal seams: (1) a network of natural fractures (cleats) which develop under shrinking or tectonic stress, and (2) matrix blocks of very low permeability and highly heterogeneous porous structure between the cleats.

With this structure, gas is stored in 4 different ways:

- free gas within the micropores and cleats;
- dissolved gas in water within the coal;
- adsorbed gas on the surfaces of micropores and cleats;
- adsorbed gas within the molecular structure of the coal molecules.

Some coals at shallow depths with good cleat development contain significant amounts of free and dissolved gas. But the proportion of adsorbed methane generally increases with the coal rank and pressure (depth). The surface area available for methane adsorption is extremely large (20-200 m<sup>2</sup>/g). Coal is hence capable of adsorbing very large quantities of methane (from 100 to 800 scf of methane per ton of coal). Saturated coal seam gas reservoirs can have five times the volume of gas contained in a conventional sandstone gas reservoir of comparable size.

Most of the gas in coal beds is stored in the adsorbed form, which is one of the main differences with shale gas, where produced volumes essentially come from free gas storage in the micropores.

Another difference with shale gas is that coal seams are usually quite close to the surface, and surface aquifers, whilst shale gas is commonly found at depths below one kilometer. Cleats are then very often initially filled with water. When the reservoir is put into production very large volumes of water are first produced before gas can start desorbing from the matrix and flow through the cleats to the wellbore, leading to a characteristic production profile.

The cleat spacing is very uniform and ranges from the order of millimeters to centimeters. Face cleat is continuous throughout the reservoir, while the butt cleat is discontinuous and terminates at intersections with the face cleat. These cleat patterns are crucial for gas production because they allow for the release of adsorbed gas within coal beds and migration to the production well. The ratio of permeabilities in the face cleat direction over the butt cleat direction may range from 1:1 to over 10:1. Because of this anisotropic permeability, drainage areas around coal bed methane wells are often elliptical in shape.

Global CBM production totals 5.8 Bcfd from 15 basins in the USA, Australia, Canada, China, and India. Despite its unconventional nature and a lot of common features with shale oil and shale gas, CSG will not be developed further in this chapter but may be in a following update.

### 1.A.4 Oil shale (*not covered in this chapter*)

There is often confusion between Shale Oil, which will be treated in this chapter, and Oil Shales. To be honest they could have picked more distinct names...

Oil shales are sedimentary rocks with significant amounts of kerogen at early maturation stage. These deposits were formed by underwater deposition of silt and organic debris. This material is slowly transformed into shale oil by heat and pressure, but in the case of the oil shales the natural maturation process is still at a very early stage and may require millions of years to be completed.

Oil shales can generate oil when the rock is heated upon pyrolysis, either underground (in-situ upgrading for deep deposits) or at surface (retorting process for shallow deposits).

Modeling in-situ upgrading and production of oil shale is extremely challenging. A numerical simulation model is required, that involves a fully compositional formulation with chemical reactions and thermal effects. The solid phase must also be correctly modeled to account for the prechar resulting from the pyrolysis. Geomechanical effects and thermal wellbore effects may also need to be included in the model.

Total worldwide oil shale resources are estimated to be equivalent to 3 to 5 trillion barrels.

Despite their unconventional nature, oil shales are not considered further in this chapter.

### 1.A.5 Hydrates (*not covered in this chapter*)

Gas hydrate is a crystalline (ice) form of water trapping gas of low molecular weight, typically methane. A gas molecule is surrounded by stable 'cages' of water molecules. Each water cage encloses a space of a particular size, and only a gas molecule small enough to fit within this site can be hosted. These structures can store a significant amount of gas, typically 160 scf of methane for 1 cf of gas hydrate.

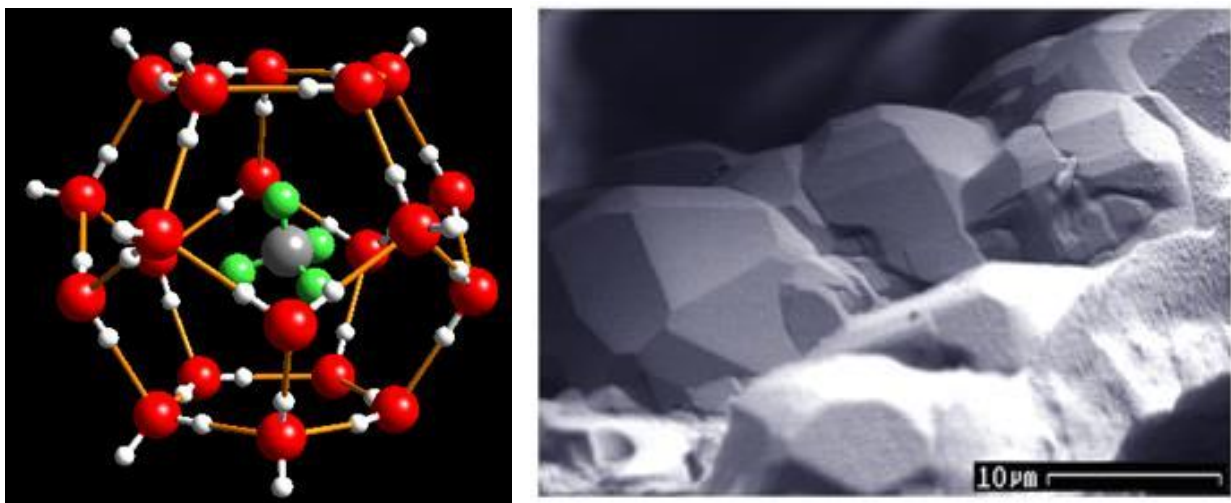


Fig. 1.A.6 – Water molecules around a methane molecule. (From USGS)

Gas hydrate occurs mostly in marine sediments of the continental shelf. In lesser quantities it also occurs in the onshore permafrost or offshore relic permafrost. Gas hydrate is stable at low temperature and high pressure. Hence, the gas can be released by depletion or heating. Injection of inhibitors is also possible.

Numerical simulation of these production processes is still at the research stage. It involves a fully-compositional formulation with chemical reactions and thermal effects.

The amount of methane sequestered globally in gas hydrate deposits is estimated to be between  $1 \times 10^5$  and  $5 \times 10^6$  trillion cubic feet. Only a fraction of this amount is likely to be commercially accessible. Despite their unconventional nature, gas hydrates are not considered further in this chapter.

## 1.B Specifics of shale plays

The most obvious difference between conventional and shale plays is the order of magnitude of the permeability. We are now speaking about micro and nano-Darcys. Without even considering the impact on the validity of the diffusion equations and unreasonably simple flow geometries, the low permeability alone will have a substantial impact;

- The flow is likely to be transient for most of the producing life of the wells.
- There are additional challenges to accurately model the system, either analytically or numerically.
- Because we are at the beginning of the life of these types of plays, we totally lack empirical knowledge of their long term production.

Then we have to question the diffusion equations we have been routinely using over the past century. A diffusion equation in a homogeneous context will be the combination of a pressure gradient law (e.g. Darcy), the principle of conservation of mass and a PVT correlation. For the gradient law the rock constant (e.g. permeability) may be sensitive to pressure and stress. Finally the reservoir may not be homogeneous and may require modeling using various networks of natural fractures and matrix blocks.

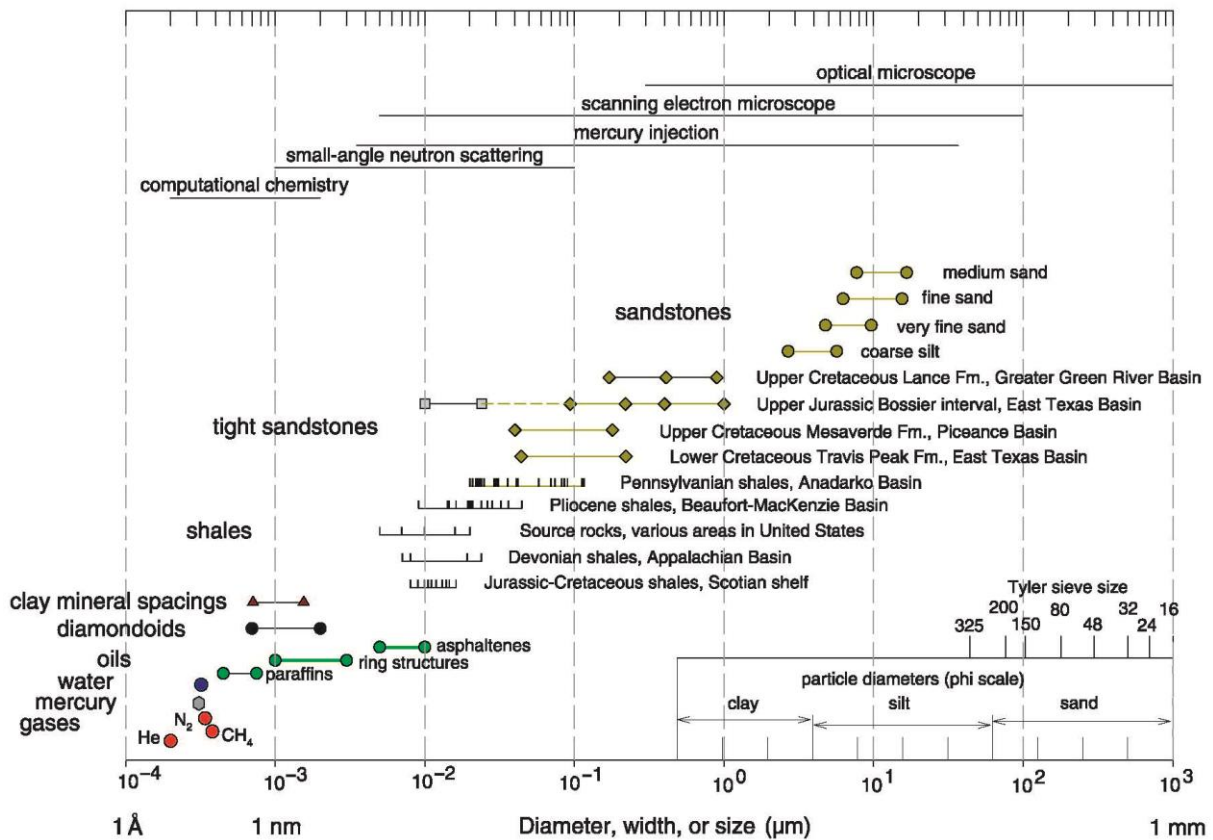


Fig. 1.B.1 – Sizes of molecules and pore throats in siliciclastic rocks. (From Nelson, USGS)

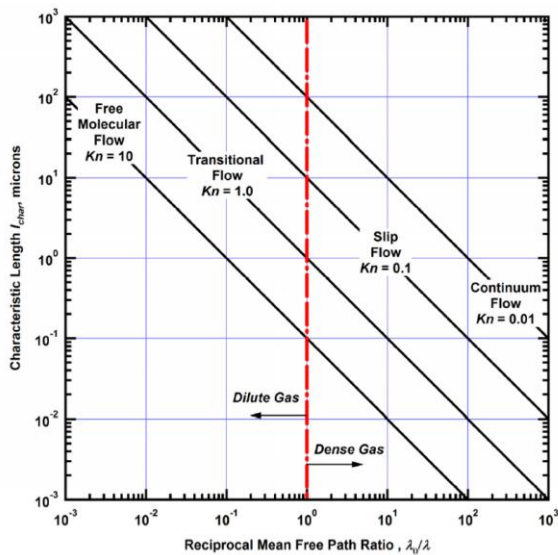


Fig. 1.B.2 – Limit of the different flow regimes (Florence, Texas A&M, 2007)

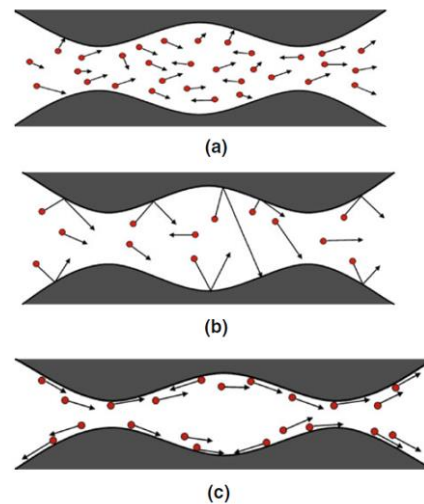


Fig. 1.B.3 – Schematic of cross section of a pore and gas molecule:

- (a) Bulk diffusion
- (b) Knudsen diffusion
- (c) Surface diffusion

The diffusion equation resulting from these components will therefore be influenced by initial and boundary conditions. In a conventional play we will start, not unreasonably, with uniform pressures and saturations. Inner boundary conditions are mainly about the wells, using again a pressure gradient relationship such as Darcy’s law. In a conventional well test the outer boundary conditions may be approximated to an infinite reservoir, but for longer term diffusion one will typically use pressure support (e.g. aquifers) or no-flow boundaries, either physical or coming from the definition of the well drainage area.

Compared to conventional plays, we might still believe in the conservation of mass but all the rest above can, and should be challenged:

- The diffusion equations are more complex, and it is accepted that one should consider at least three different scales of diffusion.
- Rock properties are highly dependent on stress.
- With pore size and molecule size converging dangerously, PVT correlations derived from lab experiments should be challenged.
- Initial producing conditions come after massive fracture jobs. Initial conditions should take into account important pressure and saturation gradients at production time zero.
- In order to compensate for the drop in permeability we increase the magnitude of the contact area between the well and the formation by the means of running multiple fractures along a drain that is generally horizontal. So the well models are much more complex, even assuming we exactly know the fractures geometries, which is seldom the case.
- The last and main challenge today is our lack of knowledge of the flow geometry in the reservoir, and the need (or not) to use discrete fracture networks (DFN).
- To add insult to injury, we typically lack quality data in shale plays.

The different specifics of unconventional plays are detailed below.

## 1.B.1 Impact of the low permeability

### Transient behavior

In a conventional play, wellbore effects and the geometry of the flow around the well will dominate the system response for a few hours or a few days for long horizontal drains. In a matter of hours or days the reservoir will exhibit its average properties upon reaching infinite acting radial flow (or equivalent) regime. Eventually, after a few weeks, the first reservoir boundaries or nearby producing wells are detected. There is no strict rule and there are exceptions, but this is generally what you would expect.

Things are radically different in unconventional plays, because the drop in mobility dramatically increases the time scale of these behaviours. As a result the flow around the well, and more specifically orthogonally to the hydraulic fractures, will last months or years, and we may wait for centuries to eventually detect the equivalent of infinite acting radial flow. This is at least the case when we lump the reservoir into a homogeneous equivalent system.

As a result we may expect that the system will be in transient behaviour for most if not all the producing life of the well. Even the SRV flow, detailed later in this chapter, is strictly speaking a transient regime.

### Lack of empirical knowledge

We have been actively producing these plays for only a few years. Considering that we are dealing with long transients, we do not yet have the experience of a complete production cycle. In the absence of such experience it is very courageous to extrapolate what we see today and predict what will happen in five or ten years. Using conventional analogs is hazardous, and we have seen this when early linear flow transients were extrapolated as if they were the final well regime, producing ridiculously high values of the 'b' decline factor.

### Modeling issues

Even keeping the simplest diffusion assumptions, the modeling of extremely low permeability formations presents new challenges for both analytical and numerical models.

Analytical models are generally computed in dimensionless terms, in real or Laplace space. Even in Laplace space the model will be accurate to at least four significant figures and would not care less about the real value of permeability, whether it is a Pico-Darcy or a Giga-Darcy. However the accuracy issue arises when converting the solution to the real fluid pressure. Because the reservoir is of extremely low permeability the pressure gradients, in commercial production, will be very high in the vicinity of the sandface, and this is a direct effect on Darcy's law. Given this pressure gradient, it would be totally wrong to assume that the fluid is slightly compressible. The resulting compressibility gradient will not only require the use of pseudopressures, which is straightforward, but also the use of pseudotime functions. The problem with pseudotime is that it requires in turn, at each time step, a reference pressure that is supposed to be the average pressure in the zone affected by the well production.

This is obtained by a material balance in a moving volume constrained by the flow geometry. This is taken into account in the generalized pseudo function approach and the dynamic pseudo time method. See more details in the chapter "13.E - The use of pseudofunctions", paragraph 13.E.5.

Numerical models do not have this issue of pseudopressure or pseudotime, as the real PVT is used in each cell. However the numerical model is very sensitive to the permeability values and requires extremely refined grids in the places where the pressure gradients are the highest, i.e. in the vicinity of the well. So in turn the numerical model needs calibration.

Model calibration can be done, for the same geometry, by going back and forth between the analytical model and the numerical model:

- The first stage is to model a slightly compressible fluid diffusion for this geometry. If the fluid is slightly compressible, and even though we know it is not the case physically, the analytical solution, if derived properly, will be exact. If we enter the same slightly compressible fluid PVT in the numerical model we will be able to check if, for a given permeability, the gridding of the numerical model is suitable to match the analytical solution. In other words we calibrate the numerical model by the analytical model in the limit case of a slightly compressible fluid.
- Once we have done this we can be fairly confident in our numerical model and we have to continue with the real fluid diffusion. Except in extreme cases of multiphase flow the calibrated grid will be sufficient and we will be able to simulate the same case integrating the nonlinearities related to the compressibility gradients. This is the time then to try the analytical model using pseudopressure and pseudotime corrections. If the correction is sufficient to match the numerical results we have calibrated the analytical model and we can be fairly confident that the result will not be off. If the data is not matched it means that the nonlinearities cannot be corrected with pseudofunctions and that we may as well focus on the numerical model.
- We have noticed that some engineers are still using numerical models with a gridding that is not adapted to the low permeability and the high pressure gradients. In this case the simulation may be substantially wrong and the simulator itself is not to blame.

## **1.B.2 Diffusion equations**

### **If we wanted to do the thing as correctly as we know how...**

The accurate description of transport phenomena in unconventional formations is still an active research area, with wide and often contradictory literature.

Many different scales (up to 5 or 6) are involved, associated with a lot of different physical processes: molecular diffusion, desorption, Knudsen / Darcy / Forchheimer flow, PVT phase behavior, stress dependence, etc.

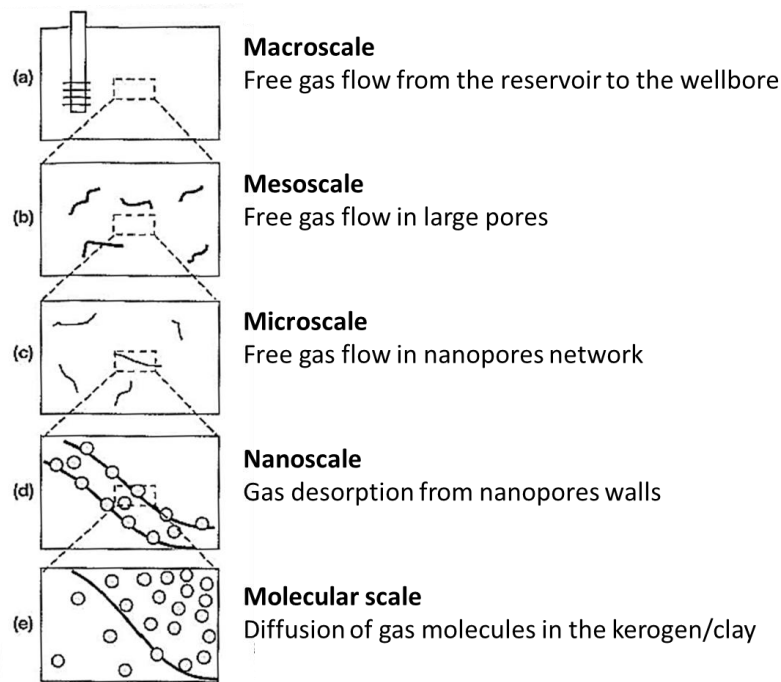


Fig. 1.B.4 – Storage and transport in shale gas sediments. (From Javadpour et al, 2007)

In order to achieve a practical model, some degree of simplification is necessary, and some scales have to be lumped together.

The general agreement is that one could consider three scales of diffusion in order to get an accurate picture of what is happening in unconventional plays: (1) At the level of micropores, (2) between micropores and (3) within the network of natural and hydraulic fractures leading to the well. For each of these scales, different storage mechanisms (solution, adsorption, free compressed fluid) and transport mechanisms (molecular diffusion, Darcy flow, etc...) may be considered. We also need to look at stress dependence and specific PVT issues.



Fig. 1.B.5 – Transport mechanisms in coal seam methane:  
(a) Desorption from internal coal surface (b) Diffusion through the matrix and micropores and  
(c) Fluid flow in the natural fracture network. (From Reeves and Pekot, 2001)

### 1.B.2.a Desorption

Desorption occurs at the level of the micropores. In coals or organic shales, gas is stored by adsorption on the walls of the micropores in quantities that depend on temperature and pressure. When the pressure is reduced in the system by producing the free fluid, some molecules are desorbed from the walls and released into the micropores.

In practice, reservoir engineers use a model  $V_{ads}(P)$  which gives the volume of adsorbed gas per unit mass of rock as a function of pressure:

$$V_{ads}(P) = V_s \cdot \theta(P)$$

The quantity  $V_s$  is a reference volume of gas adsorbed per unit mass of rock material.  $\theta(P)$  is called the adsorption isotherm. It is the coverage fraction of the surface available for adsorption (dimensionless). The most commonly used model is the Langmuir isotherm:

$$\theta(P) = \frac{P}{P_{half} + P}$$

Above, the  $P_{half}$  is the pressure for which the coverage factor is  $1/2$ :

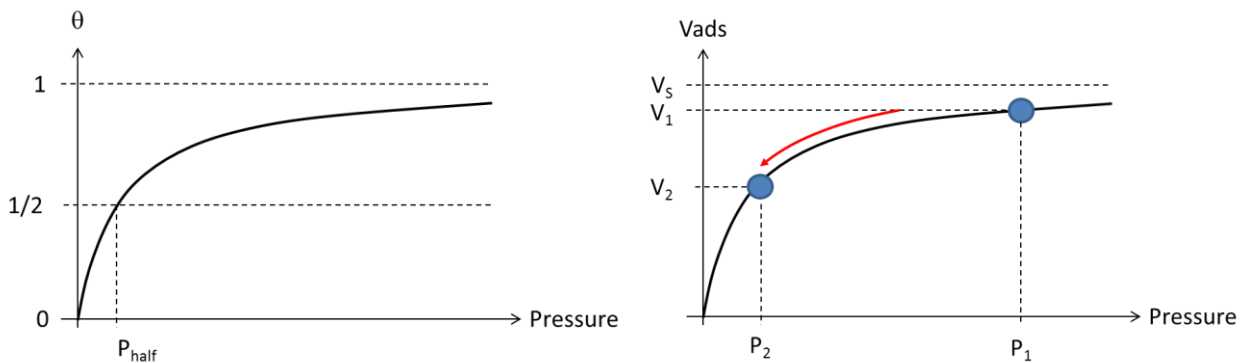


*Fig. 1.B.6 – Langmuir isotherm. When the pressure is reduced from  $P_1$  to  $P_2$ , the quantity desorbed in the system per unit mass of rock material is given by  $(V_1 - V_2)$ .*

Although Langmuir’s model is the most commonly used model in the industry, other  $\theta$  functions can be found in the literature: Freundlich, Toth, Unilan, etc.

In coal seam gas, the pores are initially filled with water and the quantity of gas initially adsorbed in the system is actually lower than the prediction of the theoretical isotherm at  $P_i$ . In this case, the pressure in the pores will have to be decreased to the saturation pressure (also called critical desorption pressure) before gas can start to desorb. The quantity initially adsorbed corresponds to the value of the isotherm at this critical pressure  $P_{crit}$ . This situation is called undersaturated initial state.

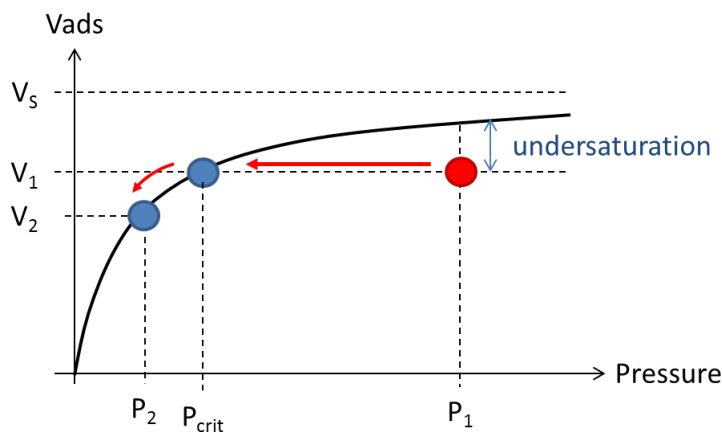


*Fig. 1.B.7 – Langmuir isotherm. Gas starts to desorb when the pressure reaches the  $P_{crit}$ , then, w the pressure is reduced from  $P_1$  to  $P_2$ , the quantity desorbed in the system per unit mass of rock material is given by  $(V_1 - V_2)$*

Isotherms used for volume estimations are typically obtained from laboratory measurements. When dealing with coal samples, two types are used for lab analysis and reporting:

- As received: the sample represents in-situ conditions, and can be used as is for in-situ volumes estimates.
- Dry and ash free: the sample is free from moisture and ash. The reference equation has to be corrected to account for the in situ moisture content  $f_m$  and the ash content  $f_a$  - in order to avoid overestimating the adsorbed quantity:  $V_{ads}(P) = V_S \cdot (1 - f_a - f_m) \cdot \theta(P)$

### 1.B.2.b Molecular diffusion and diffusion between micropores

Molecular diffusion: from desorption the concentration of the solution gas stored inside the kerogen changes between the surface and the bulk of the kerogen material. This induces a slow gas transfer by molecular diffusion inside the kerogen, following Fick's law:

$$J = -D \cdot \nabla \phi$$

where J is the diffusive flux, D is the diffusion coefficient and  $\phi$  is the gas concentration.

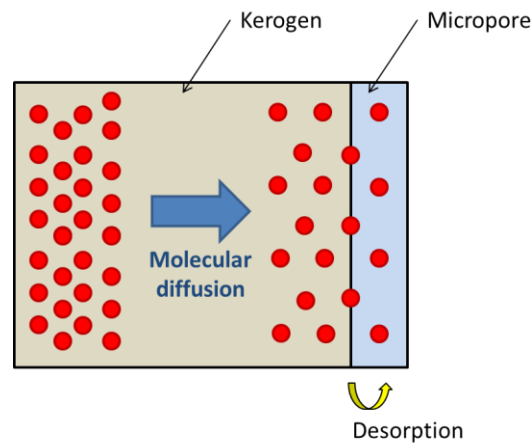


Fig. 1.B.8 – Gas diffusing from high gas concentration to low concentration.

Diffusion between micropores: This is usually modelled with continuum methods, using either Fick's diffusion (especially for coal seam methane) or a more classical diffusion based on the Darcy equation, with a very low effective permeability. However, given the size of pore throats in unconventional systems, the validity of continuum methods with no-slip conditions can be discussed.

The flow regime for a gas flowing in a micro-channel is given by the Knudsen number:  $K_n = \frac{\lambda}{l_c}$ , where  $\lambda$  is the mean free path of the gas molecules (distance between 2 consecutive collisions) and  $l_c$  is the channel radius. As long as the Knudsen number is small (ex: large pores in conventional formations), gas flows under no-slip condition, and average diffusion in the porous medium can hence be correctly described by Darcy's law using an intrinsic permeability value. But in nanoporous system, the pore size is not negligible compared to  $\lambda$  and the Knudsen number increases ( $0.01 < K_n < 0.1$ ). In this case, gas molecules freely slip on the surface of the pores and collide with the wall or other molecules (slip flow conditions).

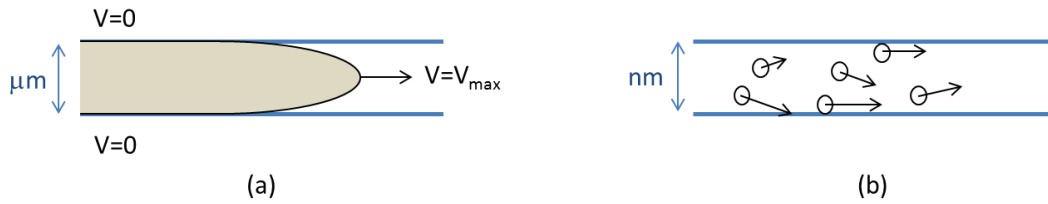


Fig. 1.B.9 – Gas flow in a pore under (a) no-slip condition with the characteristic Poiseuille velocity profile and (b) slip flow conditions. (From: Javadpour et al, *Nanoscale gas flow in shale gas sediments, Canadian J. P. T. Oct 2007*)

This induces an apparent increase of the effective permeability of the system, known as the Klinkenberg effect:

$$k = k_{\infty} \left( 1 + \frac{b}{P} \right)$$

Above,  $k$  is the effective permeability,  $k_{\infty}$  is the reference permeability measured under no-slip conditions, and  $b$  is the gas slippage factor, which depends on the rock-gas couple.

An important consequence of this effect is that if we keep using the classical Darcy's law to match and forecast production data, the estimated effective permeability will actually not be an intrinsic property of the rock, but will also depend on the properties of the gas and on the production pressure. This aspect is also discussed in the PVT paragraph below.

### 1.B.2.c Fracture diffusion

Inside fractures, the classical Darcy's law is used, and the description does not fundamentally differ from conventional situations:

$$\nabla P = -\frac{\mu}{k} \cdot \vec{u}$$

When the gas velocity increases (ex: near the drain inside hydraulic fractures), significant inertial (non-Darcy) effects can occur. This induces an additional pressure drop in the hydraulic fractures in order to maintain the production rate, also modeled as a rate-dependent skin in pressure transient analysis. In this case, an additional term is simply added to the Darcy equation, involving the Forchheimer factor  $\beta$ :

$$\nabla P = -\frac{\mu}{k} \cdot \vec{u} - \beta \cdot \rho \cdot |\vec{u}| \cdot \vec{u}$$

Darcy / Forchheimer equations may apply differently in hydraulic and natural fractures:

Hydraulic fractures are opened and propped during the injection process. Since their orientation and length have a major impact on production, they should always be explicitly included in the model.

For natural fractures two situations can be considered:

- They form a dense network of small, well-connected objects. The system behaves like a homogeneous equivalent medium with an effective large-scale permeability  $k^*$ . The geometry of the natural network can be ignored. The fractured nature of the medium may then approximate to a double-porosity model.

This is typically the case in coal seam methane, where the dense network of cleats is treated as a homogeneous equivalent medium, fed by diffusion inside the coal matrix.

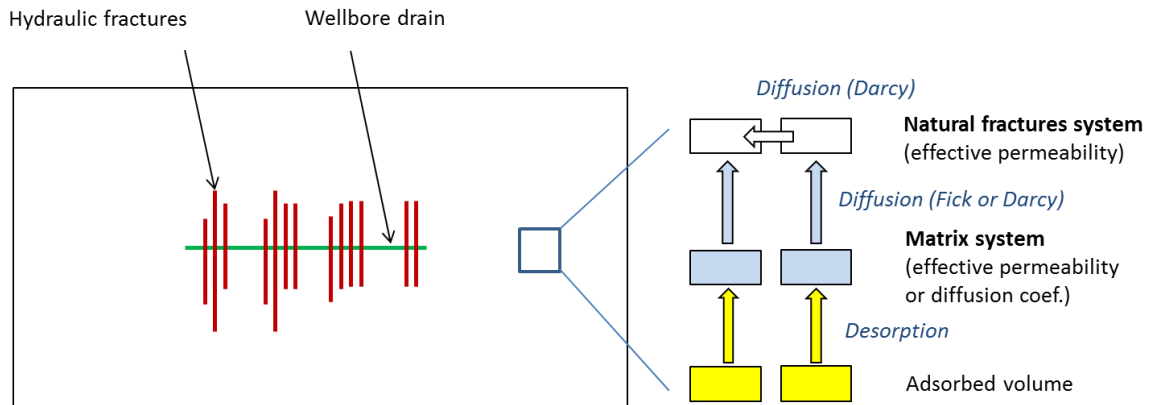


Fig. 1.B.10 – Natural fracture approximated with a double-porosity model

- The fractures are larger objects creating long-distance connections between the wells. They cannot be homogenized. The geometry of at least the main fractures is important and transport has to be described using Darcy’s law. This large-scale fractures network is connected to a homogeneous micro-porous ‘matrix’ system. Smaller scale fractures may approximate to a double-porosity model.

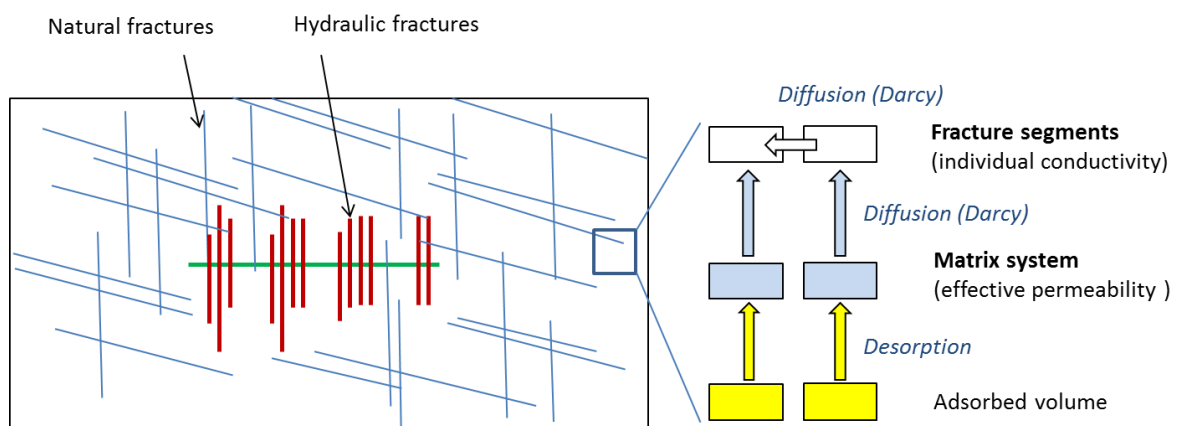


Fig. 1.B.11 – Natural fractures simulated by a fracture network connected to the matrix

### 1.B.2.d Stress and pressure-dependent properties

Modifications of the stress field ( $\sigma$ ) during operations may have a significant impact:

- During the injection fractures propagate perpendicular to the minimum principal stress, which can change with location and time, depending on the operations schedule, as the stress field is modified while injecting and fracturing.
- During the injection pressuring of existing fractures reduces the effective stress across fracture planes (closure stress,  $\sigma$ -P). This opens the fractures, increasing their width and conductivity.
- As pressure decreases (fall-off and production) the closure stress increases again. Unpropped fractures and small fissures tend to close. Propped fractures remain open but the conductivity of the proppant may decrease.
- In the matrix, the effective permeability and porosity are also dependent on modifications of the stress field due to compaction.
- In extreme cases, proppant may get embedded into the matrix, dramatically reducing the conductivity of the hydraulic fracture.

One way to address this is by coupling the geomechanics and flow equations in the same the numerical model. A simpler approach is to add pressure dependence of the permeability and the porosity in the flow model. Three relations may be used:

- One for the matrix, used essentially to simulate the compaction and reduction of the effective permeability as pressure decreases.
- One for the natural fracture system, where the closing of fractures when pressure decreases can be captured by various models, ex: cubic, Ostensen's or Walsh's laws. For example, Walsh's law gives the variation of the fractures permeability vs. pressure:

$$\frac{k}{k_0} = \left[ C \cdot \ln \left( \frac{\sigma_{ref}}{\sigma - P} \right) \right]^3$$

- One for the propped fractures, integrating the evolution of the conductivity as a function of the closure stress.

### 1.B.2.e PVT issues

There are PVT issues unique to unconventional plays. Conventionally, one may consider that methane is methane, and that the PVT behavior is therefore an independent block of the modeling process. This is unfortunately not the case when the size of the pores approaches the order of magnitude of the size of the hydrocarbon molecules. Lab experiments do not take this into account, and when we get to these extreme cases the fluid properties will not be the same under these conditions at a given pressure and temperature.

For instance, for a given composition of a hydrocarbon mixture, the phase behaviour obtained in a laboratory PVT cell may be considerably different from the behaviour in a confined environment: the phase envelope is shifted, leading to different values of the saturation pressure and an apparent bubble or dew point 'suppression effect'.

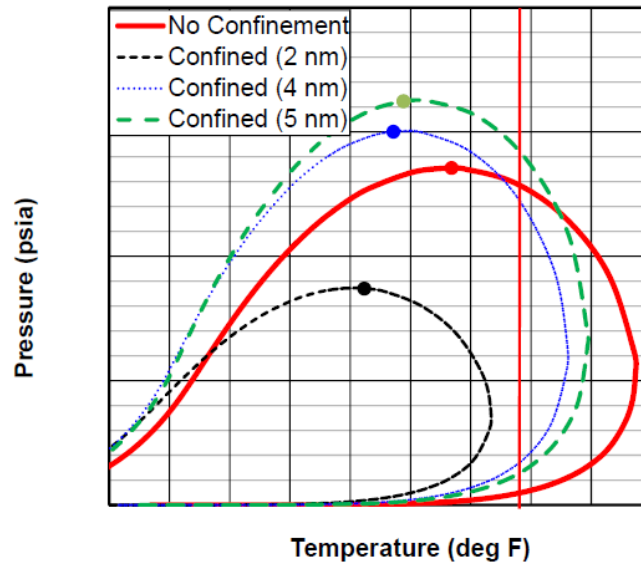


Fig. 1.B.12 – Phase diagrams of confined and unconfined gas-condensate fluid.  
(From Devegowda et al, 2012)

However, the agreement today is that this specific behaviour will only affect the estimation of the rock permeability in these particular areas. As we base our forecast on real production data, given our current knowledge, it should not dramatically affect the accuracy of our predictions. One way to approach problem is to consider that we have in the apparent permeability a component coming from the fluid and not the rock, and that all in all the errors are lumped and neutralized in the process of matching the production.

Another approach is to use a solution that takes into account the nanoporosity effects on the PVT properties.

#### 1.B.2.e.i Confined PVT solution

One solution is proposed by adding an additional condition in the Equation of State that we use to define the PVT properties of the fluid in a numerical.

This option accounts for the phase envelope modification due to strong capillary pressure related to pore size.

In the approach used in the Kappa workflow, there are two methods for taking the effect of the confinement into account:

- To correct the flash calculation due to the capillary pressure in the pore.
- To shift the component critical properties.

More details are given in the paragraph 9.N Confined PVT.

## **What we do in practice**

Often, despite the availability of data, for production analysis and forecasting purposes, engineers might use no model at all and just a decline model that may or may not account for a change in the apparent 'b' factor. This is the sad reality of our industry.

Even when engineers attempt to integrate some physics, in most flow models today the diffusion process is lumped into a homogeneous equivalent, with possibly the addition of double-porosity behaviour, pressure dependence of the permeability and a desorption equation. For analytical models these different correction parameters are integrated in pseudopressure and pseudotime functions, in addition to the usual PVT corrections.

Surprisingly the solution of these simplified diffusion equations seem to follow pretty well the first years of response we observe in these wells. This will be shown later in this chapter. The main question is whether these simplified models are sufficiently equipped to forecast longer term production, and whether or not they will be compatible with the productivity observed in future in-fill wells. Lumping the diffusion into a homogeneous equivalent has a substantial impact on our hypothesis for the extent of the Stimulated Reservoir Volume (SRV).

### 1.B.3 Fractured horizontal wells

As stated earlier the fractured horizontal wells are the only way we have found so far to make these plays commercial. If we look at Darcy's law and consider the term  $k \cdot A$ , where  $A$  is the flow area, we try to get almost reasonable pressure gradients and compensate the low value of  $k$  by increasing dramatically the value of  $A$ .

The different levels of complexity of analytical and numerical tools used to model the behaviour of these wells will be detailed throughout this chapter. From operations we may have an estimate of the number of fractures, their lengths, directions and properties. Production logs and microseismics may also refine our understanding. However this information is not certain enough to consider it as a definitive input for the models to match the observed responses.

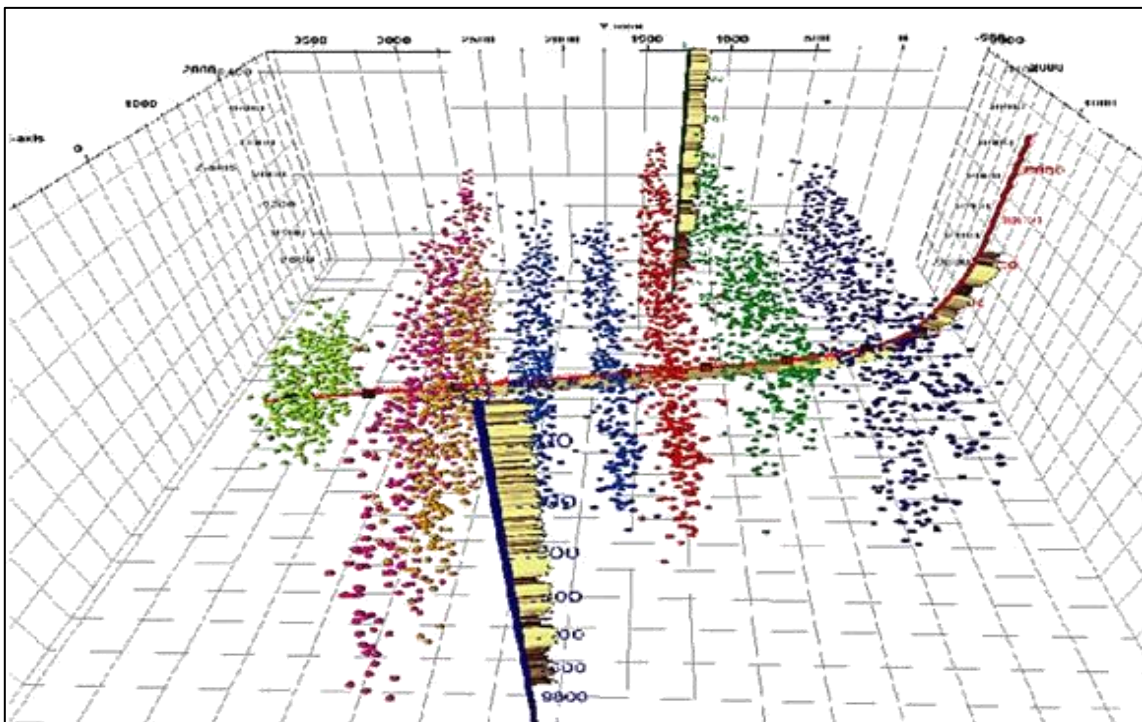


*Fig. 1.B.13 – Microseismic events (Canada National Energy Board)*

As a consequence we tend to simplify the hypotheses and lump the unknowns into a smaller number of parameters we will use to match the observed data. We are well past the illusion of a unique solution to the inverse problem. We are just looking for a proxy that is reasonably close to reality, and good enough to match observed data and forecast future production.

### 1.B.4 Initial state of the system

The well production starts after a substantial series of fracturing jobs. Typically this will involve the injection of  $Q_{inj} = 100,000$  barrels of water, proppant and various chemicals. So we start with a system that is substantially disturbed in terms of pressures, saturations and stress.

There may be four different ways to model the initial state of the system:

- We ignore this and we consider an initial uniform pressure and saturation field. This may be acceptable for long term prediction and required when using analytical models. However it will unlikely match the early time response where substantial water flow back is expected.
- The “Static Method”: we take a material balance approach and initiate a numerical model with a non-uniform initial water saturation field. 3 zones are defined: (1) the hydraulic fractures where the saturation is set to the  $S_{wmax}$  of the fractures relative permeability ( $S_{wmax}^{frac}$ ), (2) a flooded zone surrounding the fractures, where the saturation is set to the  $S_{wmax}$  of the matrix relative permeability ( $S_{wmax}^{mat}$ ), the extension of this zone derived such that its volume  $V_{tot}$  honors the material balance  $Q_{inj} = V_{tot} \cdot \phi \cdot S_{wmax}^{mat} + V_{frac} \cdot S_{wmax}^{frac}$  and (3) the remaining matrix volume, where the saturation remains unchanged at  $S_{wi}$ . This purely static approach is valid for long term predictions. It allows us to reproduce the water volumes corresponding to early time water flowback and capillary trapping, as well as the delay in gas production due to early-time dewatering. However, this is only an approximation since it does not account for the local pressure increase associated with injection, nor for any effective permeability or porosity variation due to modifications to the effective stress field during injection.

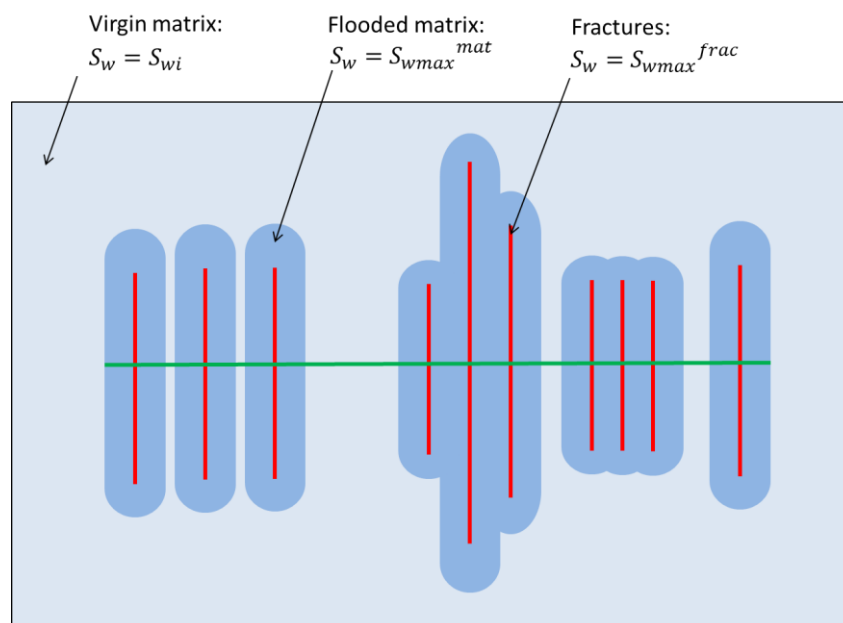
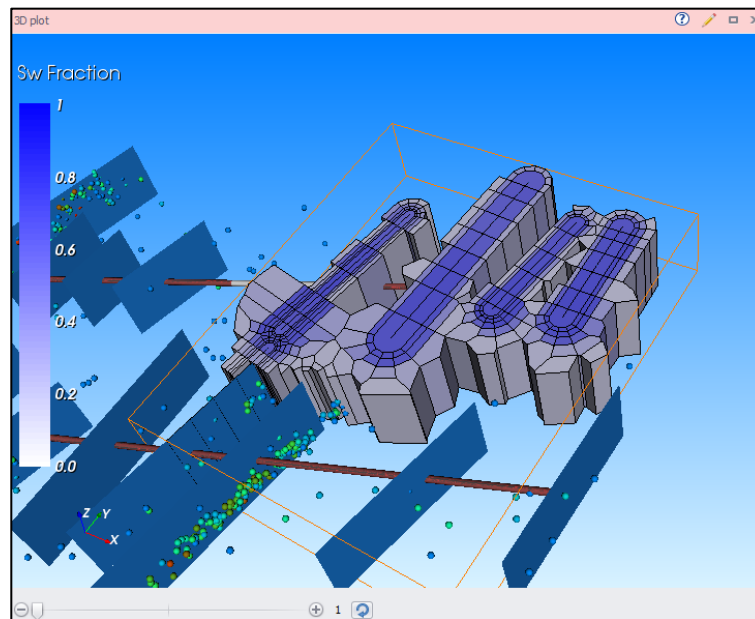


Fig. 1.B.14 – Initialization using the material balance static approach.

- The “Dynamic method”: we simulate the injection in the final fractured system, as if the hydraulic / natural fracture system already existed... before the fracturing jobs. So we start with the geometry of the final system and simulate the increases of pressure and water saturation. This model is more rigorous than the previous one. It produces a non-uniform pressure field and a more realistic distribution of water. It requires a rather complex simulation and the exact injection history. Such a model could represent a good compromise in the perspective of simulating the initial state of the system before the production starts.



*Fig. 1.B.15 – Initialization using the injection dynamic approach.*

- The realistic approach: we simulate the exact fracturing job and use the resulting stress, pressure and saturation fields as the starting point for the production. This full-physics approach is the most rigorous one for detailed modeling/analysis of the water flowback. However, it requires a flow simulator fully coupled with a mechanic simulation engine, and a very large number of inputs (initial stress field, geomechanical properties of the rock, injection schedule, proppant properties, etc). KAPPA does not have yet the ability to simulate such a system.

More details are given in 10.H.3.

### **1.B.5 Heterogeneities and DFN**

One of the big choices to make when trying to model unconventional plays is whether we consider a more or less complex diffusion at the micro-scale and extend it to the whole reservoir at the macro-scale, or if we need to consider macro-scale heterogeneities. Even if homogeneous models can, generally, pretty well explain single well production, they may quickly become insufficient to explain well interference.

Heterogeneities may have to be introduced at a point, even though it creates an even more under-defined problem. Discrete Fracture Network (DFN) models are for this reason becoming increasingly popular, whether they are generated numerically or approximated analytically.

### **1.B.6 Lack of quality data**

The elements above point to very complex systems. The potential number of unknowns is much higher than for conventional formations, and with a total lack of empirical rules of thumb. If these formations constitute our 100-year future, one might have expected that substantial effort would be made on the metrology and, more generally, the acquisition of high quality data to mitigate the complexity of the problem.

The opposite was initially observed. There was a frenzy of drill & frac, and the paradigm was that we were creating a new mining industry. The reservoir and the well would be the same thing, no real reservoir engineering would be required because, in essence, the part of the reservoir of interest would be the famous SRV, i.e. more or less the bulk volume physically delimited by the set of hydraulic fractures. If for a given well the choice was to spend the same money on an additional fracture stage or a permanent downhole gauge, the immediate choice would be about fracking.

We have certainly passed this stage today, and companies are increasingly aware that proper reservoir engineering may be required in the long term. Most companies of a certain size are now running at least pilot developments where permanent gauges are installed and well interferences are being recorded and studied.

Still today most wells are poorly equipped, and most production databases contain allocated rates, with or without a pressure that is generally recorded at surface.

## 1.C Basic production behaviour of a shale well

In order to illustrate the basic production behaviour of a shale well, we first consider the simplest possible model using typical parameter values for a shale play. We ignore most of the complex elements described in the previous section and start with the following assumptions:

- Formation Conditions:
  - Assume a uniform initial pressure scenario for the reservoir.
  - No desorption or other chemical/thermodynamic effects are considered.
  - Single-phase flow only.
- Darcy's Law is Applicable:
  - Formation is homogeneous.
  - No micro- or nano-scale heterogeneous behaviour.
  - No macro-scale fracture network(s).
- Multi-Fractured Horizontal Well:
  - Fractures have the same length, width, and permeability.
  - Fractures are orthogonal to the horizontal well.
  - Fractures are placed evenly along the horizontal section.
- Well Placement:
  - The well is located in an infinite-acting reservoir, or
  - The well is located at the center of a bounded rectangular or square reservoir.
- Well Stimulation:
  - The fracturing process is not modelled.
  - Water invasion due to stimulation is not modelled.
  - Pressure and saturation gradients due to stimulation are not modelled.

In the following graphical representation and, although it integrates a large number of simplifications, this sort of model was more or less the state-of-the-art five years ago. For our purposes, we simulate production at a constant pressure for as long as it takes to observe the main flow regimes. We show the response on an RTA log-log plot.

Although the corresponding analytical model would qualitatively reproduce the same log-log response, we utilise the numerical model in order to visualize the pressure fields. This is critical in assessing the 'stimulated reservoir volume' (or SRV). For each case, on the left there is the log-log RTA plot and on the right, the pressure profile in the reservoir. A close-up of the same plot is integrated in the loglog area to show the pressure gradients at the well.

This is a theoretical exercise. To observe the final reservoir behaviour, such test would take several thousand years and the corresponding flowrates during very late times would approach infinitesimally small values. However this example will be quite useful for a reservoir engineer with a background in PTA to orient themselves to the various flow regimes and the state of the pressure distribution in the reservoir over time.

### 1.C.1 'Early' linear flow

The first series of plots shows the response after one month. At the start of the production the flow is orthogonal (linear) to the individual fractures and, because of the very low permeability, interference between the fractures is highly unlikely for a substantial period of time. In concept, the well behaves as a single equivalent fracture with an effective length equivalent to the sum of the individual fracture lengths.

This linear flow regime is characterized by a half slope on the log-log plot for both the normalized pressure and derivative functions, with a factor of 2 between the two curves. This response would also be characterized by a linear trend on a square root of time plot, similar to that used in PTA for a single hydraulic fracture.

If we were to construct a straight line on an Arps plot we would obtain a 'b' factor equal to 2.

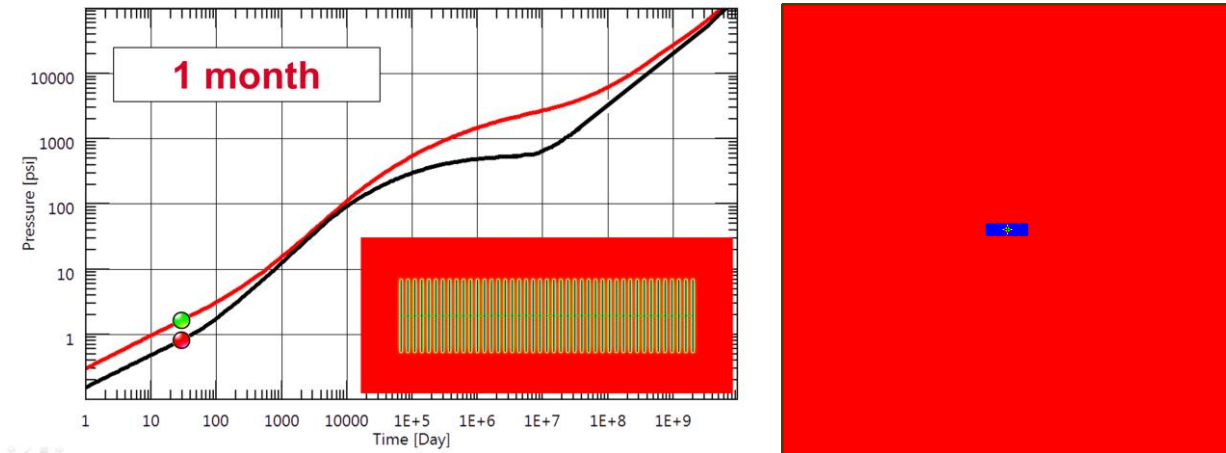


Fig. 1.C.1 – Linear flow behaviour

### 1.C.2 Transition from linear flow to SRV flow

After a certain period of production, the pressure distributions near the fractures begin to interfere. In this example, the next series of figures below show the response after three months. Both the normalized pressure and derivative begin to deviate (slightly) upwards from the expected linear flow half-slope trend where this represents a loss of productivity for the well.

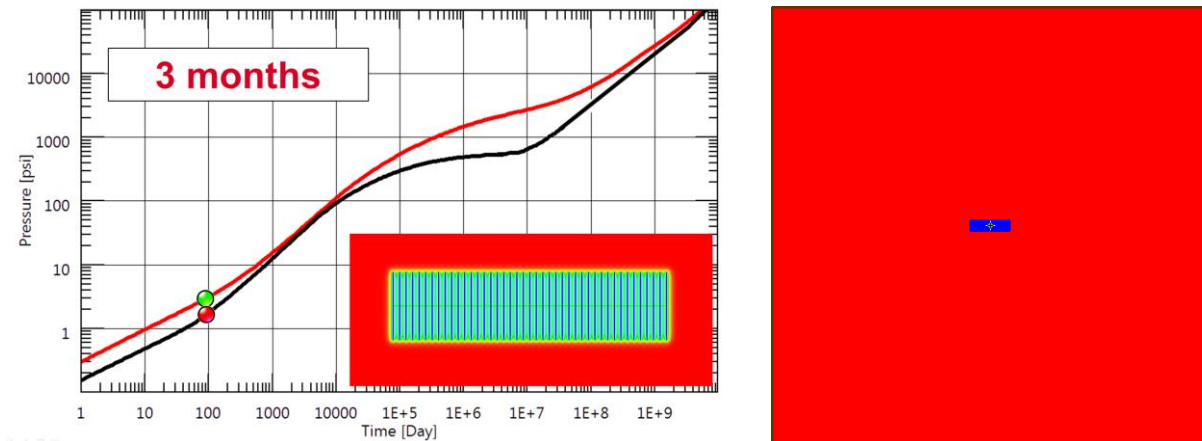


Fig. 1.C.2 – Start of interference between fractures

The next series of plots show the end of the transition from linear flow as both the normalized pressures and derivatives tend to merge onto a unit slope trend. During this transition period, the 'b' factor shown on the Arps plot continuously declines from the initial value of 2 (linear flow) the value of 0 (exponential decline).

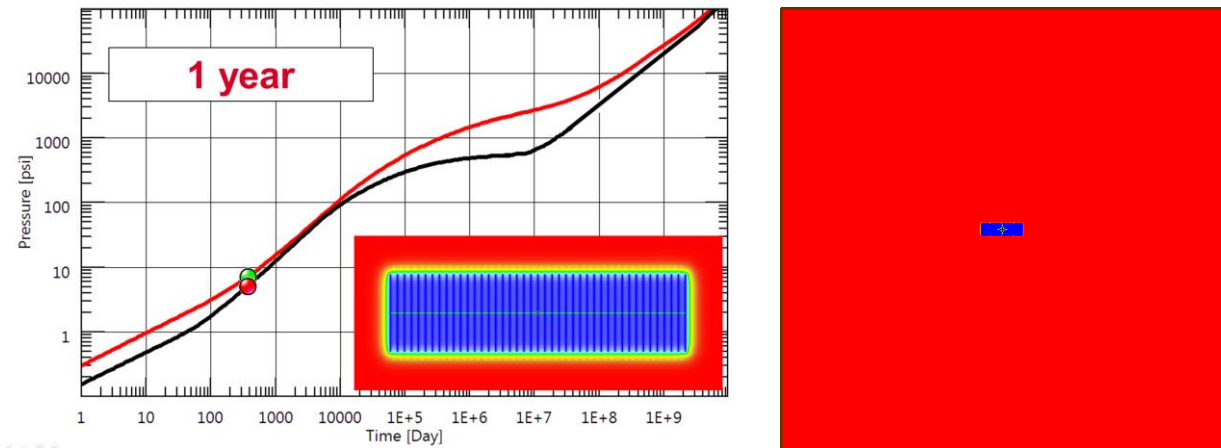


Fig. 1.C.3 – Transition period to SRV flow

### 1.C.3 SRV flow

We achieve a behaviour where both the normalized pressure and derivative functions have merged onto a unit slope, producing a regime that we will call the 'SRV flow regime' and this regime behaves exactly like the traditional Pseudo Steady state behaviour that we expect to encounter in conventional plays. The following plots show the system behaviour after five years.

The physical explanation is straightforward. During the early phase each fracture produced as if it was alone in the reservoir, so the diffusion is in all directions orthogonal to each fracture. Once the interference occurs we are taking the formation 'by surprise'. There is no diffusion expansion except at the outer face of the two extreme fractures and at the tips of all fractures. This suddenly decreases the area of contact between the well and the reservoir, and the only thing that is left to sustain the production is to deplete the volume already investigated, which we call the Stimulated Reservoir Volume, or SRV. It is not strictly Pseudo Steady state, because there is still diffusion going on at the limit of the SRV, but it will look very much like it. We could also call this flow Pseudo Pseudo Steady state.

On the right hand plot we start to see the diffusion (in yellow) at the very near border of the SRV.

During the SRV flow, the 'b' factor will be fractionally above zero.

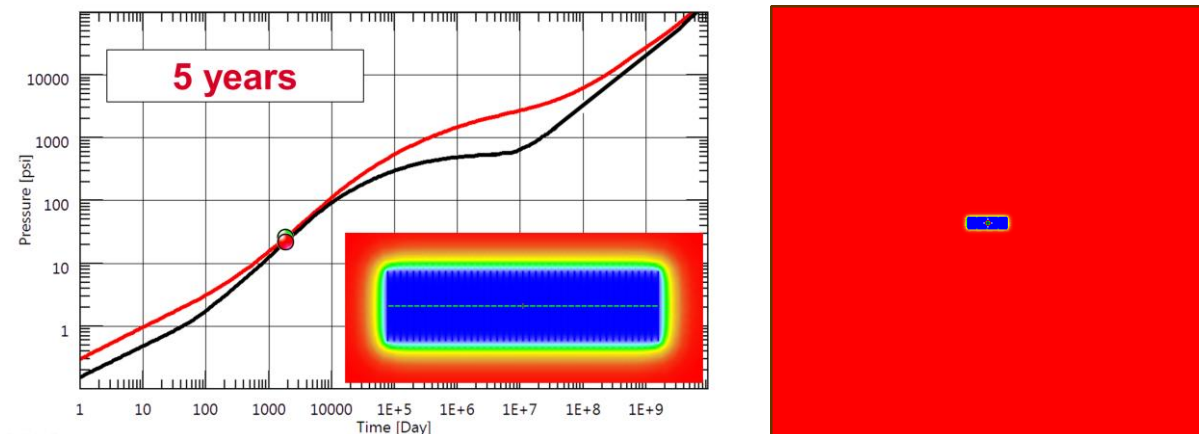


Fig. 1.C.4 – Established SRV flow

### 1.C.4 Beyond SRV

Depending on the reservoir parameters and the well-fractures system, one may see (or not) the response deviate from SRV flow once the contribution of the outer part of the SRV becomes non-negligible.

In theory, if we were to wait long enough, we could even see the system reach the more traditional Infinite Acting Radial Flow (IARF).

However this is very unlikely to happen as, by this time, the production would become infinitesimal and the well would be long abandoned. In addition, one would expect that other fractured horizontal wells would have been completed and produced in the meantime.

However, for the sake of the theoretical exercise you will find below in the three next series of plots the response of our example after 50 years, 500 years and 5,000 years, where in our case IARF is reached.

Just for fun, you can see in the fourth and last series the response after 50,000 years, where the system reaches the ‘true’, ‘final’ Pseudo Steady state response.

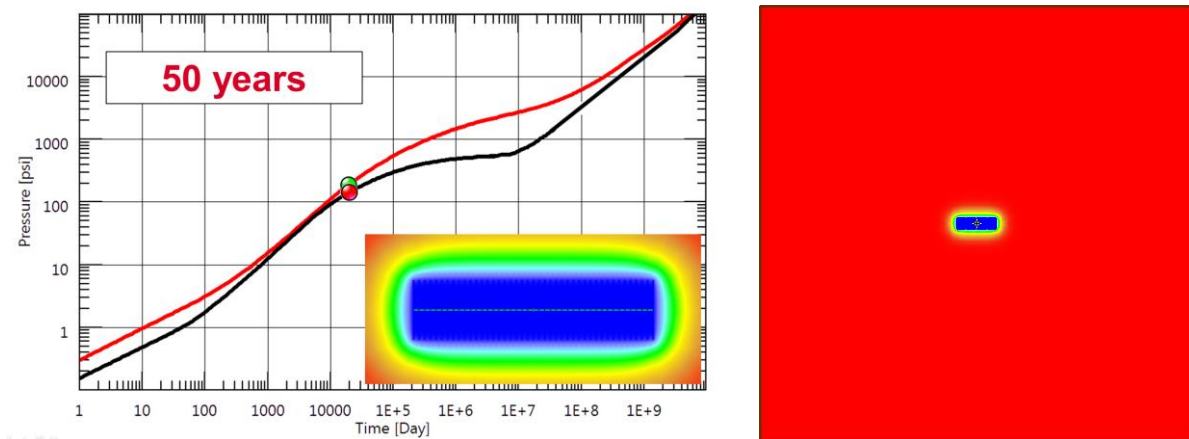


Fig. 1.C.5 – Deviation from the SRV flow

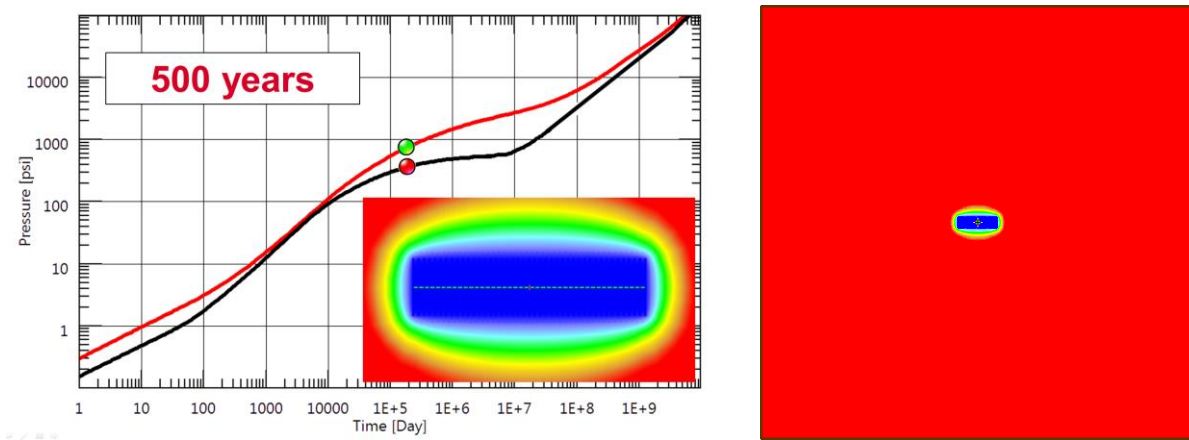


Fig. 1.C.6 – Effect of the formation out of SRV

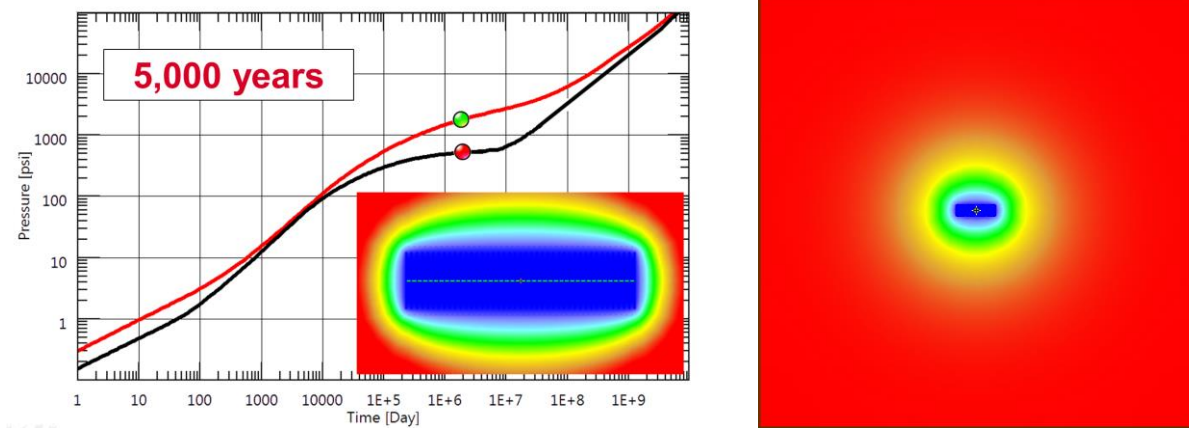


Fig. 1.C.7 – Possible IARF from the formation

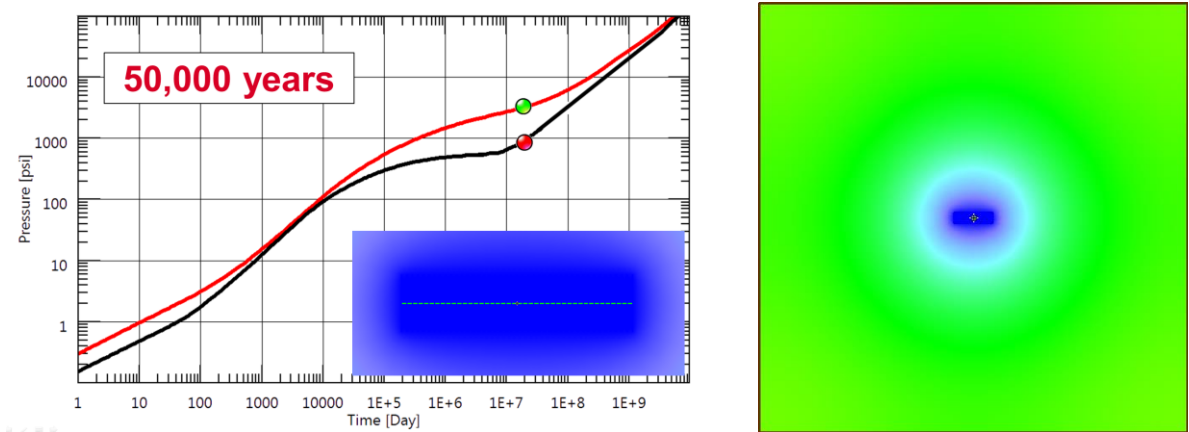


Fig. 1.C.8 – Very late final P.S.S.

Naturally all this is a theoretical exercise and there are four reasons not to get too much out of it: (1) 50,000 years may be a little long for a well test; (2) the whole idea of shale production today is to multiply the number of wells; (3) over long durations simplistic models just fail; (4) even for shorter durations we will see that a number of observations challenge this model.

If we believe this model and return to more realistic production times and abandonment rates, the conclusion is that the meaningful part of the response is constituted by the four first time log cycles (figure below). In the production life of such wells we would see the linear flow, some kind of transition towards the SRV flow, the SRV flow and, depending on the case, some late time deviation if it is not affected by the production of nearby wells.

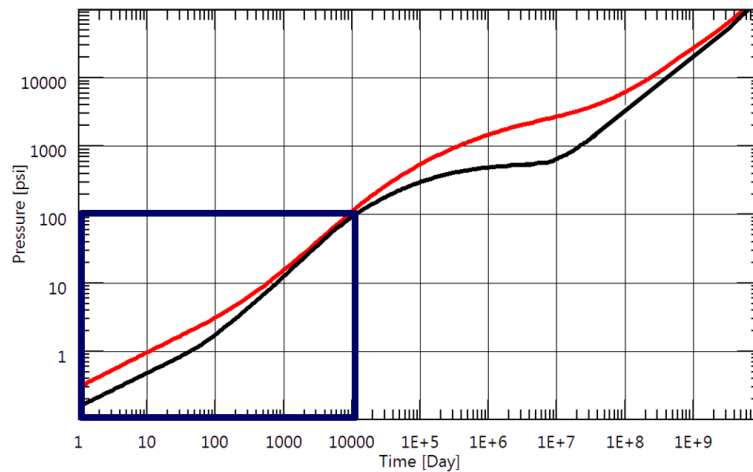


Fig. 1.C.9 – Realistic time range

This simulation reflects the state-of-the-art not so long ago. *Though an external analytical model was available in Saphir as long ago as 1999, these analytical and numerical models were integrated in Ecrin in 2009 and into Generation 5 Workstation in 2015.*

This model also represents the position of one of the main schools of thinking around these plays. Beyond the model itself, this school considers that the near totality of the production will come from an SRV that is indeed a slightly inflated version of the bulk volume determined by the series of hydraulic fractures.

This simple model is also the first occasion to introduce the difficulty of forecasting the production of these wells, as shown in the figure below. We have just started to produce these plays and we do not have yet any rule-of-thumb to anticipate these slow diffusion processes. So we only have a small number of data while the response starts with a long transient. Then we anticipate a transition and a long SRV flow. By the end of the production life we may see something else. The challenge is to use this little data and extrapolate it to get an estimate, or a probability function for EUR. The initial work that consisted of extrapolating the initial linear flow response has led to the issues we know.

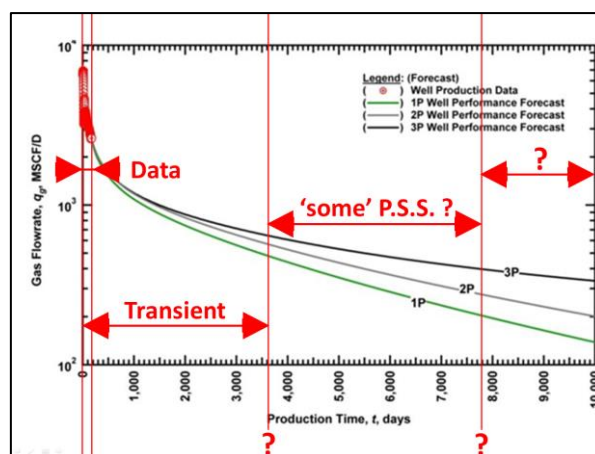


Fig. 1.C.10 – Forecast uncertainties

## 1.D Decline Curve Analysis (DCA) of unconventional plays

The application of Decline Curve Analysis (DCA) in unconventional plays could be problematic. A prerequisite to any discussion on DCA for unconventional plays is the understanding that no simplified time-rate model can accurately capture all elements of performance.

The analyst should be realistic and practical when attempting to characterize production performance of systems where permeability is in the order of the nano-Darcy. Although the hydraulic fractures enable the production performance, today we only have a basic understanding of the flow structure in the hydraulic and natural fracture systems.

From a historical perspective, DCA and production forecasting using Arps' exponential and hyperbolic relations have been the standard for evaluating Estimated Ultimate Recovery (EUR) in petroleum engineering. However, in unconventional plays such as shale gas, tight/shale oil reservoirs, these relations often yield ambiguous results due to invalid assumptions. The main assumptions which form the basis of traditional DCA can be summarized as:

- There is no significant change in operating conditions and field development during the producing life of the well
- The well is producing with a constant bottomhole flowing pressure
- There is a boundary-dominated flow regime and reservoir depletion was established

In very-low permeability reservoir systems, it is common to observe basic violations of the assumptions related to traditional DCA, hence the misapplications of the Arps' relations to production data with significant overestimation of reserves, specifically when the hyperbolic relation is extrapolated with a  $b$ -exponent greater than one.

In order to prevent overestimation of EUR, a hyperbolic trend may be coupled to an exponential decline at late time. However, this approach remains empirical and may be 'non-unique' in the hands of most users, yielding widely varying estimates of reserves.

The issues with Arps' relations have led numerous authors [Ilk et al. (Power-law exponential, 2008), Valko (Stretched exponential, 2009), Clark et al. (Logistic growth model, 2011), and Duong (2011)] to propose various rate decline relations which attempt to model the time-rate behaviour observed in unconventional plays. Specifically these relations are focused on characterizing the early time transient and transitional flow behaviour. They are based on empirical observations of characteristic behaviours of certain plays. None of them are sufficient to forecast production for all unconventional plays. In other words, one equation may work for one play and perform poorly on another one. It is therefore important to understand the behaviour of each equation, and apply these relations appropriately for production forecasts.

This chapter presents the application of the decline curve equations. The results of time-rate analyses for each equation are presented and diagnostic plots to guide analysis are described.

### 1.D.1 Main plots used in Decline Curve Analysis

Diagnostic plots are very useful while performing decline curve analysis and provide direct insight into our understanding of decline behaviour. In particular, diagnostic plots can guide the analyst and are mainly used in an effort to understand data characteristics prior to performing decline curve analysis.

Our general procedure for decline curve analysis is to simultaneously use the diagnostic plots and calibrate the parameters of each model until a reasonable match is achieved. Regression may be used to refine the model parameters once diagnostic interpretation is complete. This procedure ensures consistency and may prevent non-uniqueness associated with matching multiple model parameters only on a single plot (e.g., time-rate plot).

Though many others may be used, the four following plots are recommended, and in most cases are considered sufficient for a proper DCA workflow:

1. [Semi-log]: (Log) Rate and Time
2. [Log-log]: (Log) D-parameter and (Log) Time
3. [Log-log]: (Log) b-parameter and (Log) Time
4. [Log-log]: (Log) Rate/Cumulative Production and (Log) Time

These plots may exhibit characteristic behaviours and validate the applicability of such or such decline equation. For example, by observing the D and b parameters, one can infer the b exponent to be used in the Arps' hyperbolic relation. For reference, D-parameter and b-parameter plots are derivative plots and their definition is tied to the term called the 'loss ratio' (Johnson and Bollens (1927)). For reference, these formulations are given as:

$$D(t) \equiv -\frac{1}{q(t)} \frac{dq(t)}{dt} \quad (\text{decline parameter})$$

$$\frac{1}{D(t)} \equiv -\frac{q(t)}{dq(t)/dt} \quad (\text{loss-ratio})$$

$$b(t) \equiv \frac{d}{dt} \left[ \frac{1}{D(t)} \right] \equiv -\frac{d}{dt} \left[ \frac{q(t)}{dq(t)/dt} \right] \quad (\text{derivative of the loss-ratio})$$

The parameters are computed from the data using numerical differentiation. Such differentiation without smoothing results in noisy data. Proper editing of the time-rate data along with the Bourdet derivative are recommended.

The four plots to be used in decline curve analysis of a single well example are shown below (Figs. 1 to 4).

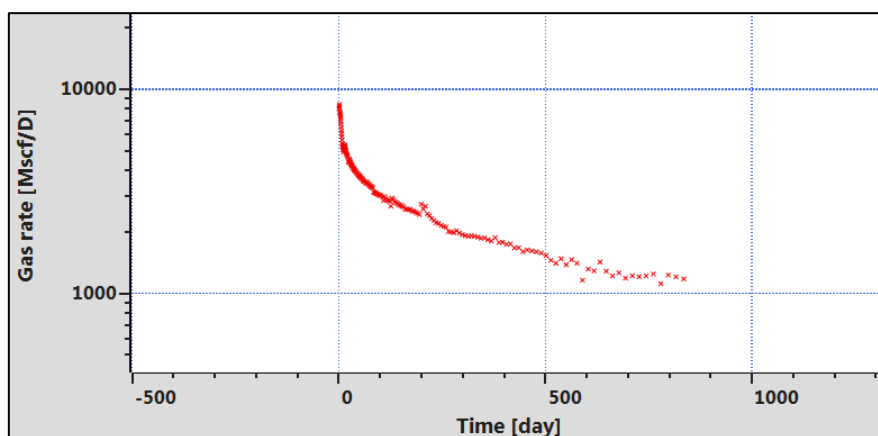


Fig. 1.D.1 – Rate and time plot.

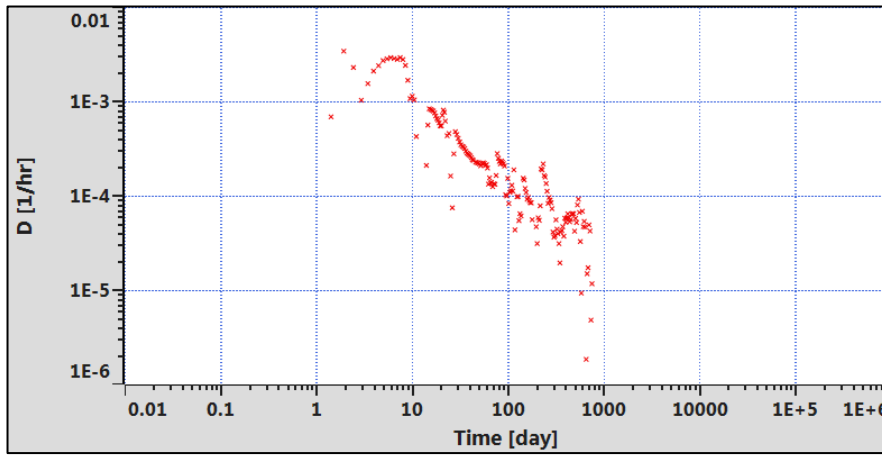


Fig. 1.D.2 - Computed D-parameter and time plot.

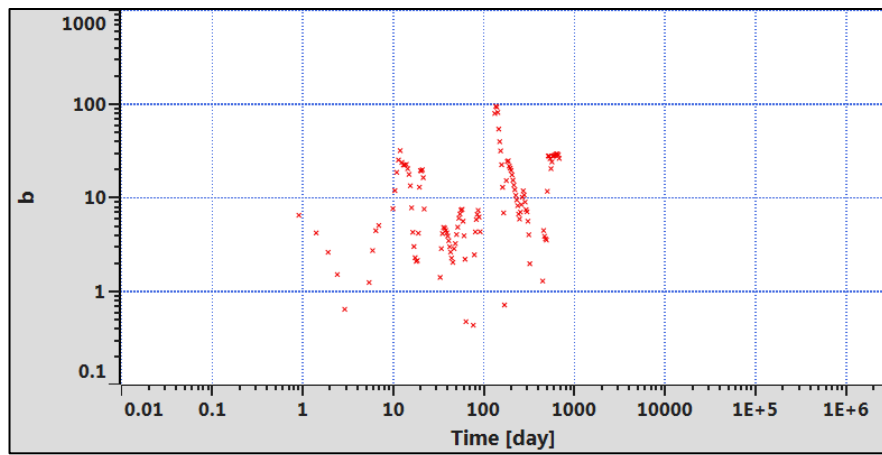


Fig. 1.D.3 - Computed b-parameter and time plot.

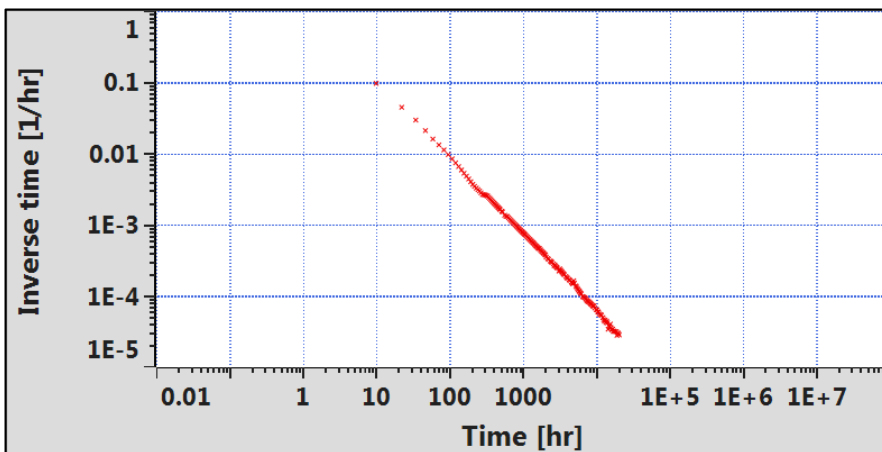


Fig. 1.D.4 - Rate/cumulative production and time plot.

## 1.D.2 The Arps equations

Arps' hyperbolic relations are widely used in DCA for production extrapolations and reserves estimations. The basis for the Arps' relations is empirical. The exponential decline corresponds to the Pseudo Steady State (PSS) flow in transient analysis. The hyperbolic relation does not have a transient equivalent. Gas flow during the boundary dominated flow regime can be approximated to a hyperbolic equation with b-values ranging between 0.4 and 0.6. For reference, exponential and hyperbolic relations are given as:

$$q(t) = q_i \exp[-D_i t] \quad (\text{Exponential rate decline})$$

$$q(t) = \frac{q_i}{(1 + bD_i t)^{1/b}} \quad (\text{Hyperbolic rate decline})$$

It is possible to infer exponential or hyperbolic behaviour by observing the D and b parameters. A constant D-parameter indicates exponential decline. A constant b-parameter indicates hyperbolic decline. For matching purposes, the user should first adjust b from the b-parameter plot, then match the D-parameter with a model. The initial rate ( $q_i$ ) can be adjusted to complete the match and obtain the production forecast. It is possible to use a segmented hyperbolic if the user identifies multiple constant trends of the b-value.

Finally it is important to note that industry wide application of the Arps' hyperbolic relation in unconventional reservoirs includes a modification with the exponential decline at later times to prevent overestimation of reserves as the hyperbolic equation is unbounded for b-values greater than one (i.e. transient flow assumption for b-values greater than one). Hyperbolic decline is switched to an exponential decline once a certain yearly decline value is reached. This yearly decline value is set by the analyst and is called as the 'terminal decline' value. This protocol yields the 'modified' hyperbolic designation. Figs. 5 to 8 describe the application of the modified hyperbolic relation on a specific field example.

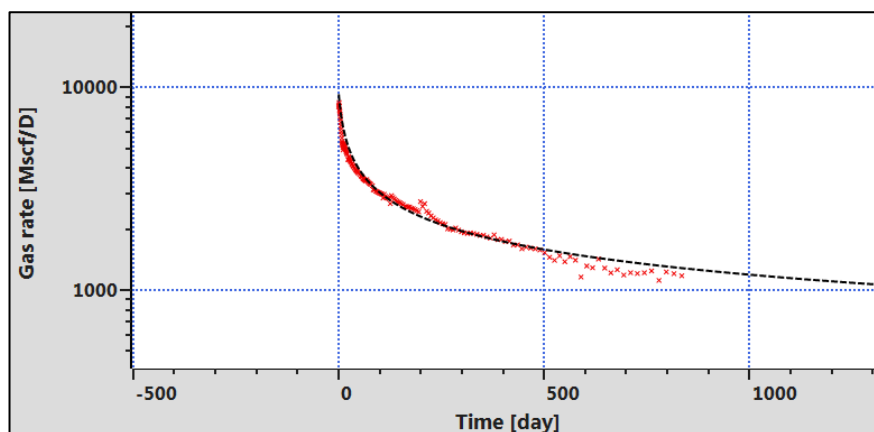


Fig. 1.D.5 – Rate and time plot  
(modified hyperbolic relation).

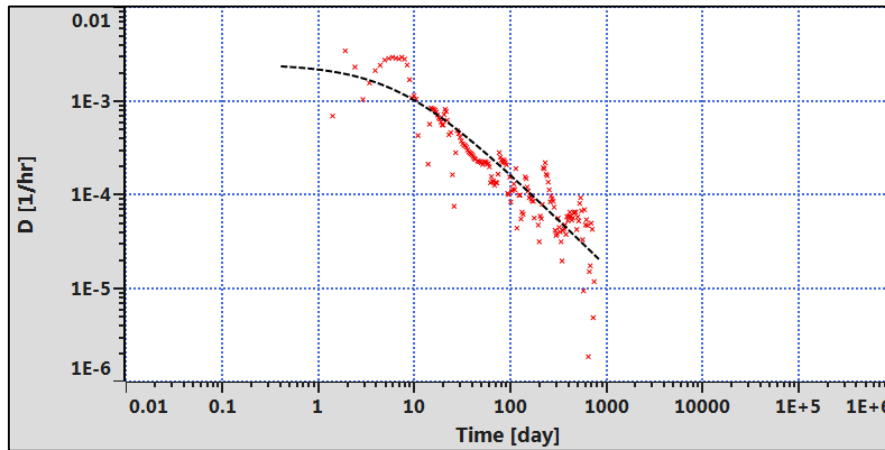


Fig. 1.D.6 – Computed D-parameter and time plot (modified hyperbolic relation).

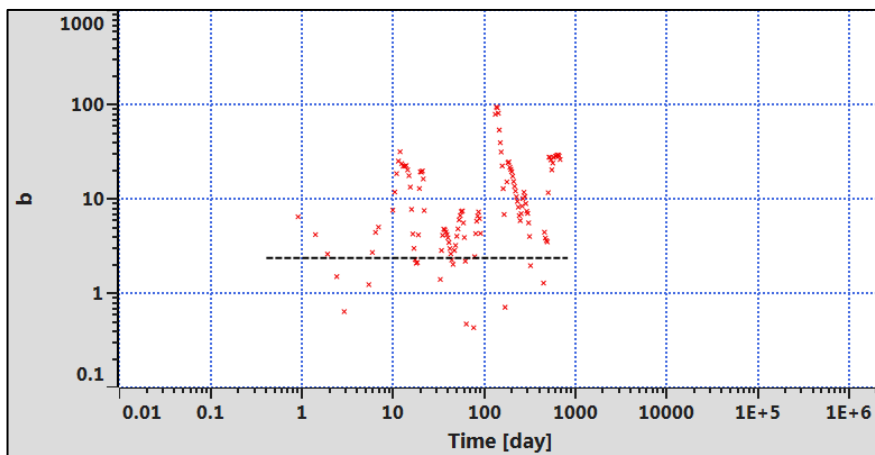


Fig. 1.D.7 – Computed b-parameter and time plot (modified hyperbolic relation). (From Ilk, 2014)

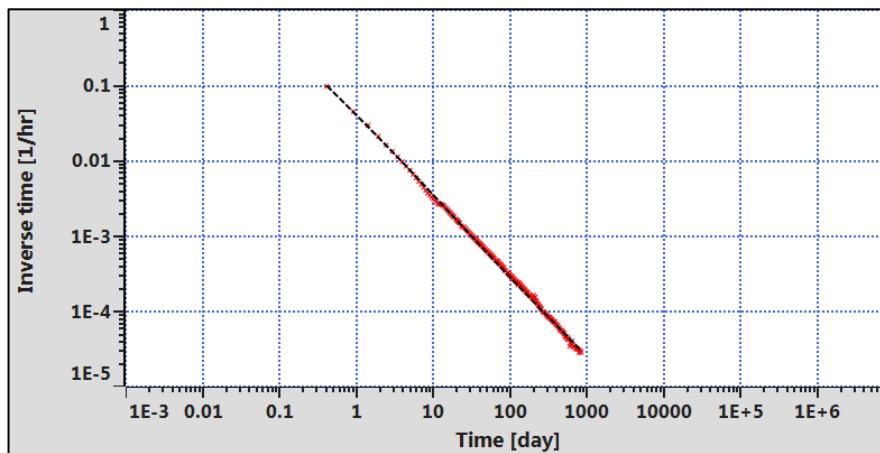


Fig. 1.D.8 – Rate/cumulative production and time plot (modified hyperbolic relation). (From Ilk, 2014)

### 1.D.3 Power-law exponential

The power-law exponential relation was derived exclusively from the observed behaviour of the D-parameter and b-parameter. Its primary assumption is that the D-parameter exhibits a straight line behaviour on a log-log scale, which essentially corresponds to a power-law model. If the D-parameter formulation (Eq. 1) is approximated to a power law model, the resulting differential equation yields the power-law exponential relation.

By introducing a constraining variable ( $D_\infty$ ), the D-parameter trend is constant at late times. This variable converts the power-law exponential equation to an exponential decline with a smooth transition. However, in almost all of the applications in unconventional reservoirs,  $D_\infty$  is not required since there has been no observation of the constant D-parameter trend and the nature of the power-law exponential relation is conservative as it models the b-parameter trend declining with time. Power-law exponential relation is given below:

$$q(t) = \hat{q}_i \exp [-\hat{D}_i t^n - D_\infty] \quad (\text{Power-law exponential relation})$$

The application of the power-law exponential relation is centered on use of the D-parameter and time plot. Once the straight line is identified, slope and intercept values associated with the  $\hat{D}_i$  and  $n$  parameters are obtained. The  $\hat{q}_i$  parameter is adjusted to achieve the match on rate and time plot. Figs. 9-12 describe the application of the power-law exponential relation on a specific field example.

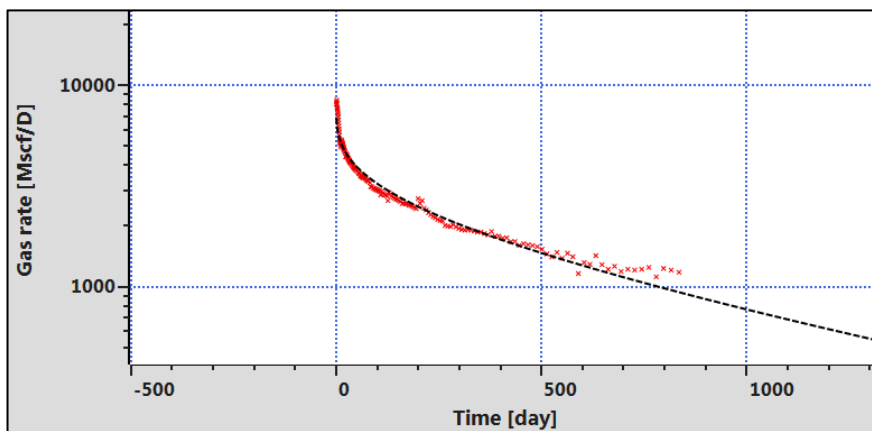


Fig. 1.D.9 – Rate and time plot (power-law exponential).

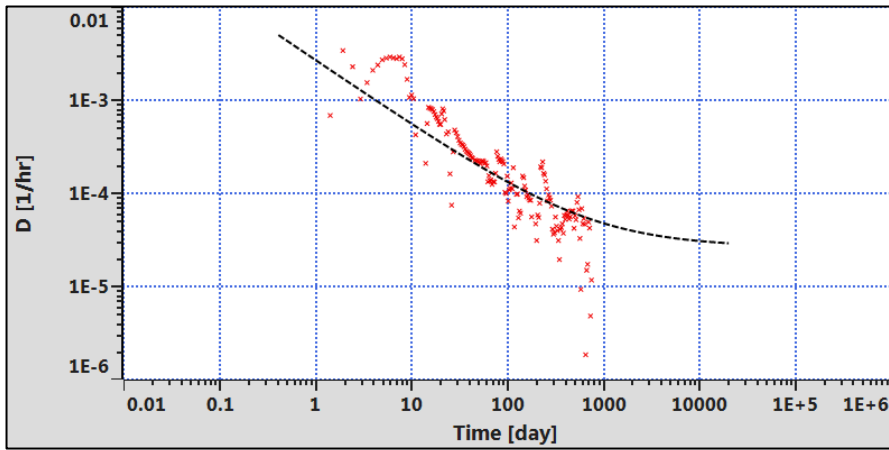


Fig. 1.D.10 – Computed *D*-parameter and time plot (power-law exponential relation).

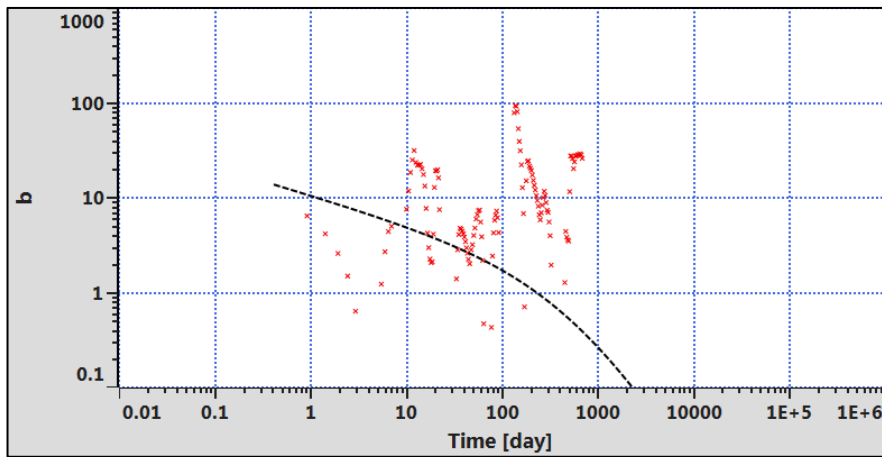


Fig. 1.D.11 – Computed *b*-parameter and time plot (power-law exponential relation).

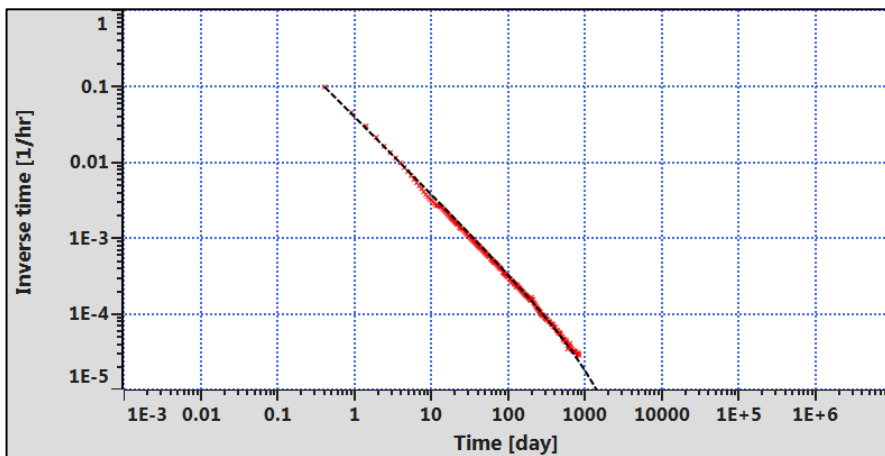


Fig. 1.D.12 – Rate/cumulative production and time plot (power-law exponential relation).

### 1.D.4 Stretched exponential function

The stretched exponential relation is essentially the same as the power-law exponential relation without the constraining variable ( $D_\infty$ ). Outside petroleum engineering, the stretched exponential relation has many applications such as in physics where numerous processes manifest this behaviour, as first described by Kohlrausch (1847), and then by various authors (Philips (1966)). In geophysics, the stretched exponential function is used to model aftershock decay rates (Kisslinger (1993)). In his seminal work (1945), Arps also provided the stretched exponential function, but no application was provided.

In general, the stretched exponential function is used to represent decays in randomly disordered, chaotic, heterogeneous systems. It can be suggested that the stretched exponential decay of a quantity is generated by a sum (superposition) of exponential decays with various time constants. This leads to the interpretation of heterogeneity where production decline in an unconventional reservoir system is determined by a great number of contributing individual volumes exhibiting exponential decays with a specific distribution of time constants. The stretched exponential function is given as (Valko (2009)):

$$q(t) = q_0 \exp[-(t/\tau)^n] \quad (\text{Stretched exponential relation})$$

The stretched exponential relation can be applied in the same manner as the power-law exponential relation using diagnostic plots or alternatively the procedure described by Valko (2009) could be applied.

Figs. 13-16 describe the application of the stretched exponential relation on a specific field example.

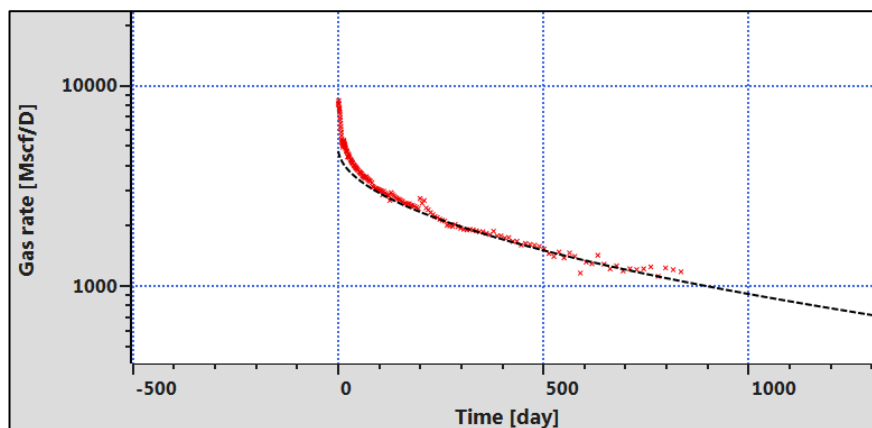


Fig. 1.D.13 – Rate and time plot  
(stretched exponential relation).

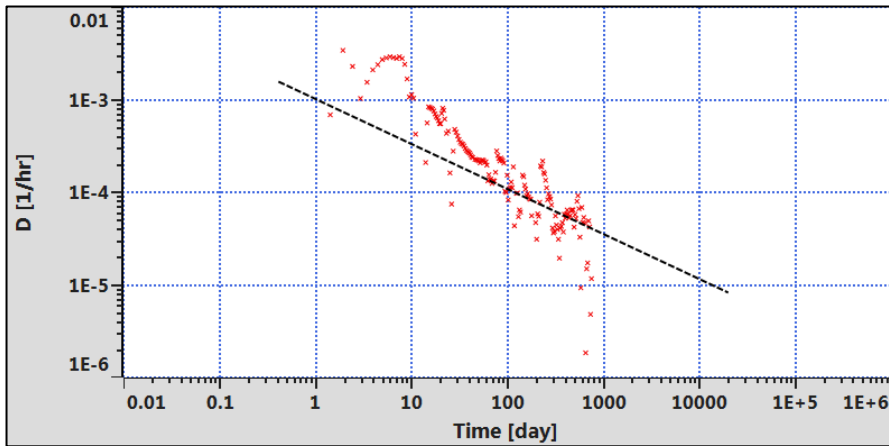


Fig. 1.D.14 – Computed D-parameter and time plot (stretched exponential relation).

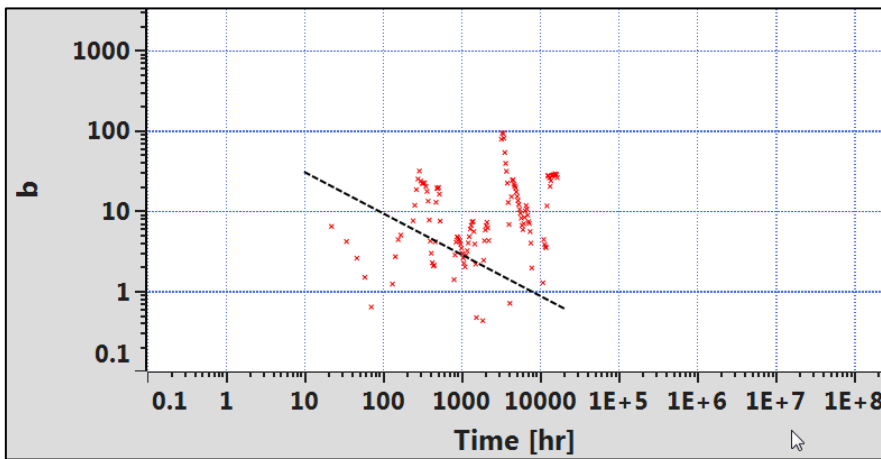


Fig. 1.D.15 – Computed b-parameter and time plot (stretched exponential relation).

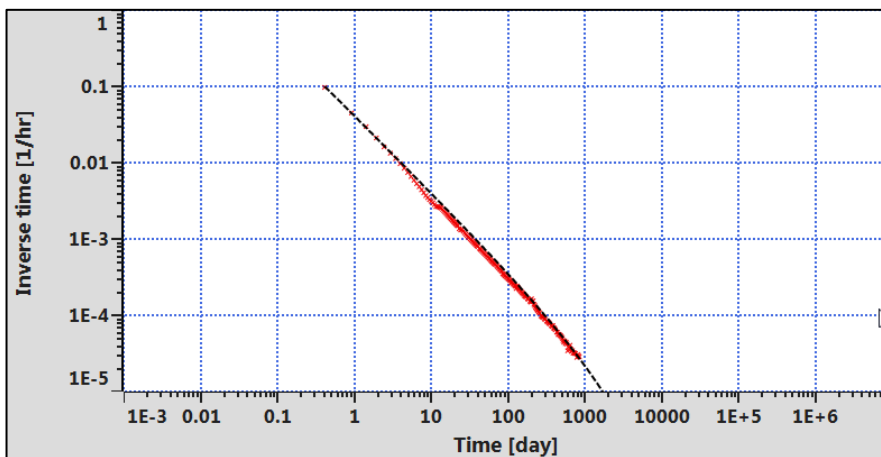


Fig. 1.D.16 – Rate/cumulative production and time plot (stretched exponential relation).

### 1.D.5 The Duong model

The Duong model is based on the assumption of dominant fracture flow and negligible matrix contribution. The fractured area increases with time and supports the fracture flow. Duong suggested that pressure depletion within fracture networks may reactivate existing faults or fractures. A log-log plot of rate and cumulative production vs. time yields a unit slope straight line regardless of the fracture type. Slopes greater than one may be due to flow regime changes and field operations. Time-rate relation can be calculated from the intercept and slope values of the log-log plot and an initial rate. The Duong's model is given as:

$$q(t) = q_1 t^{-m_{Dng}} \exp\left[\frac{a_{Dng}}{(1-m_{Dng})} [t^{(1-m_{Dng})} - 1]\right] \quad (\text{Duong model})$$

Other models, such as the power-law exponential, the stretched exponential and the logistic growth, account for deviations at later times. Such deviations also occur when a terminal decline is imposed on the modified-hyperbolic relation. The EUR estimates from Duong's model are therefore higher unless a constraining variable is also imposed. The linear flow assumption of the Duong model may hold for some plays, but it will generally need modifications to deal with changes in flow regimes (i.e. transitional flow, depletion of SRV, interference, etc).

Figs. 17 to 20 illustrate the application of the model. An important step is to establish the slope ( $m_{DNG}$ ) and intercept ( $a_{DNG}$ ) values on the rate/cumulative production trend and then adjust the  $q_1$  value to obtain the match.

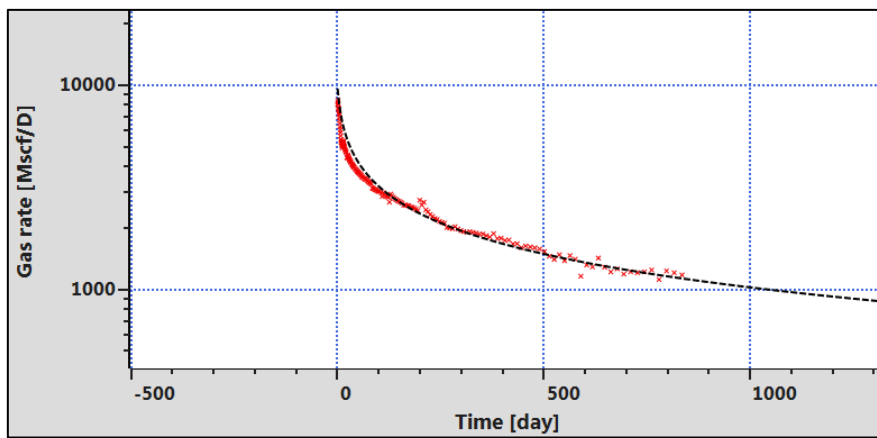


Fig. 1.D.17 – Rate and time plot (Duong model).

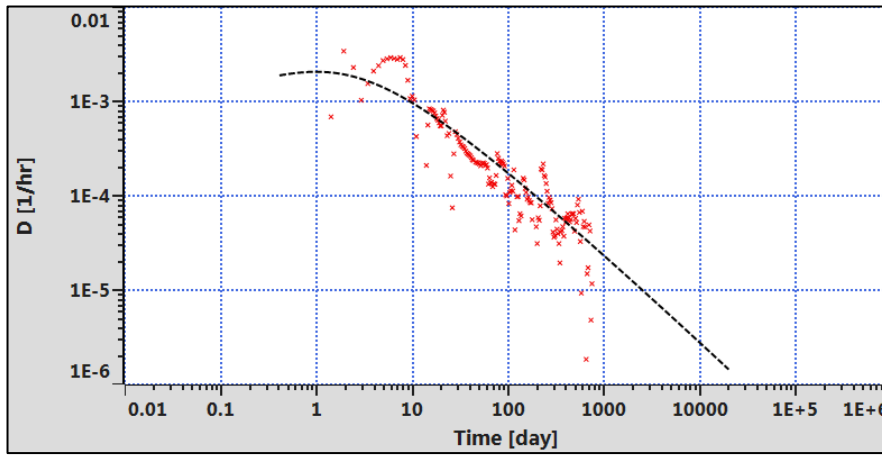


Fig. 1.D.18 – Computed D-parameter and time plot (Duong model).

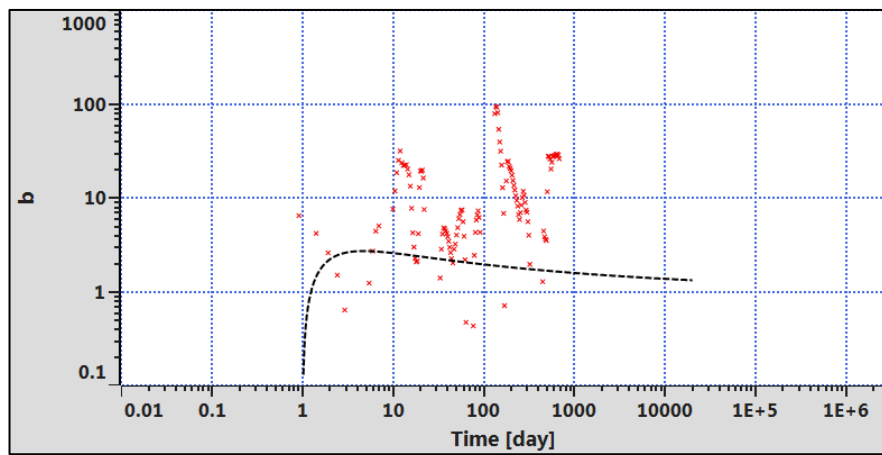


Fig. 1.D.19 – Computed b-parameter and time plot (Duong model).

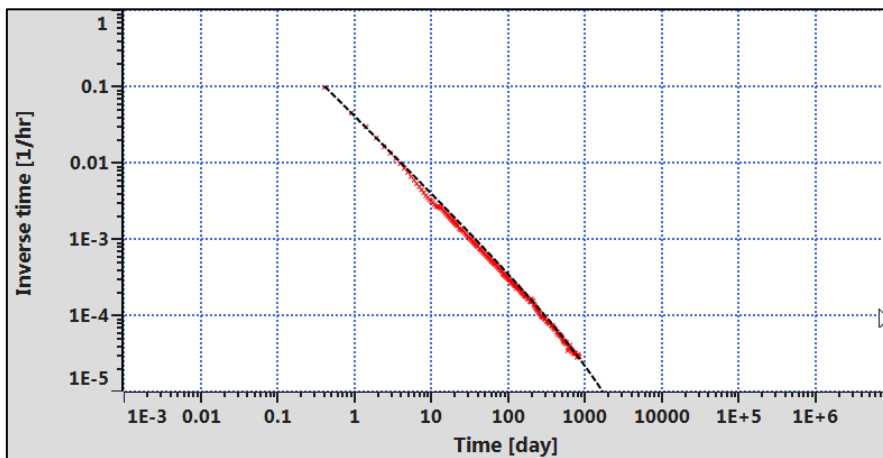


Fig. 1.D.20 – Rate/cumulative production and time plot (Duong model).

### 1.D.6 Logistic growth

Logistic growth curves are a family of mathematical models used to forecast growth (e.g., population growth, growth of agricultural products, regeneration of organs, market penetration of new products, etc.). Conceptually, logistic growth models assume that the growth variable increases then stabilizes. Logistic growth models have a term called the carrying capacity, which is the size at which the growth variable stabilizes and growth rate terminates.

Clark et al (2011) utilizes the logistic growth model for forecasting cumulative production of the wells in unconventional oil and gas reservoirs. The logistic growth model to describe cumulative production and rate is given below:

$$G_p(t) = \frac{K t^{n_{LGM}}}{[a_{LGM} + t^{n_{LGM}}]} \quad \text{(Logistic growth model)}$$

$$q(t) = \frac{dG_p(t)}{dt} = \frac{K n_{LGM} a_{LGM} t^{(n_{LGM}-1)}}{[a_{LGM} + t^{n_{LGM}}]^2} \quad \text{(Logistic growth model)}$$

The parameter  $K$  is the carrying capacity and referred to as the ultimate of oil and gas recovery from the well without any economic limits. This parameter is included in the model itself. Cumulative production will approach  $K$  while the rate tends to zero. The parameter  $n$  controls the decline. When  $n$  tends to one the decline becomes steeper. The parameter  $a$  controls the time at which half of the carrying capacity is reached. A high value of  $a$  indicates stable production. A low value of  $a$  points to a steeper decline.

Figs 21 to 24 show the application of the logistic growth model on a single well example.

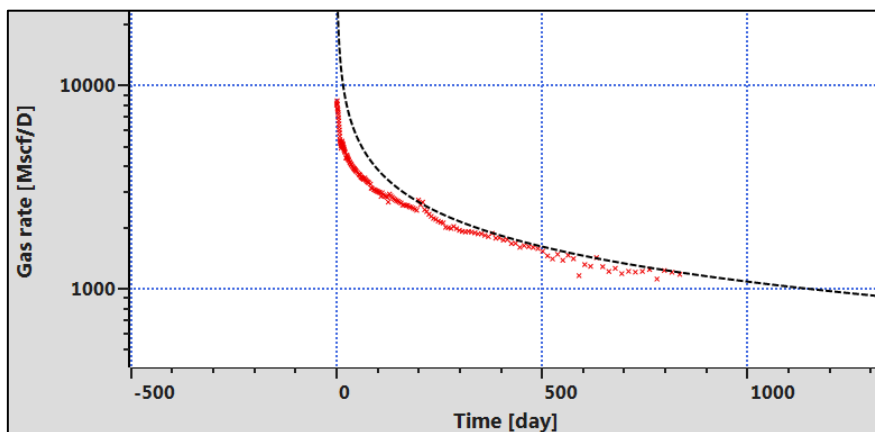


Fig. 1.D.21 – Rate and time plot (logistic growth model).

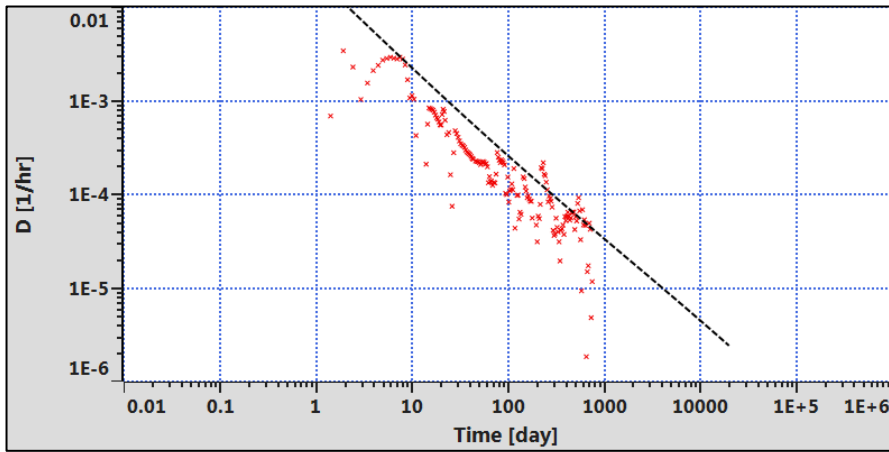


Fig. 1.D.22 – Computed D-parameter and time plot (logistic growth model).

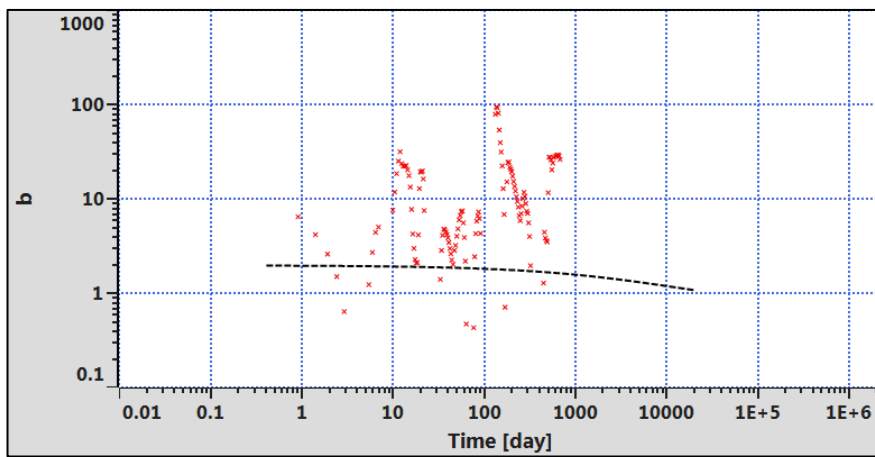


Fig. 1.D.23 – Computed b-parameter and time plot (logistic growth model).

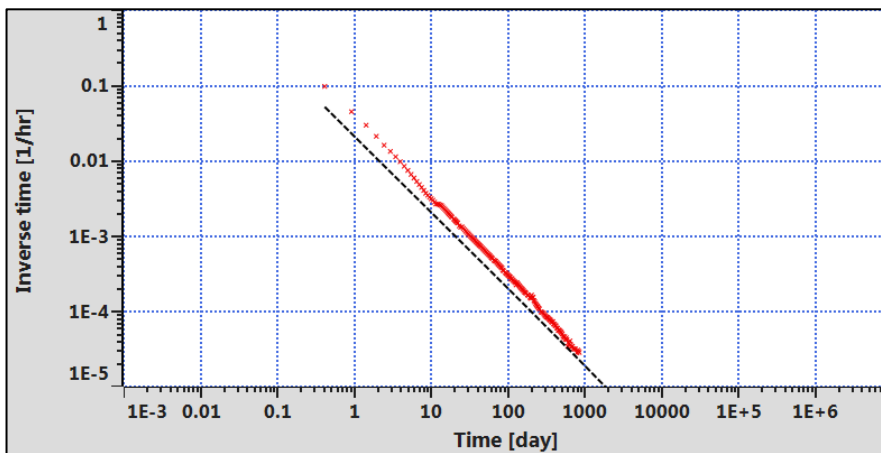


Fig. 1.D.24 – Rate/cumulative production and time plot (logistic growth model).

### 1.D.7 Stimulated Reservoir Volume Bounded decline curve

This decline curve includes the main Multi Fractured Horizontal Well flow regimes from the linear flow until the SRVB flow. The transition and the respective position of these two flow regimes are described by the three parameters:

- Initial rate  $q_i$
- The time of transition at the intersect of the  $\frac{1}{2}$  loglog slope straight line and of the unit loglog slope straight line.
- $P_a$ , the rate normalized pressure value (a.k.a.reciprocal productivity index) at the intersect of the  $\frac{1}{2}$  loglog slope straight line and of the unit loglog slope straight line.
- $\tau$  (tau), which determines the beginning and the end of the transition and has an influence on the curvature of the transition

The advantage of using this Decline Curve is that an analytical MFHW model can be initialized from it. It is sufficient to confirm the well length and the permeability and the fracture length can be then estimated.

Figs 25 to 28 show the application of the SRVB model on a single well example.

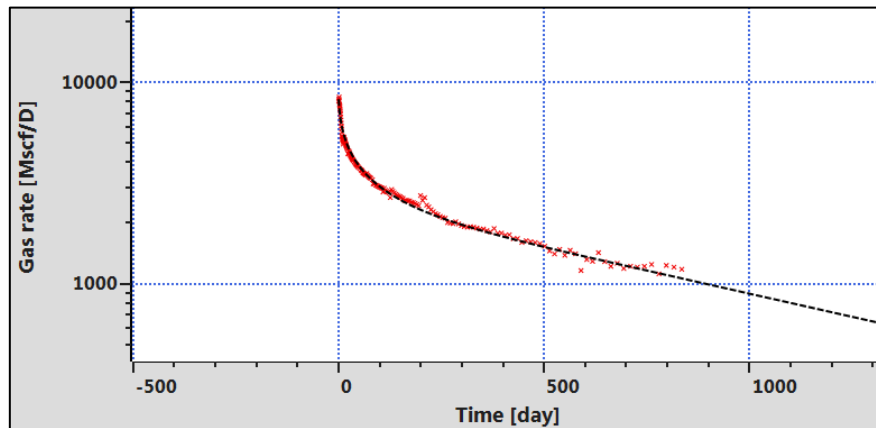


Fig. 1.D.25 – Rate and time plot  
(SRVB model).

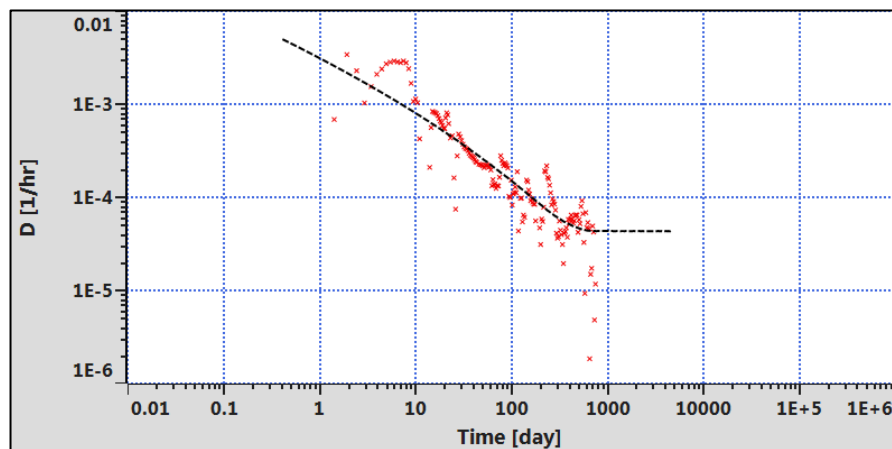


Fig. 1.D.26 – Computed  $D$ -parameter and time plot  
(SRVB model).

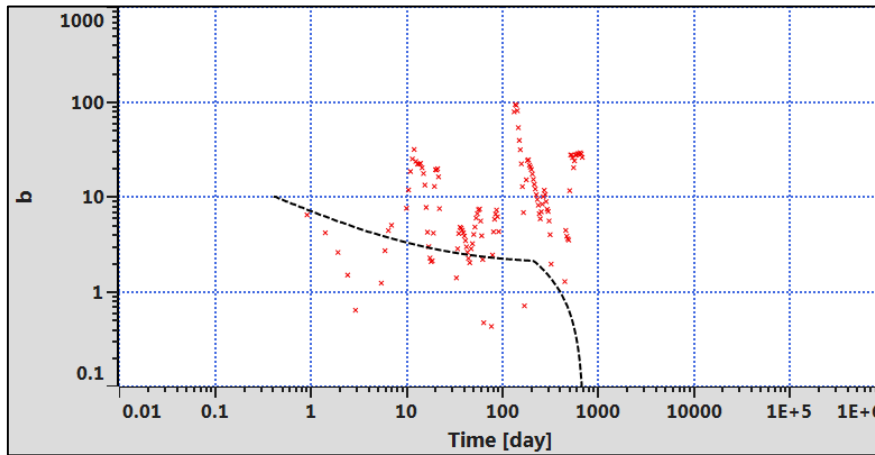


Fig. 1.D.27 – Computed *b*-parameter and time plot (SRVB model).

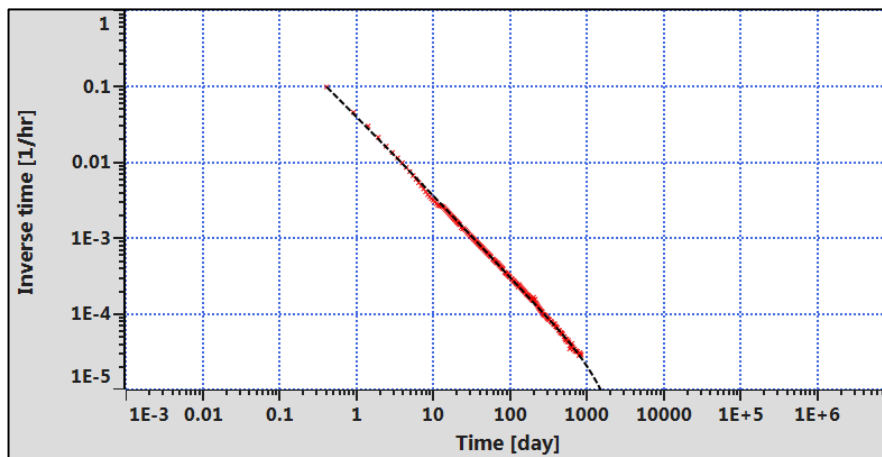


Fig. 1.D.28 – Rate/cumulative production and time plot (SRVB model).

### 1.D.8 Segmented DCA models

Long-term observation of the unconventional fields led many engineers to observe that the well behavior can exhibit not just a steady consistent power-law decline, but a sequence of them with changing parameters.

This can be due to changing production conditions, reservoir conditions or to changing reserves due to the drilling of other well in the vicinity.

For these reasons it can be perfectly reasonable and fruitful to split the history of the well production in to several segments, according to the observed behavior and to adjust different DCA model in order of study the evolution of the reserves with the time.

#### 1.D.8.a Segmented Power Law Model

On the *D* parameter plot this is manifested as a sequence of straight lines with the same slope, separated from each other, and on the *b* parameter plot the model line would show several intervals with constant values (see Figure below). Each segment in this case corresponds to an individual power-law segment of the well behavior. There are a few attempts to connect this with a physical description of a well-reservoir fractured system (e.g. the multi-zone fractional dimension model).

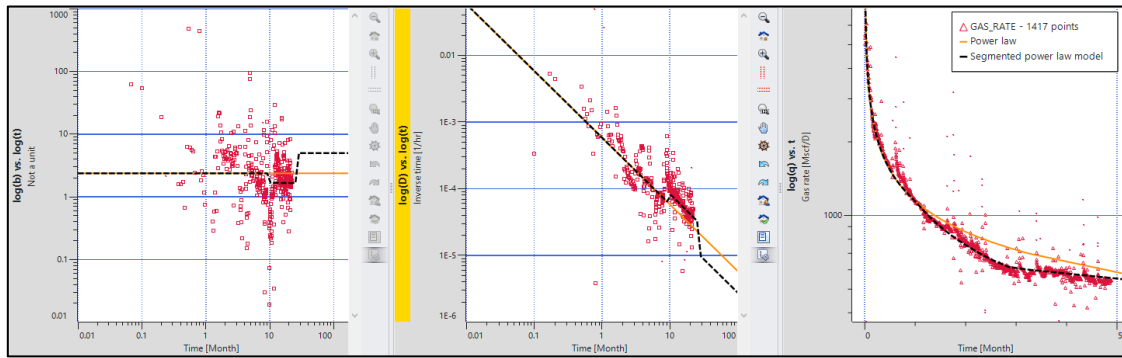


Fig. 1.D.29 – Segmented Power law model match

The model can also with the second (or latter) segment in the model forecast only to represent a situation when the expected future behavior of a well exhibits a different power-law decline from the historical one, e.g. when the production decline is sharper with stronger depletion.

**1.D.8.b Segmented Hyperbolic DCA model**

The Hyperbolic can also be used in a segmented model, it offers the possibility to adjust all the Hyperbolic DCA parameters in each segment.

The figure below shows an example of a Hyperbolic DCA model split into 5 segments and each segment automatically adjusted to the data in the interval.

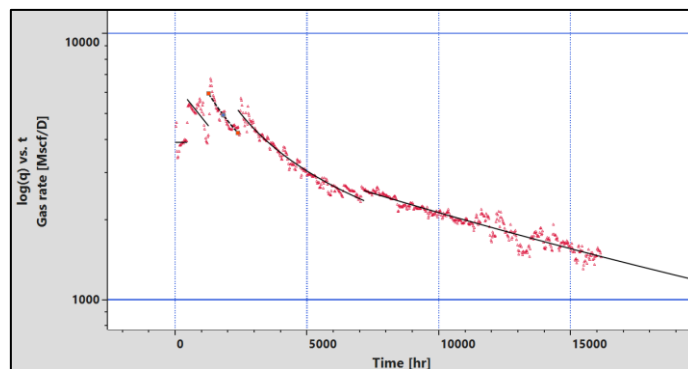


Fig. 1.D.30 – Segmented Hyperbolic DCA model match

The properties of each segment can be specified individually and several options allow the user to get the required match, for instance by imposing or not the continuity of the segments:

Decline curve bounds		
Time stamp	04/11/2011 23:00:00	
Hyperbolic Segment 1		
Segment type	Arps	
Tmin	0.00000	day
Initial rate	<input checked="" type="checkbox"/> 3901.39	Mscf/D
Decline parameter	<input checked="" type="checkbox"/> 0.01	1/year
Initial tangent effective decline rate	0.995017	%/Year
Initial secant effective decline rate	0.99255	%/Year
b exponent	<input checked="" type="checkbox"/> 0.5	
Exponential decline		
<input type="checkbox"/>		
Hyperbolic Segment 2		
Segment type	Arps	
Maintain initial rate with previous segment	<input type="checkbox"/>	
Tmin	19.0115	day
Initial rate	<input checked="" type="checkbox"/> 5661.39	Mscf/D
Decline parameter	<input checked="" type="checkbox"/> 2.49259	1/year
Initial tangent effective decline rate	91.7305	%/Year
Initial secant effective decline rate	91.7305	%/Year
b exponent	<input checked="" type="checkbox"/> 0.00000	
Exponential decline		
<input checked="" type="checkbox"/>	1.97770	1/year
Decline hyperbolic limit rate	86.1612	%/Year
Decline exponential limit rate	86.1612	%/Year
Exponential decline start time	2.05216E+304	Year
Hyperbolic Segment 3		
Segment type	Arps	
Maintain initial rate with previous segment	<input type="checkbox"/>	
Tmin	52.8673	day

Fig. 1.D.31 – Parameter input table for Segmented model

### 1.D.9 Conclusions

DCA is a fast, sometimes efficient, yet empirical way to forecast production into the future under certain assumptions. All of the equations may produce good matches across the entire production and a EUR value can be estimated associated with each model. However, Fig. 29 presents an example where all decline curve relations (previously described) match the entire production data and differences are observed at late times due to specific model behaviour.

As mentioned earlier, none of these relations have a direct link to reservoir engineering theory other than analogy. At this point one must assume that each of these models can be considered as empirical in nature and generally center on a particular flow regime and/or characteristic data behaviour. A useful way to apply decline curve analysis is to apply all equations in tandem to obtain a range of outcomes rather than a single EUR value. This range of outcomes may be associated with the uncertainty related to the production forecast and can be evaluated as a function of time.

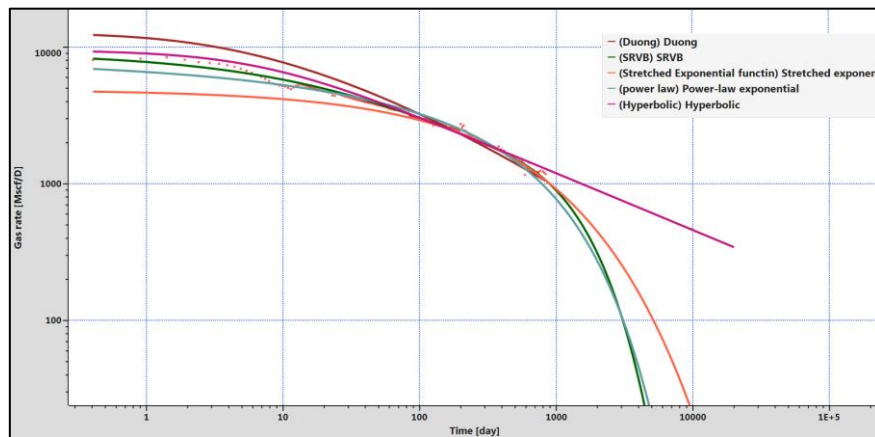


Fig. 1.D.32 – Rate and time plot (match with all models).

It is very optimistic to suggest that decline curve relations may approximate to, or match, model-based (time-pressure-rate) analysis profiles. These relations cannot capture all elements of the complexity of fluid flow behaviour in unconventional reservoirs modelled by reservoir solutions (analytically or numerically). However, the average trend can be used to approximate the behavior. Certain flow regimes can also be approximated by simpler models such as the power-law flow regime can be approximated with a constant  $b$  value in the hyperbolic model. Along these lines decline curve relations may also be used as proxies to represent model-based analysis (i.e. time-rate-pressure analysis) forecasts in economic software.

## 1.E Rate Transient Analysis (RTA) for unconventional plays

### 1.E.1 Linear flow diagnostics

The production behaviour for a fractured horizontal well exhibits the formation linear flow regime at early times, similar to the case for a single fracture. The analysis data obtained during this period gives us an estimate of the permeability-fracture half-length squared product ( $kX_{mf}^2$ ), where  $X_{mf}$  is the aggregated length of the different fractures. For the case of a simple model with  $N_f$  fractures of equal half-length  $X_f$ , the value of  $X_{mf}$  will be  $N_f X_f$ .

For oil, in the case of a constant rate, we have:

$$\frac{p_i - p_{wf}}{q_{sc}} = \frac{4.06B}{h} \sqrt{\frac{\mu}{\phi c_t k X_{mf}^2}} \sqrt{t}$$

$$p_D = \sqrt{\pi t D_{xf}}$$

$$t_{Dxf} = 0.0002637 \frac{k}{\phi \mu c_t x_f^2} t \quad (t \text{ in days})$$

$$p_D = \frac{1}{141.2} \frac{kh}{qB\mu} (p_i - p_{wf})$$

$$\frac{1}{141.2} \frac{kh}{qB\mu} (p_i - p_{wf}) = \sqrt{\pi 0.0002637 \frac{k}{\phi \mu c_t x_f^2} t}$$

$$(p_i - p_{wf}) = \frac{qB\mu}{kh} 141.2 \sqrt{\pi 0.0002637 \frac{k}{\phi \mu c_t x_f^2} t}$$

$$\frac{(p_i - p_{wf})}{q} = (141.2 \sqrt{\pi 0.0002637}) \frac{B}{h} \sqrt{\frac{\mu^2}{k^2} \frac{k}{\phi \mu c_t x_f^2} t} = 4.0641 \frac{B}{h} \sqrt{\frac{\mu}{\phi c_t k x_f^2}} \sqrt{t}$$

For gas we will have:

$$\frac{[m(p_i) - m(p_{wf})]}{q_{sc}} = 1447.8 \frac{Tp_{sc}}{hT_{sc}} \sqrt{\frac{1}{\pi(\phi \mu c_t)_i k X_{mf}^2}} \sqrt{t}$$

### Square-Root Time Plot

This relation is characterized by a linear trend on a square root plot of  $\Delta p/q_{sc}$  (for oil) or  $\Delta m/q_{sc}$  (for gas) versus  $\sqrt{t}$ . We can utilize the slope of this line ( $\alpha$ ) to estimate the  $kX_{mf}^2$  product.

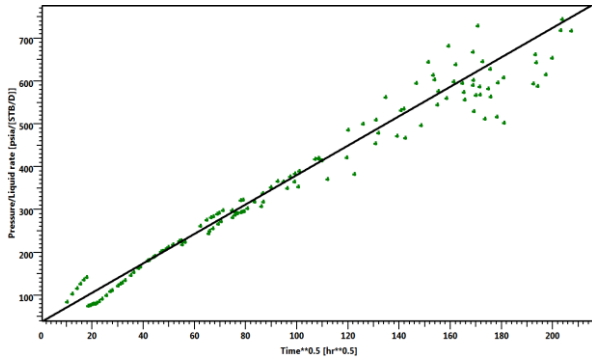


Fig. 1.E.1 – Square root plot for an oil case

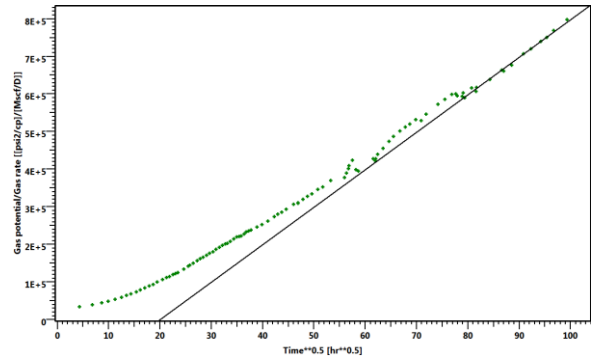


Fig. 1.E.2 – Square root plot for a gas case

For oil the slope is given by

$$\alpha = \frac{4.06 B}{X_{mf} h} \sqrt{\frac{\mu}{k \phi c_t}}$$

The permeability-fracture half-length squared product ( $kX_{mf}^2$ ) can be calculated from:

$$kX_{mf}^2 = \left( \frac{4.06 B}{\alpha h} \right)^2 \frac{\mu}{\phi c_t}$$

For gas the slope is given as:

$$\alpha = \frac{T p_{SC}}{h X_{mf} \sqrt{k T_{SC} \pi (\phi \mu c_t)_i}}$$

The permeability-fracture half-length squared product ( $kX_{mf}^2$ ) can be calculated from:

$$kX_{mf}^2 = \left( \frac{T p_{SC}}{\alpha h T_{SC}} \right)^2 \frac{1}{\pi (\phi \mu c_t)_i}$$

**Loglog and Blasingame plots**

The use of the half unit slope straight line on the Loglog plot provides an equivalent result. In the Topaze diagnosis plot, we have:

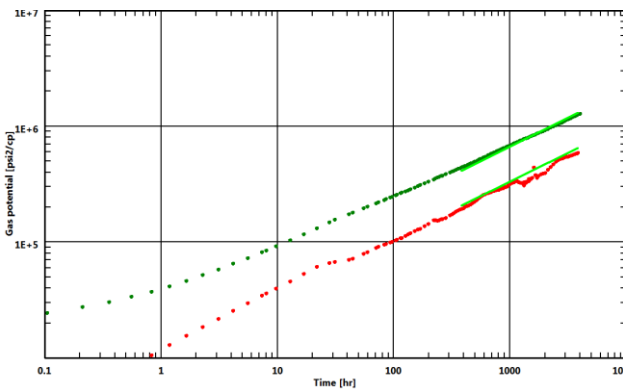


Fig. 1.E.3 – Loglog plot for production analysis

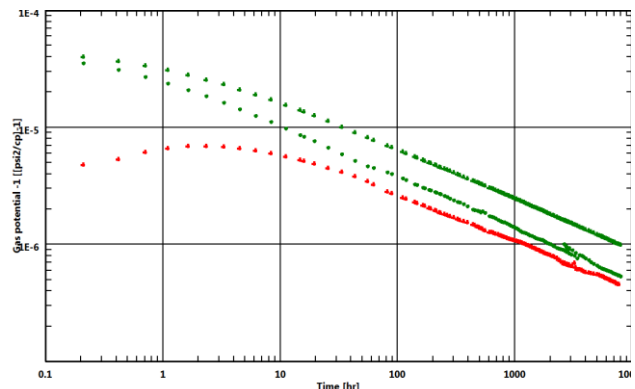


Fig. 1.E.4 – Blasingame plot for production analysis

### 1.E.2 Diagnostic of the SRV flow

The SRV flow regime is described in paragraph 10.C.3. The SRV flow regime exhibits behaviour similar to the traditional Pseudo Steady state (PSS) and the same diagnostics and analysis methods can be used. This flow regime has been called the 'Pseudo Pseudo Steady state'. The difference with conventional reservoirs is that for the unconventional reservoirs this flow does not describe the entire reservoir volume, but only from the SRV, which is thought to be the maximum practical volume for fluid production. The flow from beyond the SRV will be minor and will take from years to decades to manifest itself and will generally be ignored for any practical purpose.

In addition, the conventional Pseudo Steady state (or boundary-dominated flow) methods are only strictly valid when a distinct unit slope straight line is observed on a diagnostic Loglog or Blasingame plot.

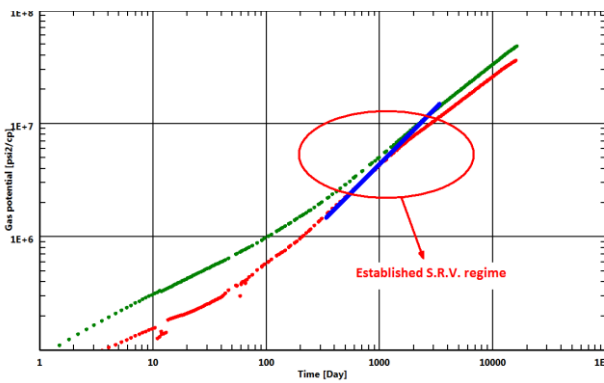


Fig. 1.E.5 – Loglog plot for production analysis

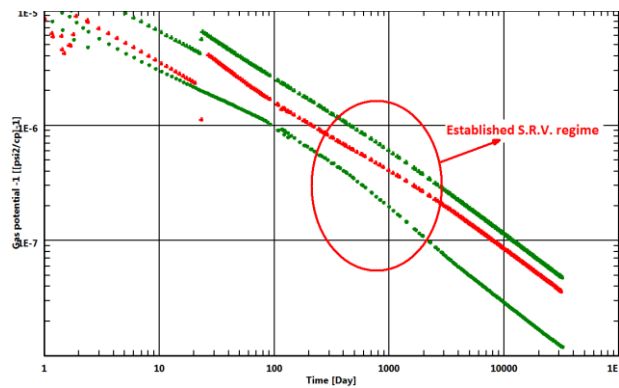


Fig. 1.E.6 – Blasingame plot for production analysis

Using the conventional PSS concepts, we can utilize a straight-line analysis on this portion of the data such that we can estimate a 'drainage area' (essentially the SRV). The governing relations are given as:

For oil, with the observation of a straight-line on a plot of  $\Delta p/q$  vs.  $t_e$ , the slope is:

$$m = 0.234 \frac{B}{\phi c_i h A}$$

For gas, with the observation of a straight-line on a plot of  $\Delta m/q_{sc}$  vs.  $t_e$ , the slope is:

$$m = 2348 \frac{TP_{sc}}{\phi c_{ii} h \mu_{gi} A T_{sc}}$$

Relating this value to the fractured region area, one can estimate the  $L X_f$  product.

In addition to plots of  $\Delta p/q$  vs.  $t_e$  (oil) and  $\Delta m/q_{sc}$  vs.  $t_e$  (gas), the material balance approach (using the Normalized Rate Cumulative plot) can also be used on the portion of the data exhibiting the SRV flow behaviour as shown in the figure below.

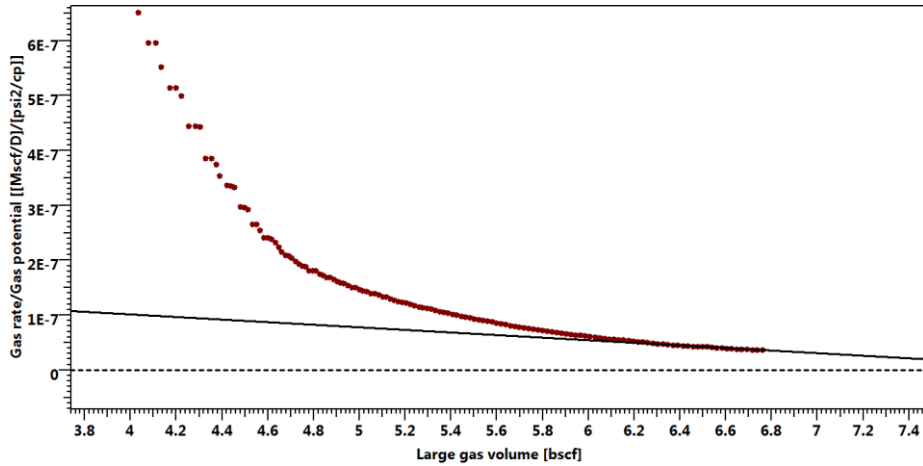


Fig. 1.E.7 – Normalized rate cumulative plot for an example gas case

### 1.E.3 Simultaneous diagnostic of several flow regimes

#### Loglog straight line diagnostics

We typically observe certain straight lines on the Loglog plot for conventional reservoirs (i.e., wellbore storage (unit slope), formation linear flow (half-slope), bilinear flow (quarter slope), and reservoir limits (unit slope)). There is also the special case of the 'zero-slope' trend which occurs for infinite-acting radial flow. The same principles apply for unconventional reservoirs, but it is unlikely that we will (ever) see certain flow regimes in the performance data for unconventional reservoirs. As guidance, we have:

- Very early time: unit slope      governed by wellbore storage (material balance)
- Bilinear flow:      1/4 slope      governed by fracture conductivity ( $k_{rf}$ )
- Linear flow:      1/2 slope      governed by  $kX_{mf}^2$
- SRV flow:      unit slope      governed by SRV drainage area (or volume)
- IARF:      zero slope      governed by  $k$  (*IARF regime is extremely unlikely in shales*)



Fig. 1.E.8 – Multiple straight lines diagnostic plot

When we consider the case of the analytical multi-fracture horizontal well model (MFHW), we have the following primary unknowns:

- The horizontal well length ( $L$ ) (this is typically treated as a 'known' or 'fixed' variable)
- The number of fractures ( $N_f$ )
- The fracture half-length ( $X_f$ )
- The fracture conductivity ( $k_f w_f$ )
- The formation permeability ( $k$ )

In most cases we can observe and analyze the linear flow and possibly the SRV flow. With them we can determine one or two of the unknowns, even assuming we know the  $L$  value.

- The Linear flow analysis provides a  $k(NX_f)^2$  value
- The SRV flow analysis provides a  $LX_f$  value
- The IARF horizontal line which should provide a permeability  $k$  value

The 'ideal' workflow should be:

- Input the well length from completion records.
- Estimate permeability ( $k$ ) using the IARF line.
- Use the permeability value in the linear flow analysis, estimate  $X_f$ .
- Using the results of the linear flow analysis, we compute the number of fractures ( $N_f$ ).

Unfortunately, in practice, the IARF is never reached for unconventional and  $k$  has to be estimated by other means, and is often found iteratively. Therefore, the 'practical' workflow is:

- Input the well length from completion records.
- Select a permeability value, maintain as constant for the given analysis cycle.
- Use the permeability value in the linear flow analysis to estimate  $X_f$ .
- Use the results of the linear flow analysis to compute the number of fractures ( $N_f$ ).
- Make sensitivity estimates on each parameter, focus on relationship of  $k$  and  $X_f$  (i.e., hold one constant and vary the other).

### **Using the linear flow to SRV model**

The transition period between Linear flow and SRV flow regime, as described in paragraph 10.C.2, represents a deviation from linear flow due to the interference of the pressure distributions between fractures. There is no simple (i.e., straight-line) model that can be used to match this transition behaviour.

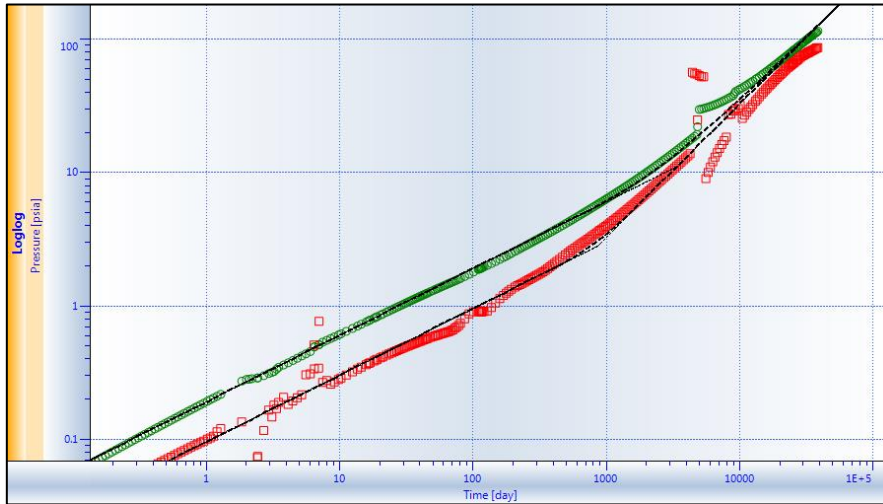


Fig. 1.E.9 – Loglog plot for production analysis (MFHW model)

### Using the trilinear flow model

Another option is to consider the 'trilinear flow model'. This is analogous to the case for a single fracture where there three linear flow components: the flow inside the fracture, the flow into the fracture, and an 'external' flow component into the linear flow 'cell'. This model has gained extensive use because it is easier and quicker to model than the multi-fracture horizontal well and because it serves as a useful 'proxy' for SRV flow in the limiting case where a boundary is assumed. Although the characterization of the flow behaviour is an 'analog' when the trilinear flow model is used, this model does provide some diagnostic capability.

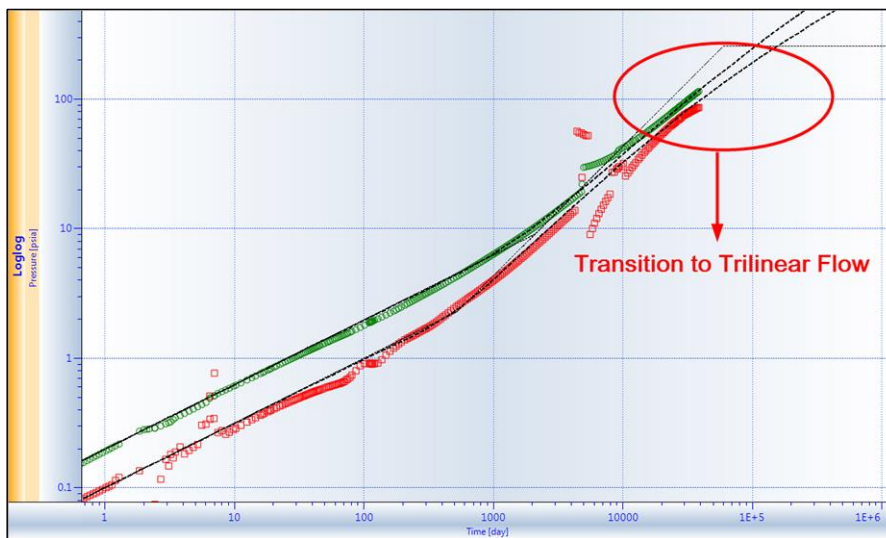


Fig. 1.E.10 – Loglog plot for production analysis (trilinear flow model)

### 1.E.4 Matching data with a model

The Loglog and Blasingame plots (see chapter 10.04.C) are designed to account for the non-constant flowing pressure and rate, generating an 'equivalent constant rate' response for comparison of data and model behaviour.

For the Blasingame plot (log-log plot) we have:

$$y = \frac{q(t)}{p_i - p_w(t)} \text{ and } y' = PI \text{ Int. Derivative} = \frac{\partial(PI_{Int})}{\partial \ln(t_e)}$$

$$x = t_{cr} = \frac{Q(t)}{q(t)} \text{ (cumulative rate equivalent time).}$$

For the Loglog plot

$$y = \frac{p_i - p_w(t)}{q(t)} \text{ and } y' = \text{derivative or integral function of } \frac{p_i - p_w(t)}{q(t)}$$

$$x = t_{cr} = \frac{Q(t)}{q(t)} \text{ (cumulative rate equivalent time).}$$

These functions can be used for diagnostic purpose and also to adjust the match of the model compared to the measured data functions on log-log scales (see before and after adjustment plots below).

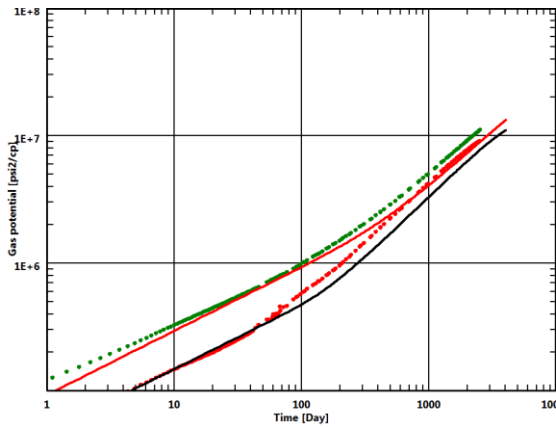


Fig. 1.E.11 – Loglog plot before adjustment.

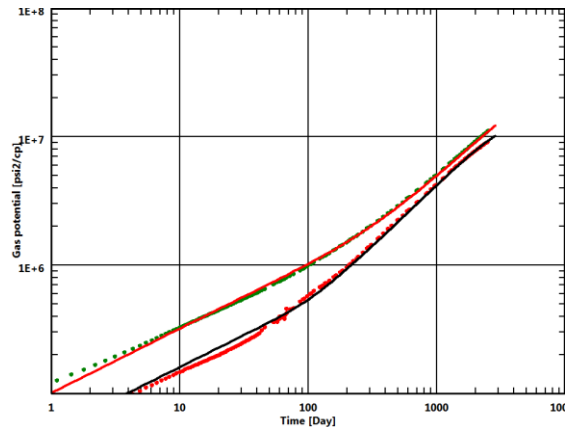


Fig. 1.E.12 – Loglog plot after adjustment.

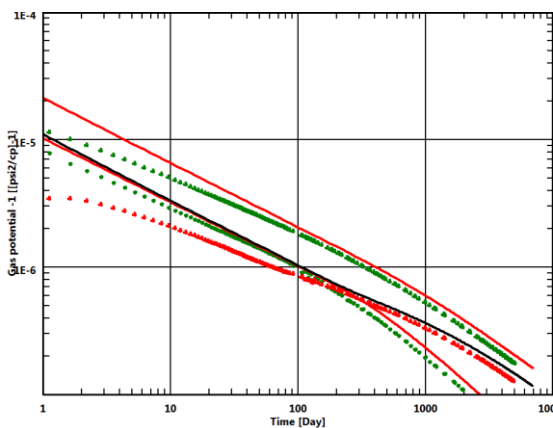


Fig. 1.E.13 – Blasingame plot before adjustment.

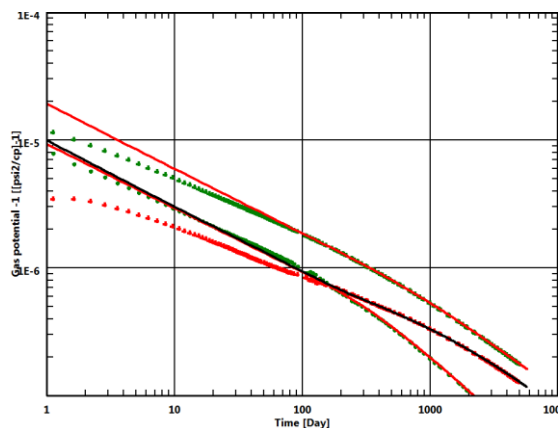


Fig. 1.E.14 – Blasingame plot after adjustment.

In the KAPPA formulation of the Loglog and Blasingame plots, the raw data functions can be compared to any model (analytical, semi-analytical, or numerical), the model parameters can be adjusted manually or using a regression model.

### 1.E.5 History matching

In addition to matching diagnostic functions for a specific flow regime, we utilize methods that permit automated and semi-automated matching of pressure and rate functions to a specified model using regressions methods. We acknowledge that the two classical plots (Loglog and Blasingame) are extremely well-suited for diagnostic purposes, but are less useful for matching time or pressure dependent parameters (i.e., quasi-linear and non-linear models).

In addition to the Loglog and Blasingame diagnostic plots, the history plots (q vs. t and P. vs t) are very convenient for observing the quality of a given model match. The 'history' plots shown below are perhaps the most effective presentation of model and data matches.

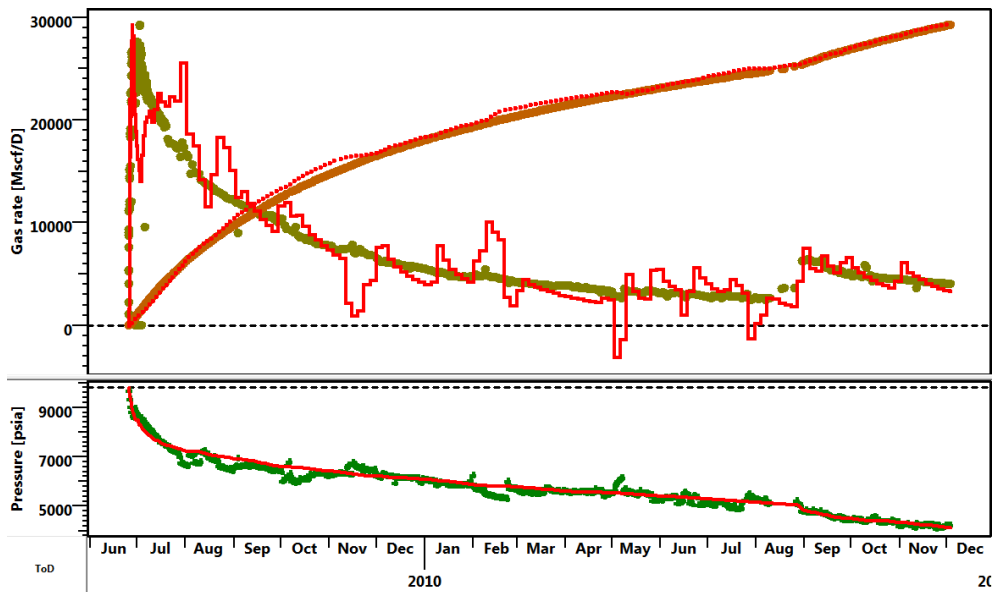


Fig. 1.E.15 – History plot for production analysis (rate, cumulative, and pressure vs. time).

Another valuable aspect of the 'history' plot is that changes in well behaviour as a function of time are more clearly visible than on the diagnostic plots. In the case shown below, a variable flowing condition can be observed (most likely a choke change, which is often seen in the surface pressures record). In such cases where a pressure-rate mismatch occurs, a time-dependent skin factor can be used to represent the changing well condition.

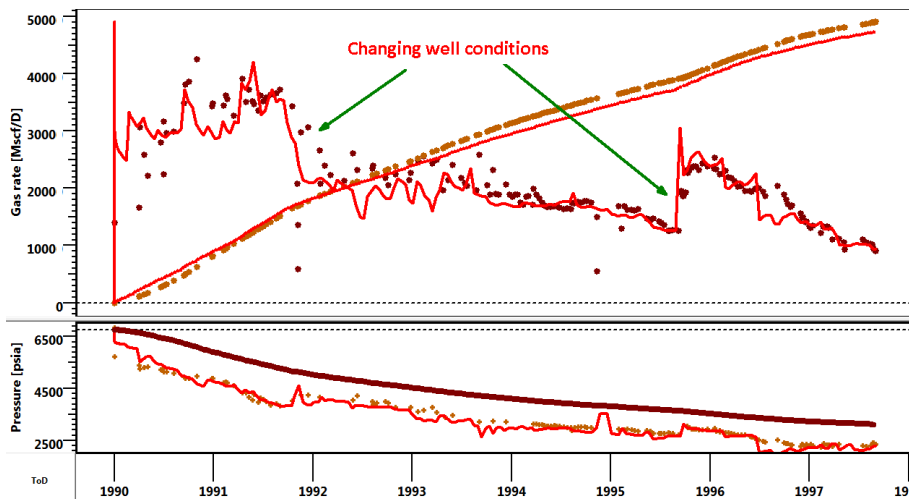


Fig. 1.E.16 – History matching with changing well conditions (analytical model).

The analytical models in Topaze include the detailed multi-fractured horizontal well (MFHW), but these analytical models are limited to the linear, liquid single phase, case. For the gas case, the pseudopressure function is used to compensate for non-linearities associated with pressure-dependent gas properties (i.e.,  $Z$ ,  $\mu_g$ ,  $C_g$ ).

The numerical model implicitly allows essentially any non-linear condition such as:

- Non-Darcy flow,
- Pressure dependent permeability and porosity,
- Multiphase flow,
- Desorption,
- Compositional fluid behaviour, and
- Combinations of these effects.

These parameters and functions can be adjusted using regression. As seen in the example below, the dew point effect (condensate drop-out) has a dramatic influence on the production character.

Typically, the analytical model is used to address diagnostic features and the numerical model is used to account for the time-dependent production effects.

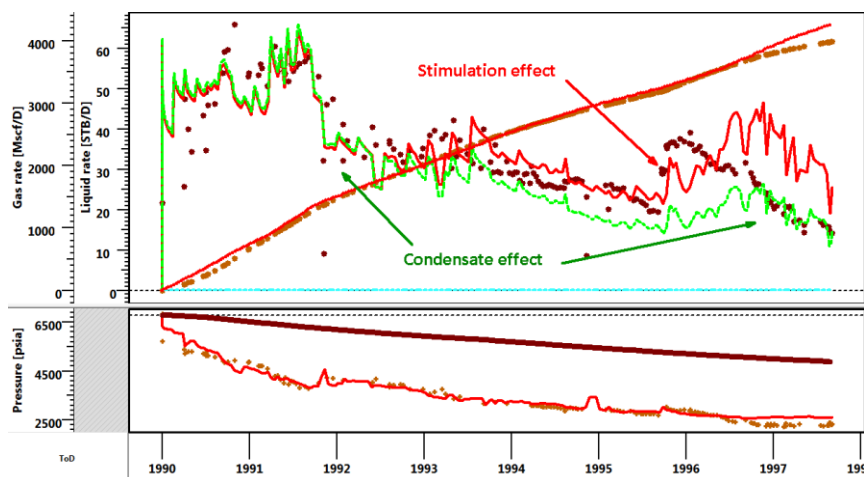


Fig. 1.E.17 – History matching with changing well conditions (numerical model).

In addition, history matching with a numerical model allows multi-well models which take into account interference from the well(s) in the immediate vicinity. The 'unconsolidated formation' option (i.e., pressure-dependent porosity and permeability) allows the user to differentiate between cases with and without the influence of pressure-dependent properties. The example below clearly indicates the need to include pressure-dependent effects.

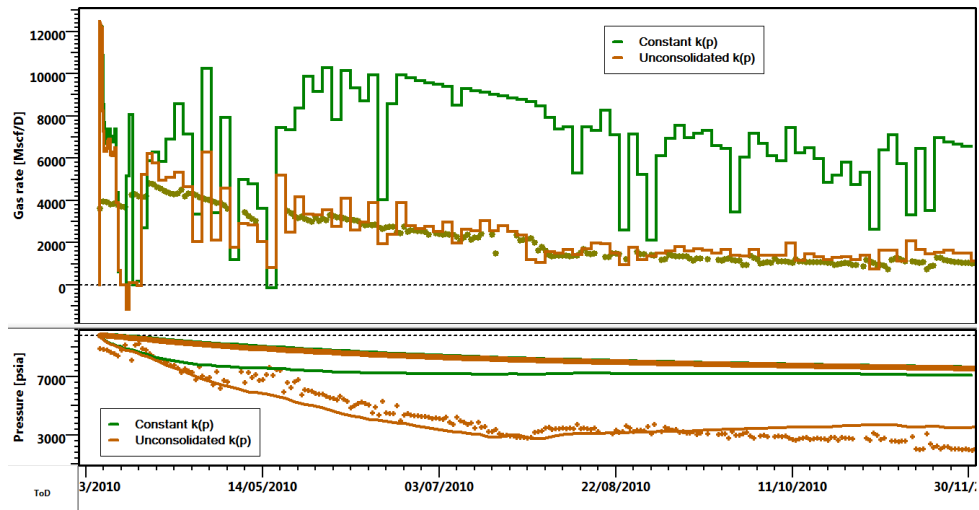


Fig. 1.E.18 – History matching – numerical model with  $k(p)$ .

### 1.E.6 Production forecasting and EUR

Once an analytical or numerical model is tuned to a historical data set, this model can then be used to forecast long-term performance and estimate hydrocarbon recovery. Such forecasts are only reliable in the case where the producing conditions remain constant. The practical approach is to establish a history match then extrapolate rate performance assuming a constant pressure or a prescribed pressure decline profile. There exists some subjectivity in this approach, but model-based forecasts are still the most robust and reliable.

An example of production extrapolation is shown in the figure below, note that the pressure forecast is set to a constant value.

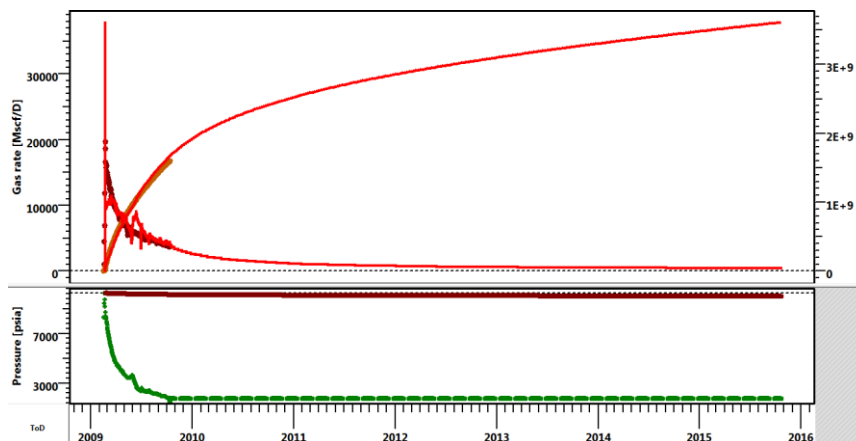


Fig. 1.E.19 – Performance extrapolation (extrapolated constant pressure profile).

Using a specified abandonment rate (or economic limit rate), the estimated ultimate recovery (EUR) can be established.

### 1.E.7 EUR statistics

In the the Rate Transient Analysis Topaze application there are two different modes for production forecasting: the 'standard' approach of imposing a rate or a pressure schedule (as described above), or the 'EUR mode'. In the latter, the simulation is run until a termination criteria is met (e.g., an abandonment rate, a maximum production time, or even limiting pressure).

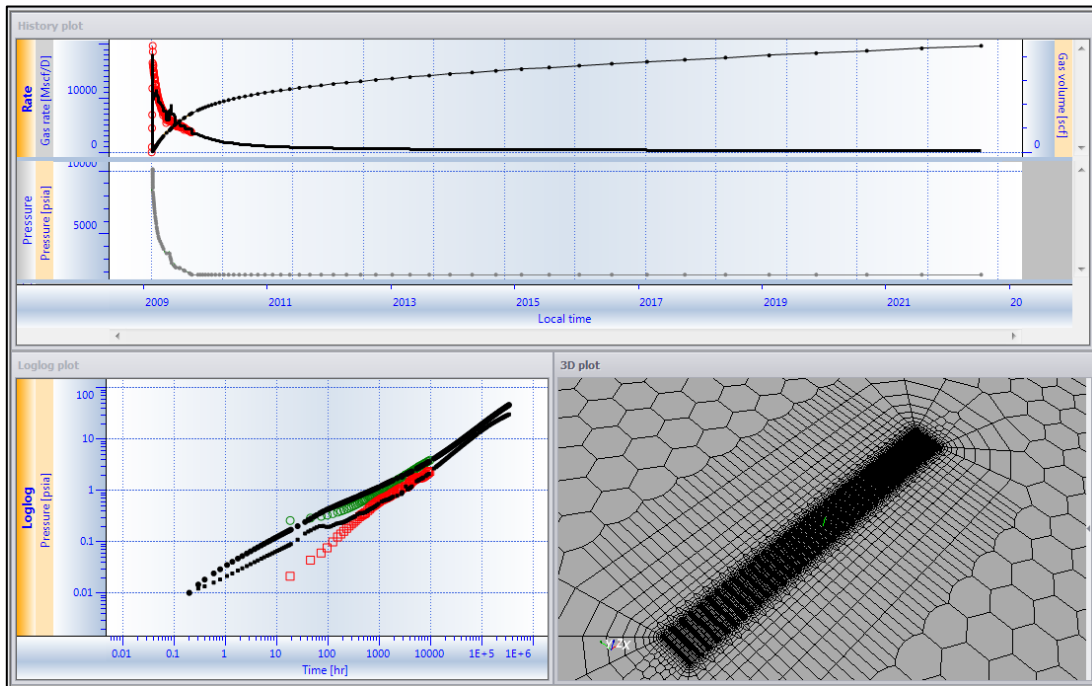


Fig. 1.E.20 – History match and performance extrapolation using a numerical model.

In our matching process we recognize the non-uniqueness of our parameter estimates, in particular the formation permeability, the fracture half-length, and on occasion, the fracture conductivity. These parameters are interdependent due to the ultra-low permeability nature of the formation and the strong influence of early-time flow regimes, in particular, linear flow. The most uncertain of these variables is formation permeability. But we accept this because, at least at present, there are no explicit model which can 'uncouple' the influence of early-time linear flow. One approach that is being used at present is to consider the effect of the distribution of various reservoir properties on the production forecasts and EUR predictions.

In the KW Rate Transient Analysis application, Monte Carlo simulation is run to randomly select parameter values from their probability distributions (most often these are permeability and fracture half-lengths) and then generate production forecasts and EUR predictions with the specified reservoir model. For reference, there are several different distribution profiles that can be used, and the user is able to select one they believe best represents a given parameter.

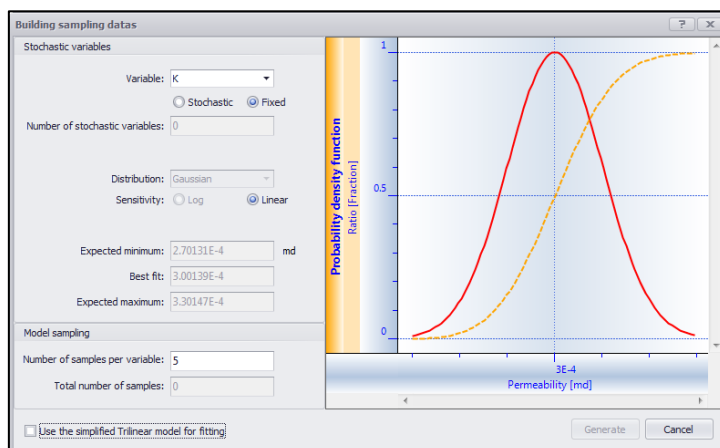


Fig. 1.E.21 – Permeability distribution plot.

As an example, we consider a case where permeability is being statistically sampled. The user specifies an appropriate number of samples, the model is generated for each permeability sample and a nonlinear regression is conducted on  $X_f$  and  $N$  to adjust the model for each permeability value and then a forecast is made to obtain the corresponding EUR values. The individual history matches and extrapolations are shown in the figure below.

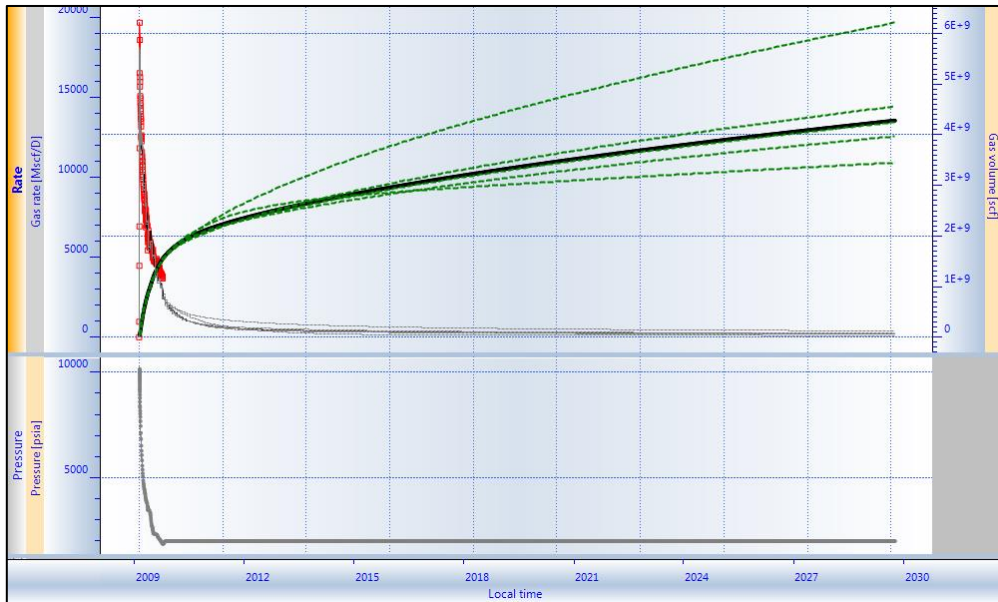


Fig. 1.E.22 – Multiple forecast plot.

Using these production extrapolations, the corresponding EUR values are then estimated based on the termination criteria specified by the user. The result is a probability distribution for the EUR and P10, P50 and P90 values can be estimated.

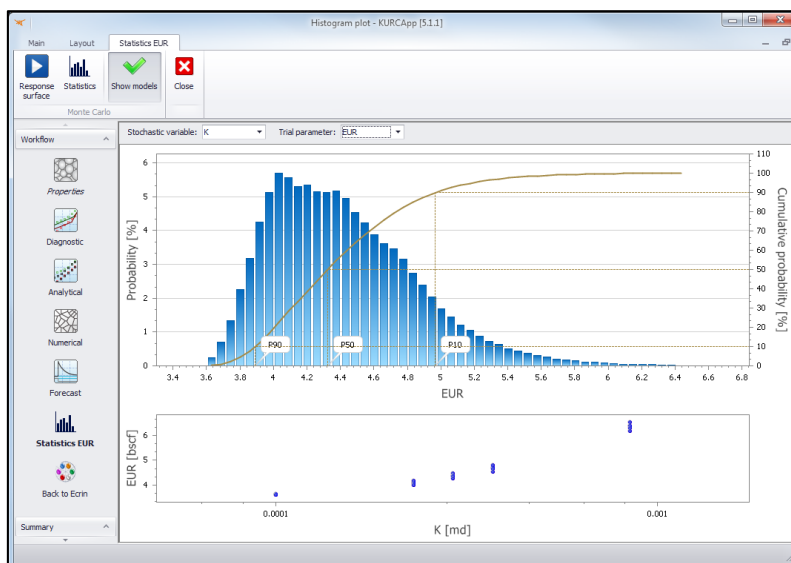


Fig. 1.E.23 – P10, P50 and P90 probability plot for EUR (as a function of permeability)

## 1.F Simple models

In this section we review the three most fundamental models that are used to represent the standard well design for unconventional reservoirs; the multi-fractured horizontal well (MFHW) case. These models can reproduce the flow regimes and rate and pressure performance as previously described in paragraph C. In the current versions of KAPPA software these models are available as either analytical or numerical models and are fully supported with a variety of options for either case.

These 'simple' models share the following assumptions:

- Reservoir:
  - The reservoir is homogeneous.
  - The traditional Darcy's law applies.
- Fractures:
  - There are  $N_f$  fully penetrating fractures and they;
    - are orthogonal to the horizontal well.
    - are evenly distributed along the horizontal well.
    - intersect the horizontal well at their mid-point.
    - all have the same half-length  $X_f$
    - all have the same fracture conductivity.

The models differ in terms of the boundary conditions and configurations.

### 1.F.1 'Classic' Multi-Fractured Horizontal Well (MFHW)

We assume the reservoir to be of infinite extent (analytical), or at least large enough for boundaries to be never seen during the producing life of the well (numerical). This classical model can also be combined with traditional simple boundary geometries such as a rectangle. This specific model was introduced in Topaze and Saphir more than ten years ago and was initially an 'external' analytical model. It was later fully integrated analytically and numerically as an 'internal' model.

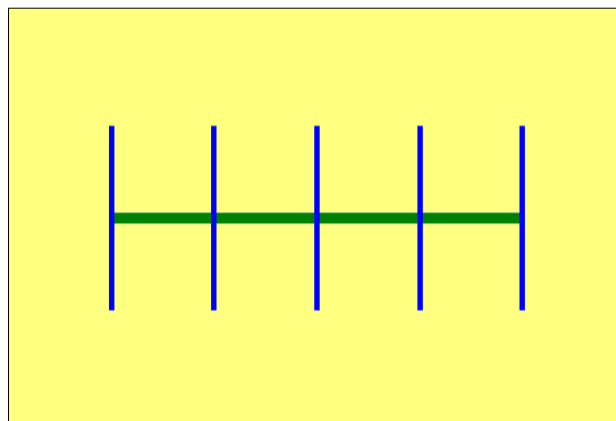


*Fig. 1.F.1 – Schematic of the classic Multi-Fractured Horizontal Well (MFHW).*

#### Analytical model

The typical behaviour of this model for an infinite reservoir is shown on the Loglog plot and a Blasingame plot below. One can observe the early-time (formation) linear flow, transition, and an SRV flow regime (also known as 'Pseudo Pseudo Steady state'), which, at unreasonably long times (years to decades depending on permeability) tends towards a hypothetical Infinite

Acting Radial Flow (IARF) regime. This model, as with all analytical models in the KAPPA software suite, can be used for gas cases using pseudopressure and pseudotime functions.

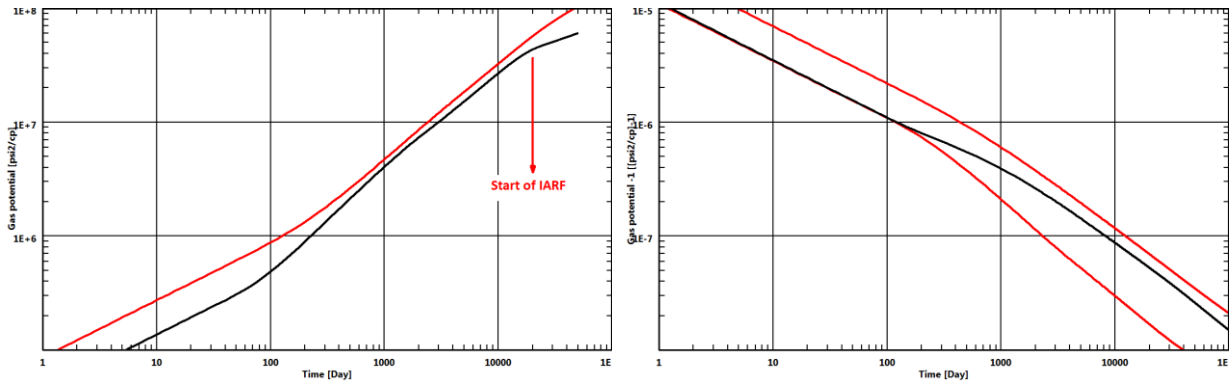


Fig. 1.F.2 – Classic MFHW – Loglog and Blasingame plots (analytical model).

**Numerical model**

The gridding used in the numerical version of this model is shown in the figure below. In each cell the system formally accounts for PVT (real gas compressibility, complex phase behaviour, etc.), pressure-dependent permeability and porosity, gas desorption, and complex diffusion if required (Forchheimer, Klinkenberg effect, Fickian diffusion, etc.).

In most situations, the horizontal well (i.e., the drain) is isolated and production is only coming from the fractures. If the fractures are fully penetrating the flow will be horizontal and this will be essentially a 2D problem, which is solved relatively fast. However, if we want to consider convergence of the flow towards the horizontal drain (which should be minimal), or if the fractures only partially penetrate the formation, this yields a full 3D problem which must be addressed by a fairly complex 3D grid.

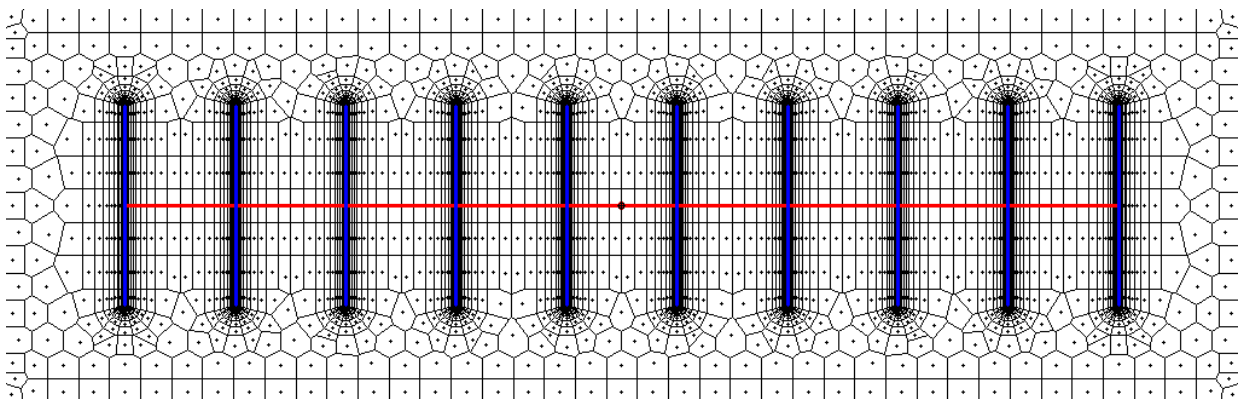


Fig. 1.F.3 – Gridding of the classic numerical model for MFHW.

Due to the high pressure gradients in the vicinity of the fractures, very fine-scale grid refinement is used to ensure that early-time pressure transients are properly represented. The size of the smallest cells connected to the fractures also depends on the fluid mobility. A large number of cells is also required when the fluid in place is a volatile oil or condensate gas, in order to accurately describe the evolution of the GOR.

### 1.F.2 SRV bounded model

The hypothesis for the SRV bounded model is that the reservoir is geometrically limited to the area defined by the series of fractures. The reservoir size along the horizontal drain is increased on each side by half of the fracture spacing to provide the same diffusion area for the fractures at the end of the well.

Because of the symmetry of the problem, each fracture has strictly the same contribution and a solution can be generated focusing on only one symmetry element corresponding to a quarter of the drainage volume of a given fracture (see below). By the use of the symmetry element, both analytical and numerical solutions are extremely fast, the speed not being dependent on the number of fractures. Once the elementary system has been simulated, the instantaneous rates are multiplied by  $4 \cdot N_F$  to get the answer of the global SRV-bounded system.

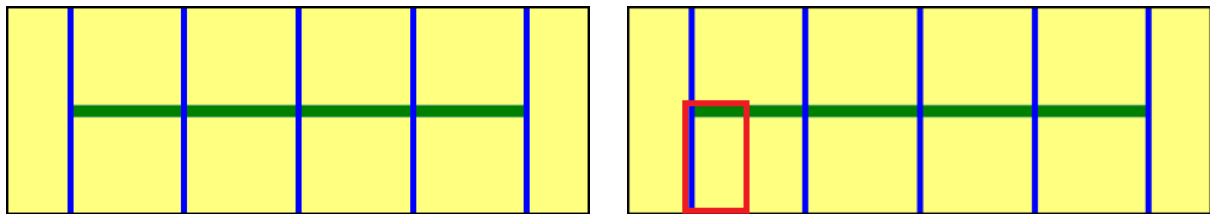


Fig. 1.F.4 – Schematic of the SRV bounded model (left), with basic symmetry element (right)

This simplistic model has been extensively used by other technical groups as their reference analytical model. It does not account for diffusion beyond the SRV, which is generally acceptable during the first years of production. Understandably, for a given well the EUR will be conservative.

### Analytical model

The typical behaviour of this model is shown below on the Loglog and Blasingame plots. As one may expect the early behaviour is linear, characterized by a half slope on the loglog plot, and after a transition the final behaviour is the SRV flow (actual Pseudo Steady state in this case), characterized by a unit slope.

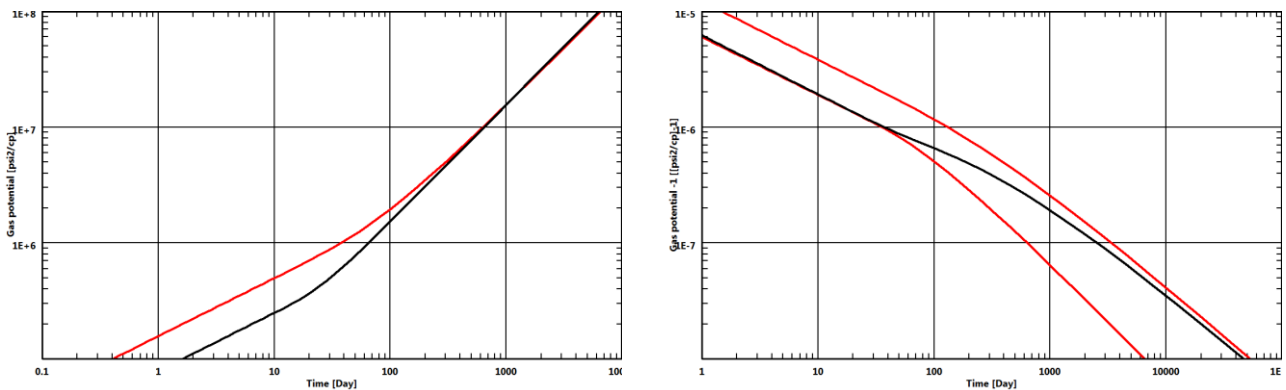


Fig. 1.F.5 – SRV model: Loglog and Blasingame plots.

The speed of the analytical model allowed us, in the KAPPA Workstation, to use it as an instantaneous, interactive ‘glorified’ straight line. A simple adjustment of the data allows a simultaneous match of the linear and the SRV flow regimes, providing instant parameters estimates.

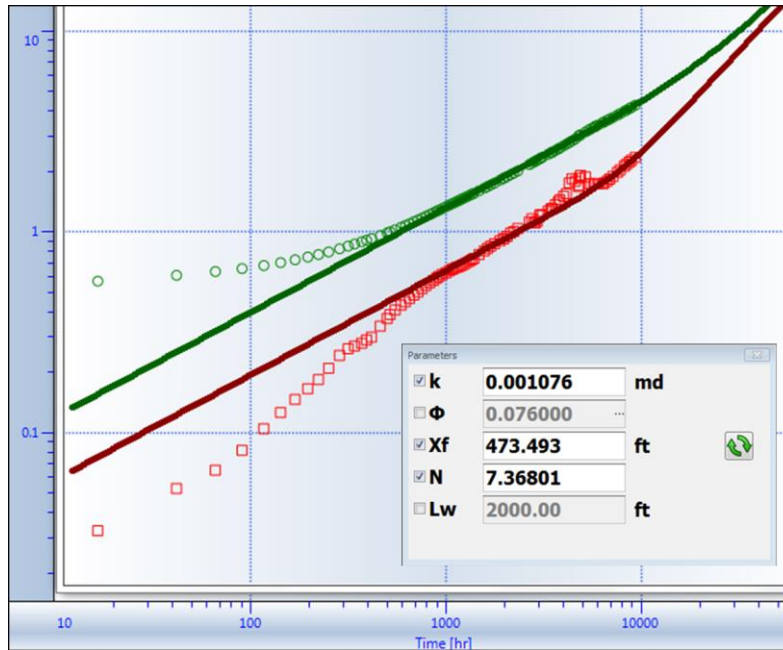


Fig. 1.F.6 – Using the SRV model as a diagnostic tool .

**Numerical model**

The SRV bounded model can be generated using the same symmetry element as for the analytical model. The result, in terms of speed, is even more spectacular. This problem is simulated by filling the symmetry element with a geometric 1-D grid (see below). As a result the numerical model is even faster than an analytical model. The behaviour is qualitatively the same as for the analytical model for the simplest diffusion cases.

This remarkable speed can be precious to test complex diffusion effects. Rather than running cases on the classic model, one can use the SRV model to assess the sensitivity of the system to complex hypotheses related to the diffusion equations, compositional PVT, stress dependence, etc. This model is even fast enough to run a nonlinear regression on the most complex diffusion hypotheses.

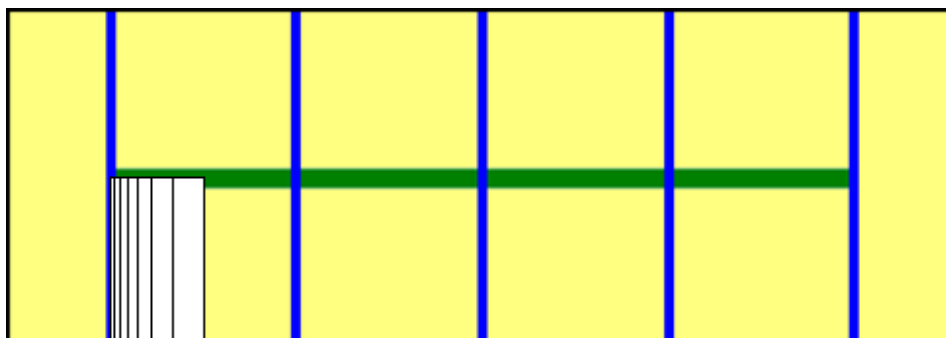


Fig. 1.F.7 – SRV Model – gridding of the symmetry element.

### 1.F.3 Trilinear model

This is an extension of the SRV-bounded model to which a linear flow was added from the outer unstimulated, reservoir matrix zone toward the inner SRV zone. Petrophysical properties (permeability, porosity, rock compressibility...) may be different in the two zones. Because of the influx from the outer zone, this model may be considered an intermediate between the SRV model and the 'classic' model.

As for the SRV model, the trilinear problem can be solved by focusing on a single symmetry element (see below) corresponding to a quarter of the drainage area of a given fracture. In both analytical and numerical cases, the speed is very high and not dependent on the number of fractures.

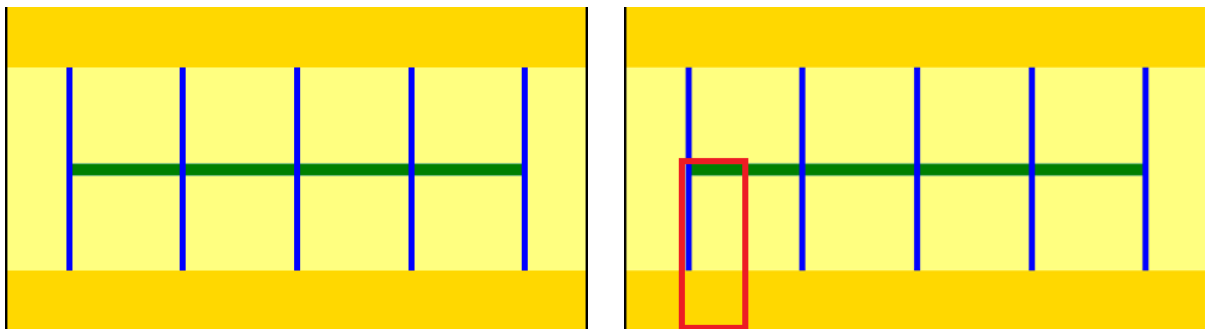


Fig. 1.F.8 – Schematic of the trilinear bounded model (left), with basic symmetry component (right).

### Analytical model

The typical behaviour of this model is shown below on the loglog plot and Blasingame plots. It starts with an initial linear flow, followed by the transition to the SRV flow, but it deviates at late times when the impact of the outer zone is felt. Because the final flow regime is the linear diffusion from the outer zone, the late time behaviour may once again exhibit a half slope on the Loglog plot. The position of this straight line depends on the well length and external reservoir permeability.

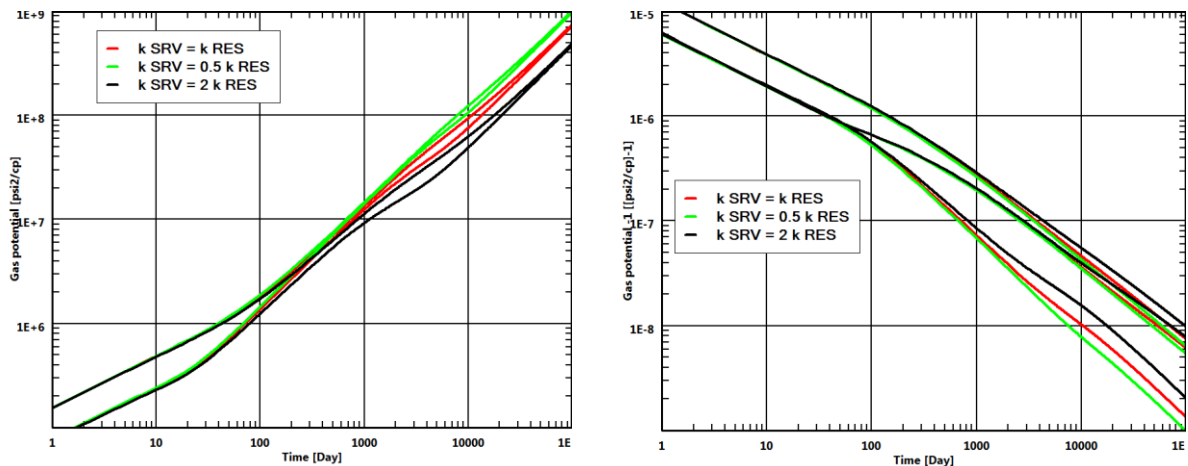
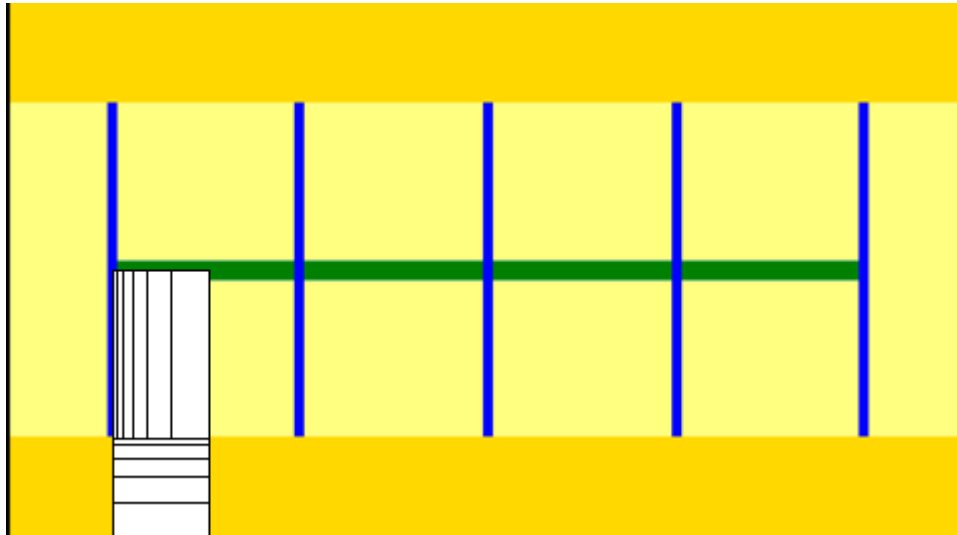


Fig. 1.F.9 – Trilinear model – Loglog and Blasingame plots.

## Numerical model

The numerical model is generated using the same symmetry element. To the 1D-grid of the SRV model, a second 1D grid is added to simulate the linear flow in the outer zone. The resulting solution is also extremely fast.



*Fig. 1.F.10 – Trilinear model – gridding of the symmetry element.*

To be totally honest, at KAPPA we are not very fond of this model, for three reasons:

- The existence of a composite zone outside the SRV is subject to discussion
- Because you have one more parameter related to the outer zone it is a flexible model that can match virtually anything. It is to RTA in unconventional plays what the radial composite model is to PTA in conventional formations. This model is too often selected for its flexibility rather than for its physical relevance.
- Because the final regime is linear we are back to the magic of  $b=2$ . It is as if this model had been designed to retroactively justify the unreasonably high values of  $b$  carelessly calculated from the initial linear flow.

As often in this case the trilinear model can have a valid usage if and only if its assumptions are validated by physical evidence, and not just the outcome of a regression process.

## 1.G Field example – Demonstration of simple models

To illustrate the basic concepts presented in the previous section we will show the summary of a study done in 2010 with the tools that were then available. We will not get into the details of the analysis and we will just scan through the main phases and main conclusions. Though some parameters are given in the next paragraph the results will not be discussed here.

This horizontal gas well had a length of around 3,900 ft, and 42 hydraulic fractures were expected to be present with an average half-length of around 300 ft. Expected permeability was in the order of  $10^{-4}$  md, water saturation of 25%, pay zone of 100 ft, temperature of 305 °F, initial pressure of 11,300 psia. Desorption data were available. The well was initially produced from casing, then production was switched to the tubing.

We were initially given 8 month of production data, with both rates and surface pressure. Water flow back was noted during the clean-up and the first hundred hours of production. A series of analyses were done using the different tools available at the time. All these tools history matched the data and forecasts were done assuming a constant final flowing pressure. The three forecasts, matching the same data, gave different forecasts and EUR.

A year later we were given 10 more months of data. We used the results of the three previous interpretations and ran a simulation, but now using the effective 10 months of pressure data. These simulations were compared to the effective 10 months of production to see how these different models behaved in this double-blind process.

### 1.G.1 First eight months of production

Rates and surface pressure were provided for the first months of data as shown on the history plot below. Pressure were available at surface and they had to be corrected to sandface.

This correction has to take into account the fact that the well was first produced through the casing, then after completion, through the tubing. The lift curves used to apply this correction correspond to the two different conditions. Extracting the production we get the loglog plot and the Blasingame plot. Both plots indicate that, after the initial water flow back that dominated for around 100 hours, the main regime during these first months was the linear flow orthogonal to the fractures.

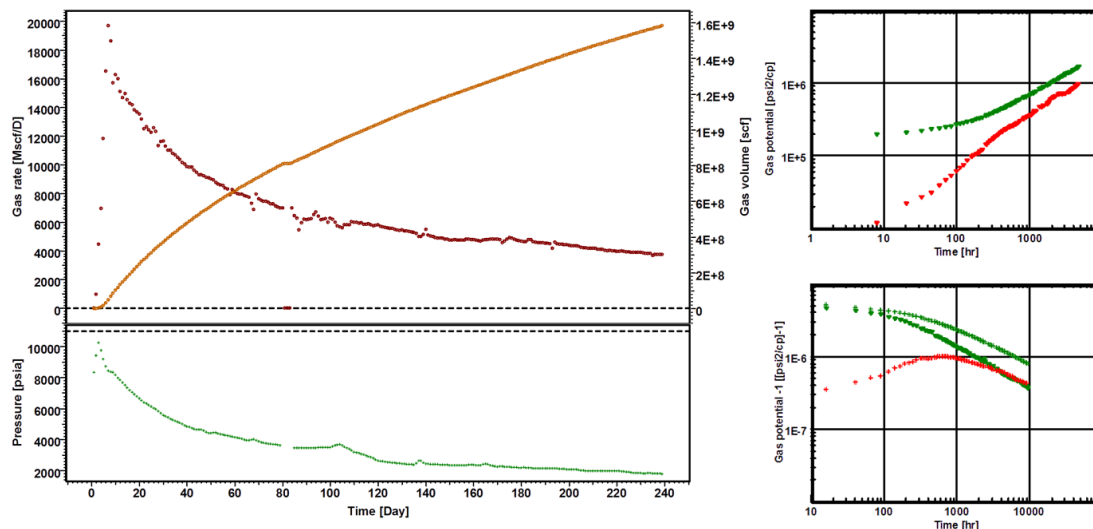


Fig. 1.G.1 – History, Loglog and Blasingame plots for 240 days of production.

### 1.G.2 Linear flow model

We started focusing on the linear flow. A square root plot would exhibit a linear behaviour during this period, allowing an early estimation of  $k \cdot (N \cdot X_f)^2$ , where  $N$  is the effective number of fractures,  $k$  is the matrix permeability and  $X_f$  the average fracture half-length.

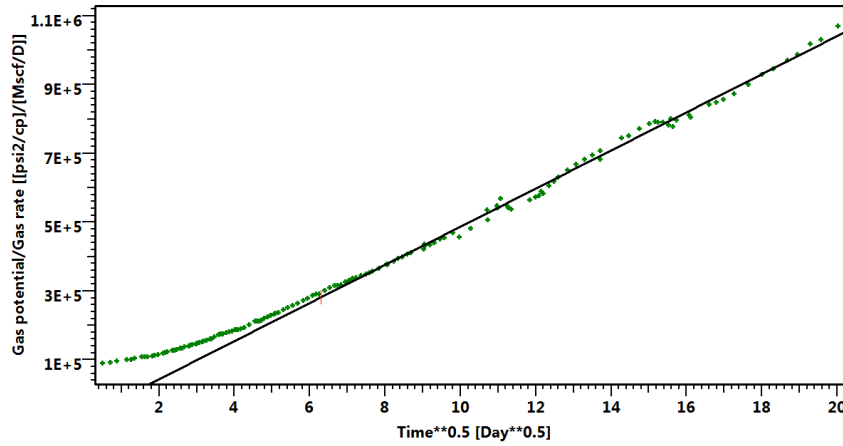


Fig. 1.G.2 – Square-root time plot.

In order to implement superposition and forecast in the model, we simulated this linear flow using the analytical model of a single infinite conductivity fracture in a homogeneous reservoir.

The indefinite linear flow from this model was ensured by setting the permeability to an arbitrarily low value. The fracture half-length was then adjusted to match the observed linear flow in the data. A nonlinear regression was then the resulting loglog match and history match are shown below. A production forecast was then calculated and is shown in the paragraph G.5.

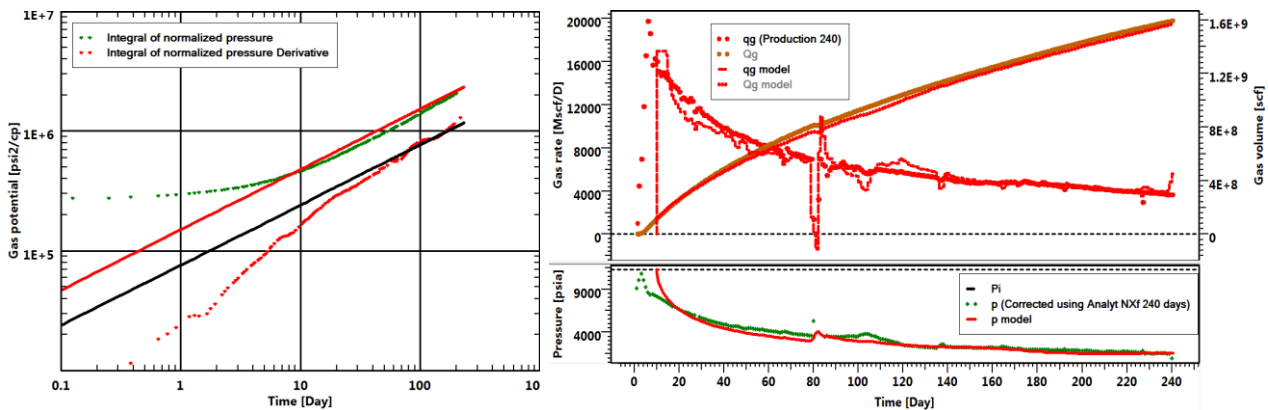


Fig. 1.G.3 – Match with a single fracture model on the Loglog and history plots.

### 1.G.3 Analytical Multi Fractures Horizontal Well (MFHW)

The analytical multi-fracture horizontal well model is described in the paragraph 1.B.3. This model has the advantage over the equivalent single fracture model of accounting for the real geometry of the system, and in particular the interference between the different fractures.

This time the permeability was set to a realistic value, as well as the number of fractures and the fracture half-length corresponding to the total length calculated above divided by the number of fractures. After nonlinear regression the loglog and history matches were calculated and shown below. Even though it was not clear on the data the model would tend to show that the interference between the fractures would start to occur after 8 months. A production forecast was then calculated and is shown in the paragraph G.5 below.

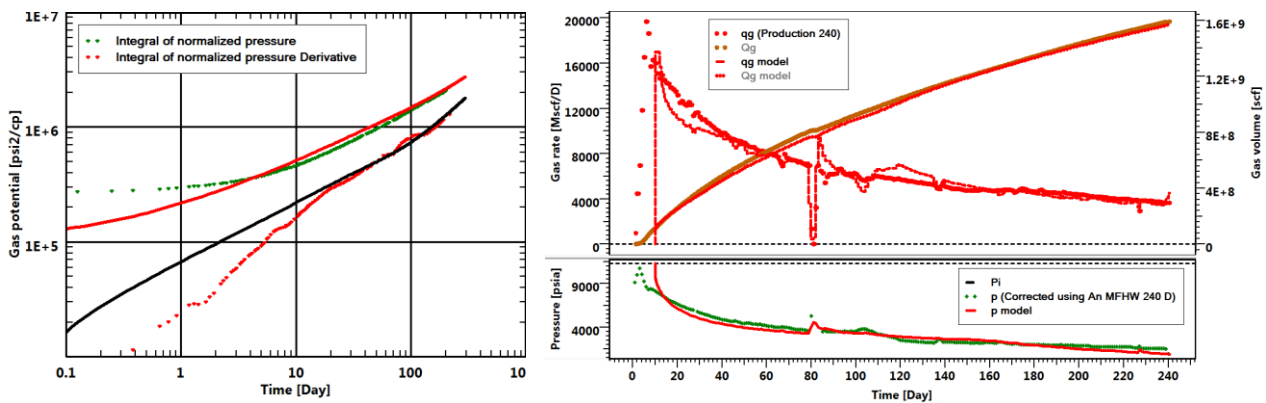


Fig. 1.G.4 – Analytical match on the Loglog and history plots.

### 1.G.4 Numerical MFHW

Again, and in a process similar to what was done with the analytical model, a numerical model was initiated and simulated. The figures below show the main grid, together with a zoom on the pressure profile around a few fractures after 1 month and 8 months. As we can see in the last representation, interference between the fractures started to be felt after 8 months.

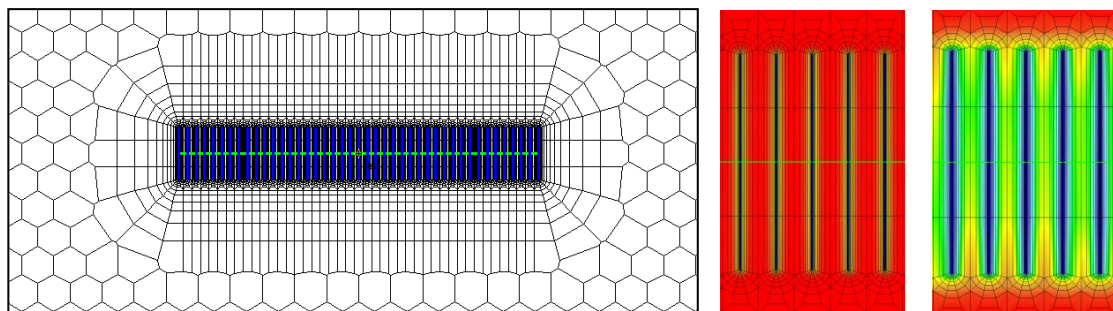


Fig. 1.G.5 – Numerical MFHW grid with a zoom on pressures after 1 month and 8 months.

The data was history matched and the resulting loglog and history plots are shown in the next page. This exercise was done with and without the integration of desorption in the model.

Note on material balance time and models: the apparent noise in the numerical model on the loglog plot comes from the material balance time function and not the model itself. In the previous section the analytical model was smooth because it was displayed as an equivalent constant pressure solution. This is not possible with numerical models. As for the other models a production forecast was then calculated, with and without the desorption effect (the paragraph G.5 below).

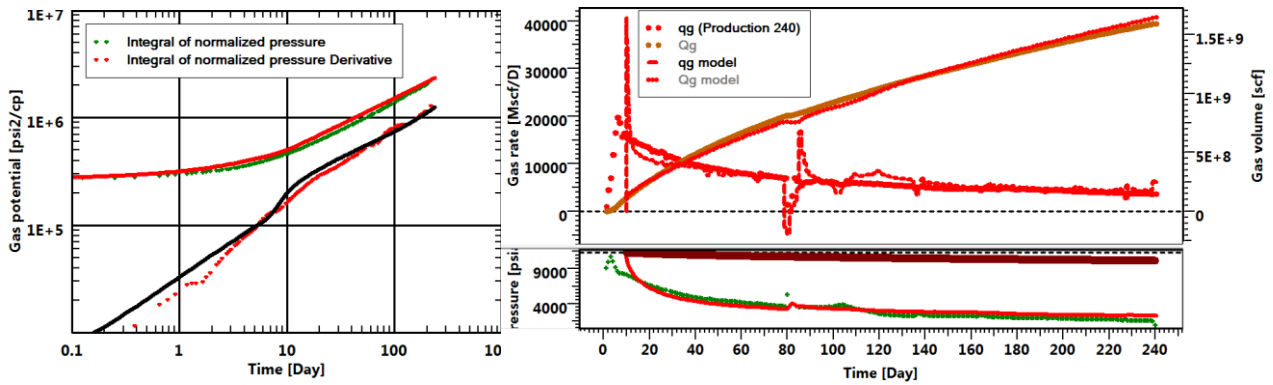


Fig. 1.G.6 – History match using the numerical model

### 1.G.5 Comparing production forecasts

The three models described above were all matching pretty well the production data, given that they were allowed to converge with different parameters. However, because the underlying assumptions are substantially different they are bound to provide very different long term production forecasts and EUR. In the plot below the linear model, the analytical model and the numerical model with and without desorption are compared with a 10-year forecast using a constant pressure taking the last flowing value.

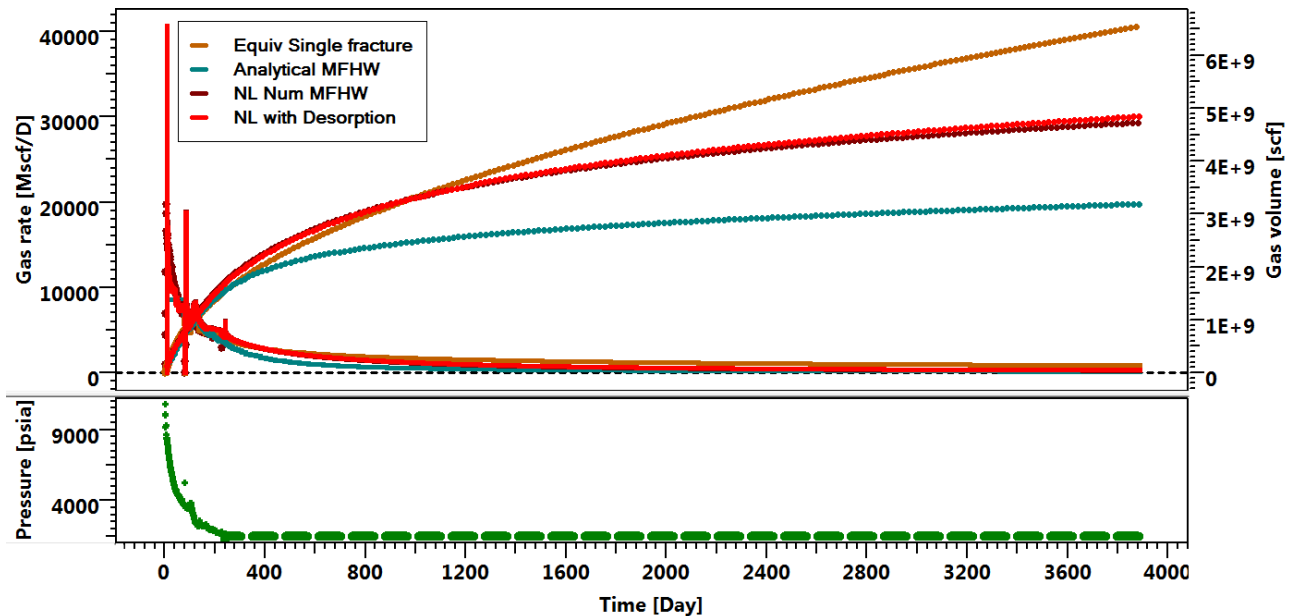


Fig. 1.G.7 – 10-year forecast – analytical and numerical (with and without desorption) models.

The equivalent single fracture model, with indefinite linear flow is definitely the most optimistic, as it does not take into account the inevitable interference between the fractures.

The analytical model is the most pessimistic. It takes into account the bad news that fractures will interfere, but it does not take into account the fact that compressibility of the fluid will improve when pressure is depleted. To be fair to this solution, at the time this study was done the pseudotime correction was not applied. With pseudotime correction the simulation would be much closer to the result of the numerical model.

The numerical model is a priori the most realistic. It takes into account all our hypotheses, if these hypotheses are correct. The numerical model with desorption is a little more optimistic as it adds the additional desorption observed after eight months. The numerical model without desorption matched the eight first months of data, hence the result of the initial desorption. So the difference between the two models is only marginal.

The loglog plot below shows the 10-year forecast of the numerical model, the pressure profile after 10 years of production is also shown.

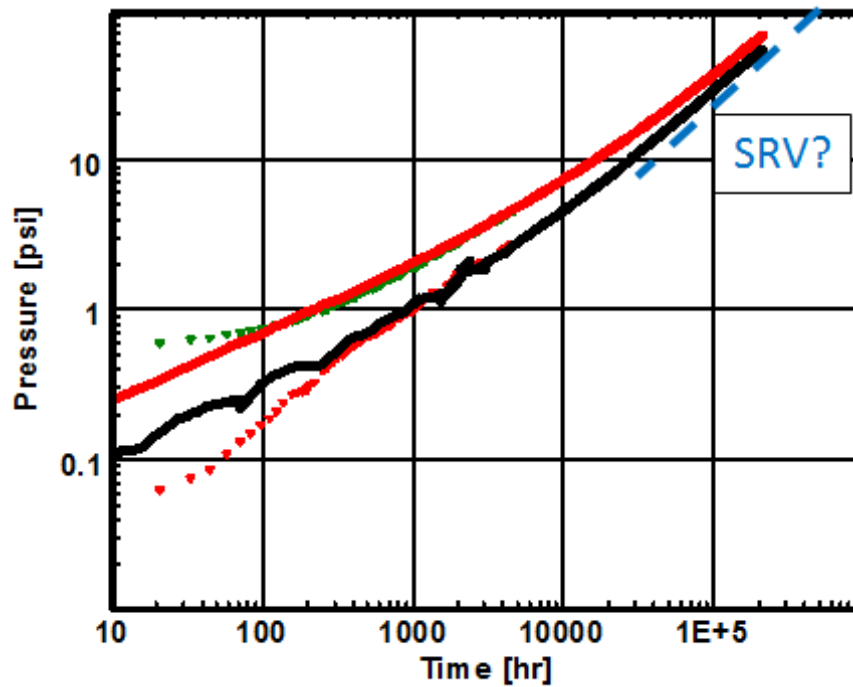


Fig. 1.G.8 – Long-term SRV flow.

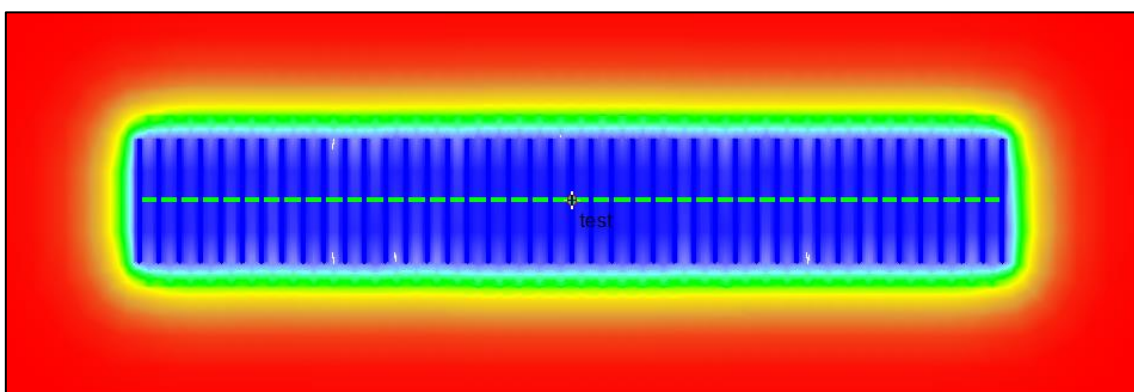


Fig. 1.G.9 – Pressure profile after 10 years of production.

### 1.G.6 Receiving ten more months of production data

One year after our initial interpretation shown in the five previous sections, we received 10 more months of data and it was the occasion to check how our initial forecast matched the observed behaviour.

The data was extracted again on a loglog plot and the three models re-generated with the same parameters. The main difference with the initial forecast of paragraph G.5 was that the real producing pressure was used instead of the constant pressure of the previous exercise.

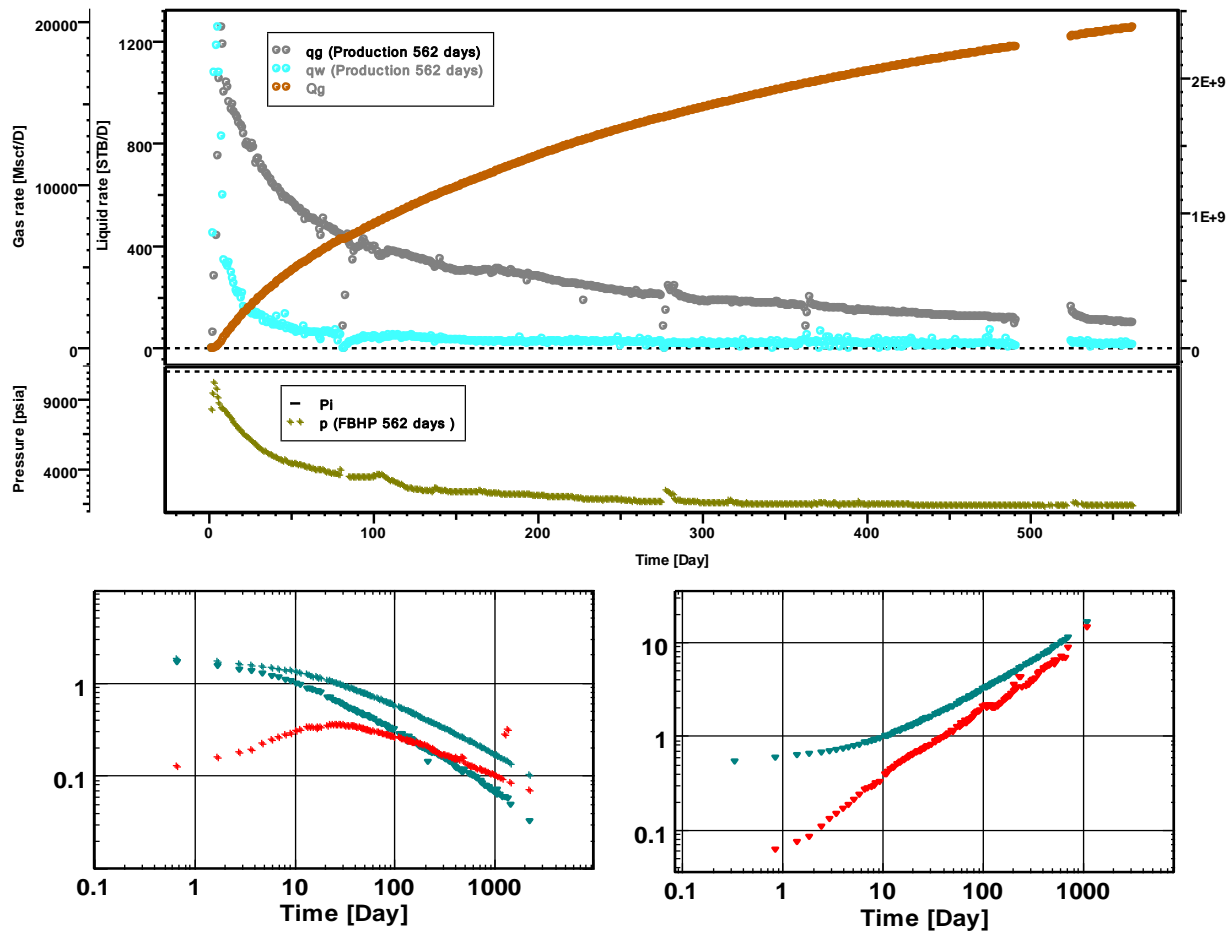


Fig. 1.G.10 – 10 more months of data on the history, Blasingame and Loglog plots.

The three loglog plots below show how the three models match the observed response:

- As expected the single fracture model stayed on its initial trend while the observed data deviates due to the interference between the fractures. The model, which corresponds to a 'b' factor remaining at 2, is naturally over-optimistic.
- As expected again the analytical model, without pseudotime correction, deviates towards SRV flow without taking into account the improvement of the permeability. It is therefore over-pessimistic;
- Finally and although the numerical model does not match the data exactly, it is pretty close.

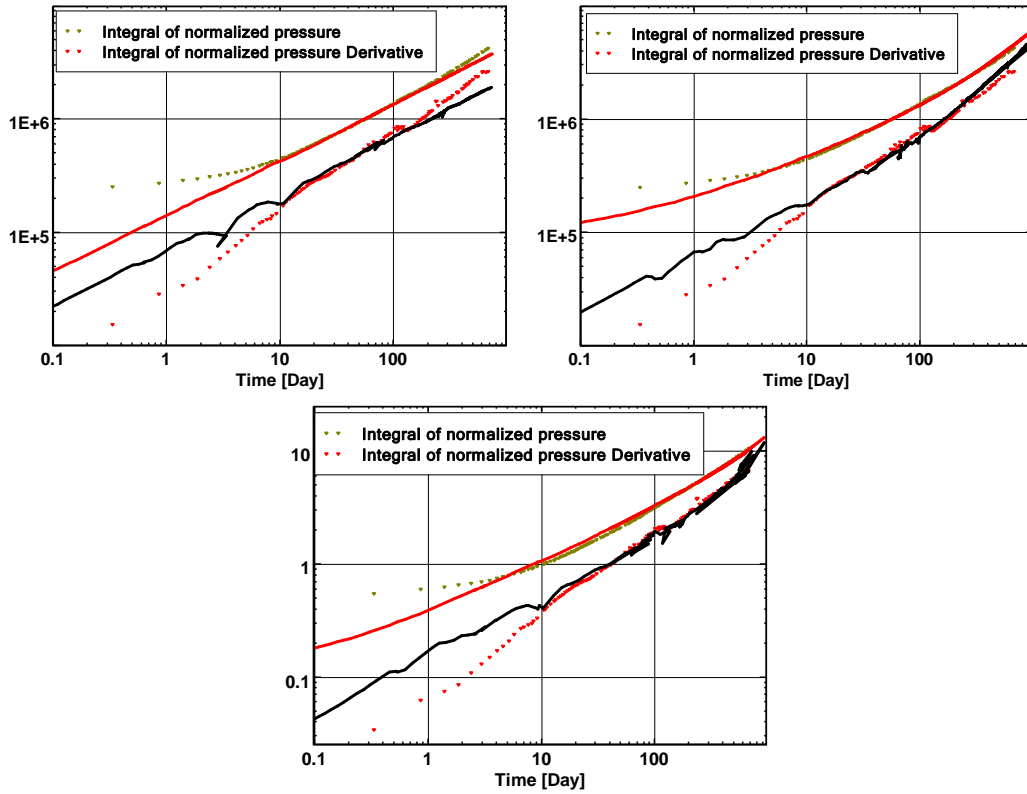


Fig. 1.G.11 – Loglog match with the linear, analytical, and numerical models.

A direct comparison is made on the history match plot, which shows how close the numerical model is to the observed behaviour.

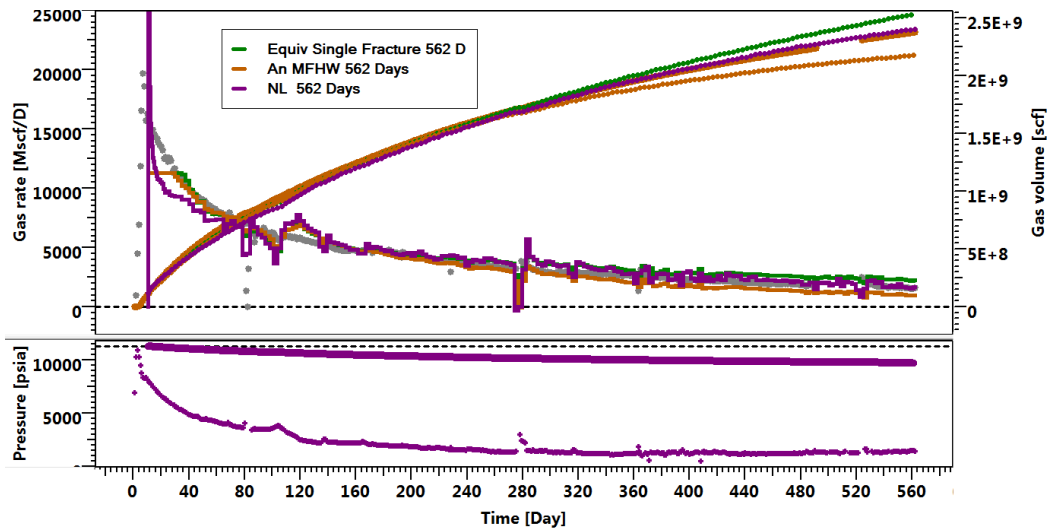


Fig. 1.G.12 – History plot with comparison of the 10-year forecasts.

## 1.G.7 Discussion

The example of this section was published in 2011. It is in no way a smoking gun proving that the numerical model used at this time is a long term solution to all our problems.

However, we can see from these examples that a relatively simple numerical model carrying the basic assumptions of diffusion and PVT can match pretty well, in some cases, the early years of responses of these wells.

Extrapolating this relatively satisfactory result to long term multiwell production would certainly be an excessive leap of faith. There are actually a lot of mitigating factors:

- Poor data: recorded pressures were at surface. It is a shame considering the cost of these wells, but this is the way the industry operates on these fields. In the absence of permanent downhole gauges, sandface pressures had to be calculated using a flow model. To add insult to injury the change of production mode from casing to tubing implied a change of model. Some truth may have gone in these cracks.
- Later operational issues: Data received on this same well, several years later, were not that brilliant. In the absence of PDG it was very difficult to exploit this data. The well head pressure data had to be corrected for depth, but the changing flowing conditions made the correction uncertain. The later forecast deviated from the initial numerical models, but data was so poor that it was nearly impossible to explain it either by the changing well conditions or by the uncertain BHP calculation.
- Other elements, such as well interference, well damage, the contribution of natural fractures, a geometric reality much more complex than these simplified models, clearly highlight the limitations of these simplistic models, even if they are already a challenge to properly model.

As a result it became clear that these simplified proxies, whether analytical or numerical, could not constitute a satisfactory answer to our long term needs. Several technical groups in the industry have been working on more sophisticated models. In the case of KAPPA the efforts were made in the framework of KURC, i.e. KAPPA Unconventional Resources Consortium.

## 1.H Advanced models

The simple models described in paragraph F assume that all hydraulic fractures share common features: same length, same conductivity, evenly spaced and orthogonal to the horizontal drain. This allows models, whether analytical or numerical, to be determined using a limited number of parameters: number of fractures, fracture half-length and conductivity. Given the poor level of data we have this is already enough to make the problem under-defined.

However, there are cases where one has other information, or sometimes the simple models just do not explain the observed behavior. In such cases you may need to simulate more complex models, probably closer to reality, but with the risk of having insufficient data to nail the problem down.

Part of the work in the KAPPA Unconventional Resources Consortium was to develop such analytical and numerical models.

### 1.H.1 Complex geometries (analytical + numerical)

The first way to refine the models is to keep the same assumptions related to global homogeneous diffusion equations, but refine the geometry of the hydraulic fractures. We want here to substantially increase the range of possible geometries, analytically if we can, numerically if we must.

So the basic model, beyond the even more simplified SRV and trilinear models described in the paragraph F, assumes a homogeneous infinite reservoir with the simplest case of fractured horizontal well. All fractures have the same length, they are centered on the well drain, orthogonal to this drain and evenly spaced. This model is available analytically and numerically in the standard KAPPA suite (Saphir, Topaze and Rubis).

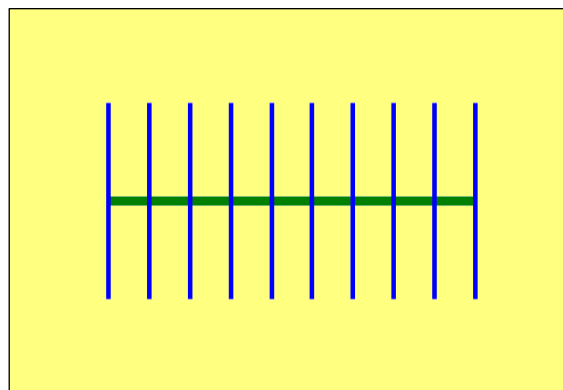


*Fig. 1.H.1 – Standard model (analytical and numerical).*

The first step towards a more complex geometry is to allow the fractures to have individual lengths and individual intersection with the well drain. They are still orthogonal to the well and their intersection is at the center of the fracture. This is shown in the next figure, right. In complement we can apply a global angle between the well and the set of fractures. This is shown in the next figure, left.

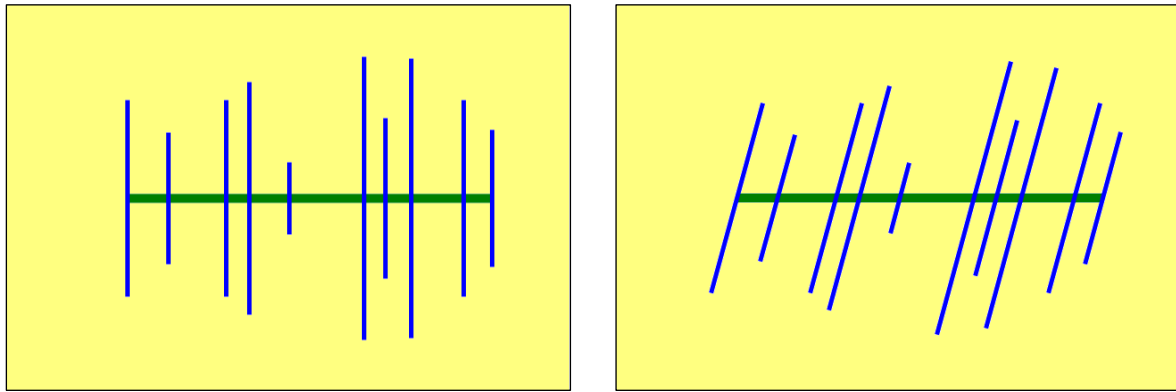


*Fig. 1.H.2 – Left: Fractures (individual lengths) + uneven spacing along the well.*

*Fig. 1.H.3 – Right: Fractures + uniform fracture angles.  
(analytical and numerical)*

Apart from rigorously accounting for nonlinearities, numerical models allow us to simulate almost any type of geometry, as long as a suitable grid can be designed. For this reason numerical models can get one step closer to reality in terms of flexibility, allowing fractures to have their own angle and an intersection with the horizontal drain that is off-centered.

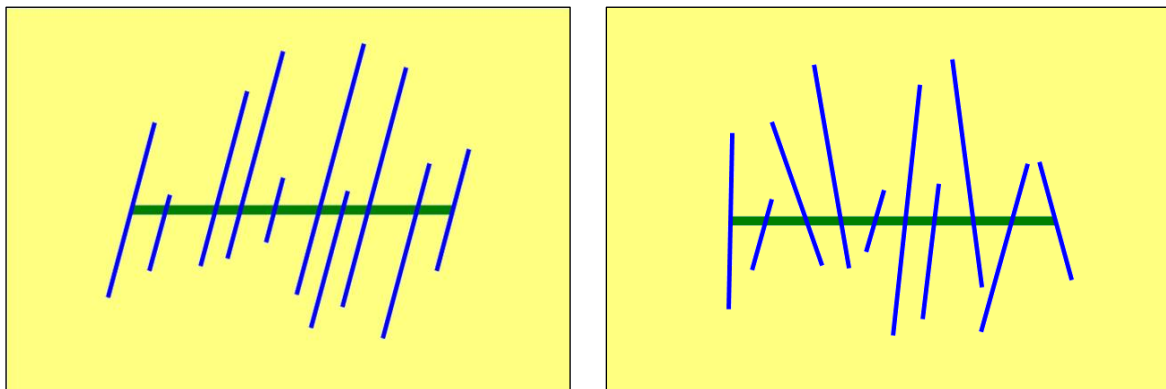


*Fig. 1.H.4 – Left: Off-center fractures (individual lengths) + uneven spacing along the well.*

*Fig. 1.H.5 – Right: Off-center fractures + arbitrary fracture angles.  
(numerical only)*

Since we are working with unstructured grids, the problem consists of rigorously constraining the grid to the direction of the fractures, while ensuring we do not lose the continuous refinements specifically made to capture transients, and without creating too much distortion.

This is a complex yet manageable task, as long as we deal with (1) planar vertical fractures (2) that do not intersect and (3) a cased wellbore. These 3 restrictions being defined, our model is fully flexible: fractures can be non-uniformly distributed along the drain, have different half-lengths and be intercepted by the drain with any (individual) angle or offset.

Fractures can also be partially penetrating, with individual penetration. In this case, a 3D grid is built around each fracture to ensure that we properly simulate the radial flow from the matrix toward the fracture plane. The drain can intercept the fractures at any depth.

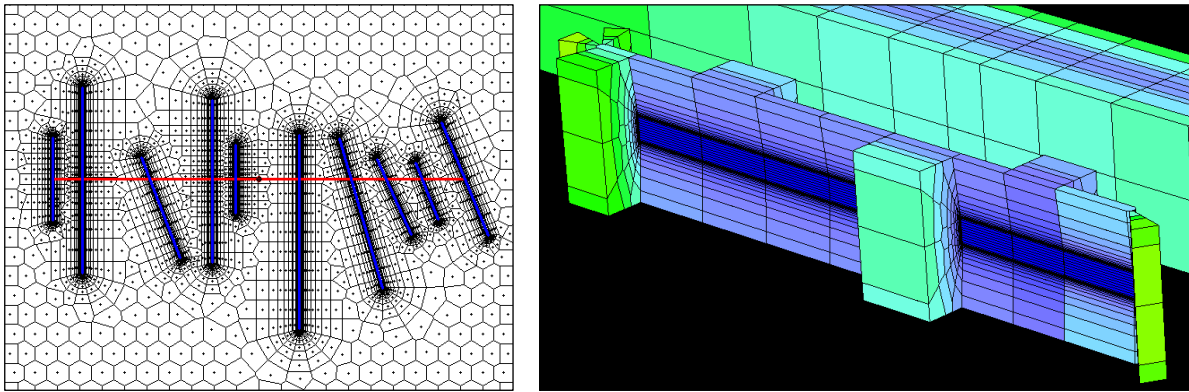


Fig. 1.H.6 – Left: previous complexity, representation of the grid pattern.

Fig. 1.H.7 – Right: 3D refinement for partially penetrating fractures (both numerical only).

The conductivity, the width and/or the porosity can be redefined for each fracture. Relative permeability curves and pressure-dependent properties ( $k/k_0$  and  $\phi/\phi_0$ ) can be different for the fractures and the matrix, but they are identical for all the fractures.

## 1.H.2 DFN models (numerical + analytical)

The next level of complexity is to challenge the assumption that we can model the reservoir response using a more or less complex diffusion equation that would be applied in a homogeneous way. The Discrete Fracture Network (DFN) model considers a network of pre-existing natural fractures that may have been stimulated, or even simply produced after the stimulation jobs. DFN can be combined with the complex hydraulic fracture geometries of the previous sections. Given the complexity of the problem and the probable stochastic nature of its definition, the numerical model is the natural way to go, though we will see at the end of this section that a first analytical pass can be run to narrow the problem.

### 1.H.2.a Numerical DFN

When various objects (e.g. hydraulic or natural fractures, boundaries...) intersect each other, the problem of constraining the Voronoi grid becomes fairly complex.

This is precisely the case when one wants to simulate the effect of the natural network of fractures by connecting the multiple fractures horizontal well model to a DFN.

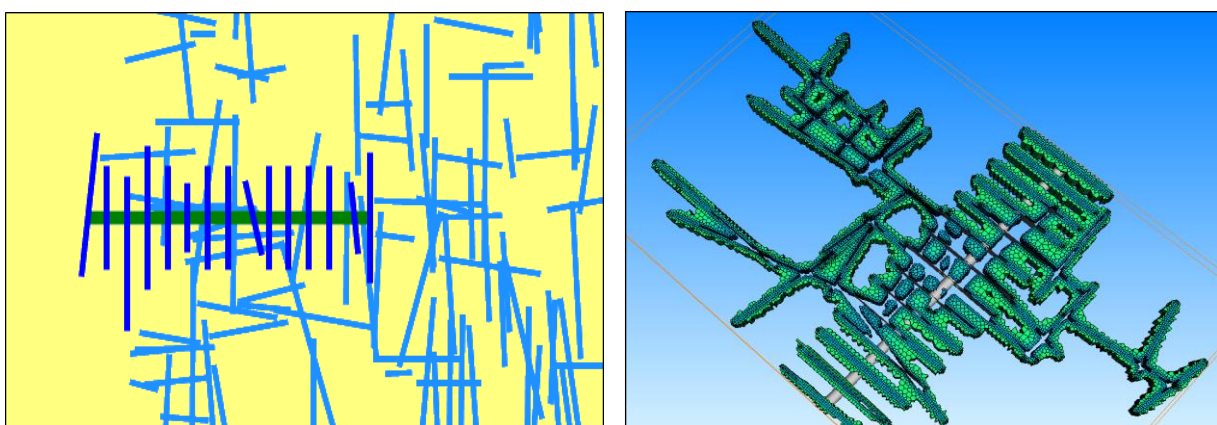
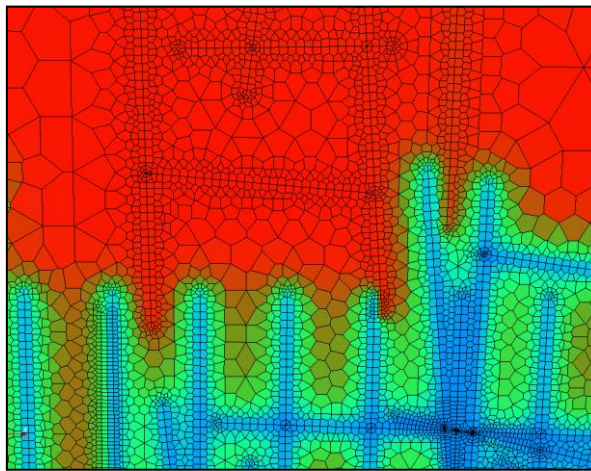


Fig. 1.H.8 – 2D (left) and 3D (right) representation of a numerical DFN.

A specific algorithm was developed for this situation, with the assumption that:

- All the fractures (hydraulic and natural) are made of individual, vertical planes.
- All the fractures (hydraulic and natural) fully penetrate the pay thickness.
- The wellbore is cased, i.e. it only connects hydraulic fractures (not the matrix).

With these assumptions, we can limit ourselves to a 2D or a 2.5D background Voronoi grid, which is iteratively refined in the vicinity of the fractures, so that transients in the matrix are properly captured. The grid portions in contact with the fractures are rigorously constrained to the geometry of the network, so that we do not create nor lose any intersection.



*Fig. 1.H.9 – Pressure fields in a numerical DFN.*

The various fracture segments can take any direction or length. This means the numerical model can handle the two regular patterns offered by the analytical option, but also simulate more complex, stochastically generated networks.

The conductivity, the width and/or the porosity can be redefined for each natural or hydraulic fracture. Also, three groups of relative permeability curves and pressure-dependent properties ( $k/k_0$  and  $\phi/\phi_0$ ) can be defined for the:

- matrix,
- hydraulic fractures,
- natural fractures.

Although in theory, an individual redefinition of these curves at the level of each fracture could be handled by the simulator.

For networks of finite conductivity, the transmissibilities at fracture intersections are derived using a specific algorithm which ensures that fluxes within the network are properly derived, even when multiple segments intersect at the same location.

### 1.H.2.b Stochastic DFN

Considering the natural origin of this fracture network it is totally logical to think about the description, then the generation of the DFN according to a random algorithm but in the same time constrained by certain aspects and information.

The principle is set a total number of expected natural fractures, then to define several families of natural fractures and to specify for each one the following characteristics:

- Fraction: percentage of each family in the final DFN
- Minimum, maximum fissure lengths
- Power: controls the fracture lengths distribution (power law)
- Strike angle: “average” fracture angle
- K strike: K parameter for the Fisher law angle distribution (dimensionless number)

The position of the region where we want to generate this DFN in the map can be set with respect to the well(s).



*Fig. 1.H.10 – Stochastic distribution of DFN with two families crossed by two wells*

The fractures can be connected or not to the well and to possible artificial fractures:

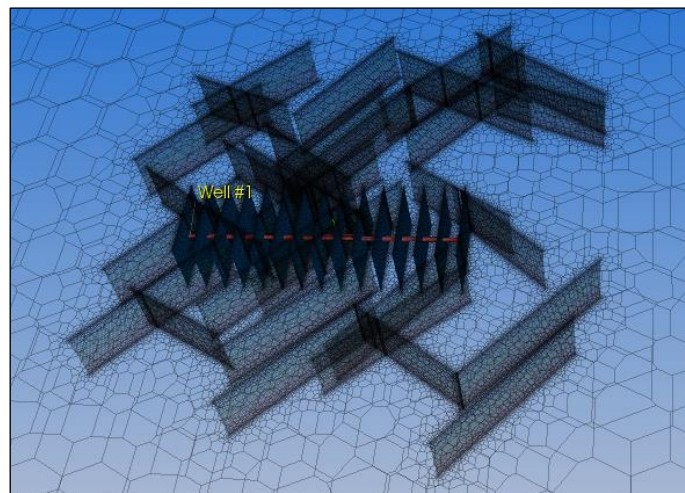


*Fig. 1.H.11 – Stochastic DFN connected to a multiple fractured horizontal well*

If microseismic events are available they can be used as a constraint on the DFN generation:

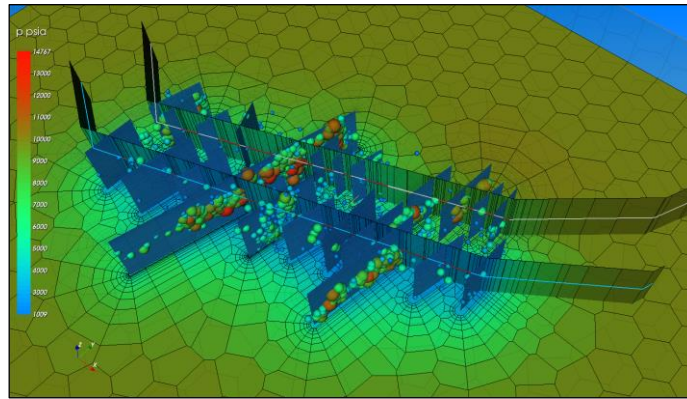


*Fig. 1.H.12 – DFN constrained by seismic events*

When the fracture network is crossed by two horizontal wells and that an interference test has been performed, the stochastic DFN generator can be connected to an optimization algorithm (called Fast Marching Method) in order to select the stochastic DFN realizations compatible with the observed interference time.

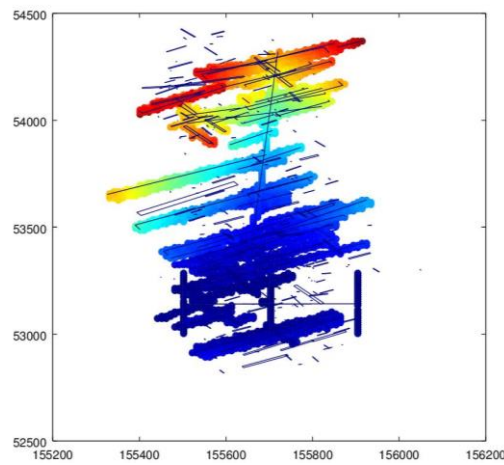


*Fig. 1.H.13 – DFN selected by the FMM from the interference test information*

### 1.H.2.c Analytical DFN

Analytical models are certainly insufficient to model a DFN, but they may be used to arrive at a first estimate of the parameters (density, orientation, etc.) that may be used as a seed to simulate the numerical DFN. In order to achieve this one may use a model such as the conjugate fractures. This model complements the hydraulic fractures with a set of evenly spaced natural fractures orthogonal to them, hence parallel to the horizontal drain. These fractures may be totally connected (left) or of insufficient length to directly connect the hydraulic fractures (right).

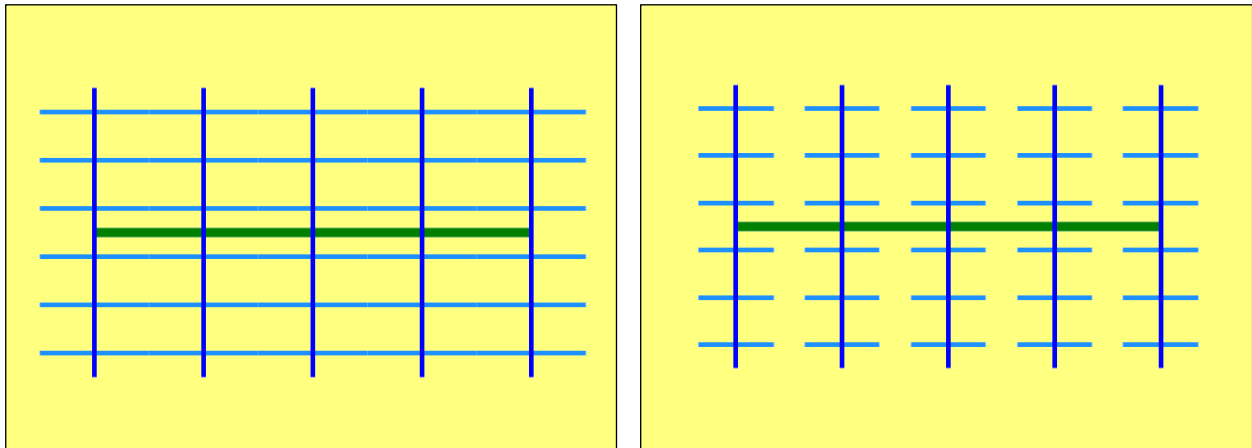


Fig. 1.H.14 – Analytical approximations of a DFN.

### 1.H.3 Modeling water flowback (numerical)

Fracturing jobs involve the injection of massive volumes of water, combined with proppant and chemicals. When the well is put on production, large quantities of water are produced during the clean-up phase. If the associated rates and pressures have been recorded, this may provide valuable information for reservoir characterization.

Furthermore, since very often only a fraction of the injected water flows back during production, one may want to evaluate the various scenarios to explain the volume difference and figure out how the missing water may impact the gas flow.

The first issue for the simulation of water flowback is in starting with a perturbed initial state, in order to account for the presence of injected fluids in the reservoir. We chose to use the material balance approach described in a previous section, i.e. to initiate the numerical model for flowback with a non-uniform initial water saturation field. The initial pressure field is uniform at  $P_i$ .

Two methods are available, the Static and the Dynamic methods, as will be illustrated in 10.B.4.

#### 1.H.3.a Static initialization

When the “Static method” is used for initialization, the volume of the flooded zone is derived so that the total amount of water added to the system (i.e. in excess to  $S_{wi}$ ) is equal to the volume of water pumped during fracturing operations.

Fractures and matrix can be associated to different relative permeability curves, hence they can be initialized with different values of water saturation in the flooded areas ( $S_{wmax}$ ).

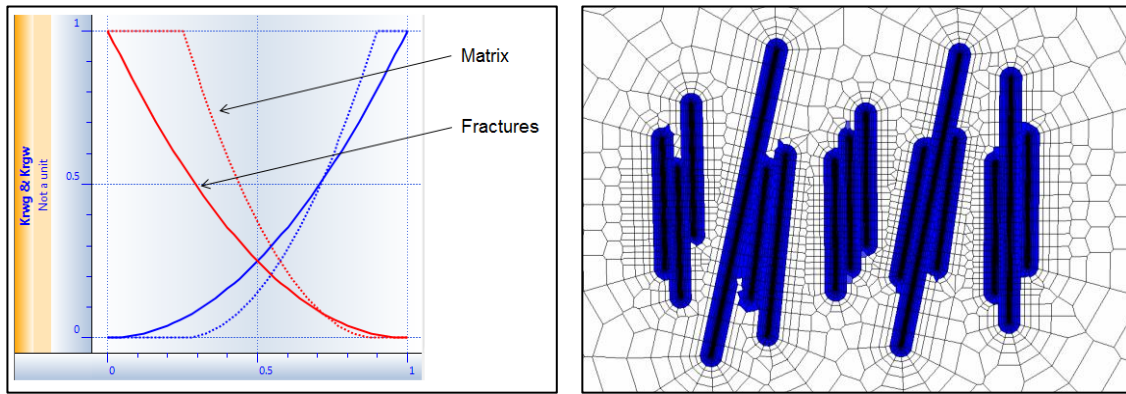


Fig. 1.H.15 – Relative permeability curves and simplified initial water saturation state.

Three different zones are defined:

- The background system, with cells initialized at  $S_{wi}$
- Hydraulic fractures, where cells are assigned  $S_{wmax}^{HF}$ .
- A flooded zone in the matrix, where cells are assigned  $S_{wmax}^{matrix}$ .

This purely static approach allows us to represent the delay in gas production due to early-time dewatering of the system:

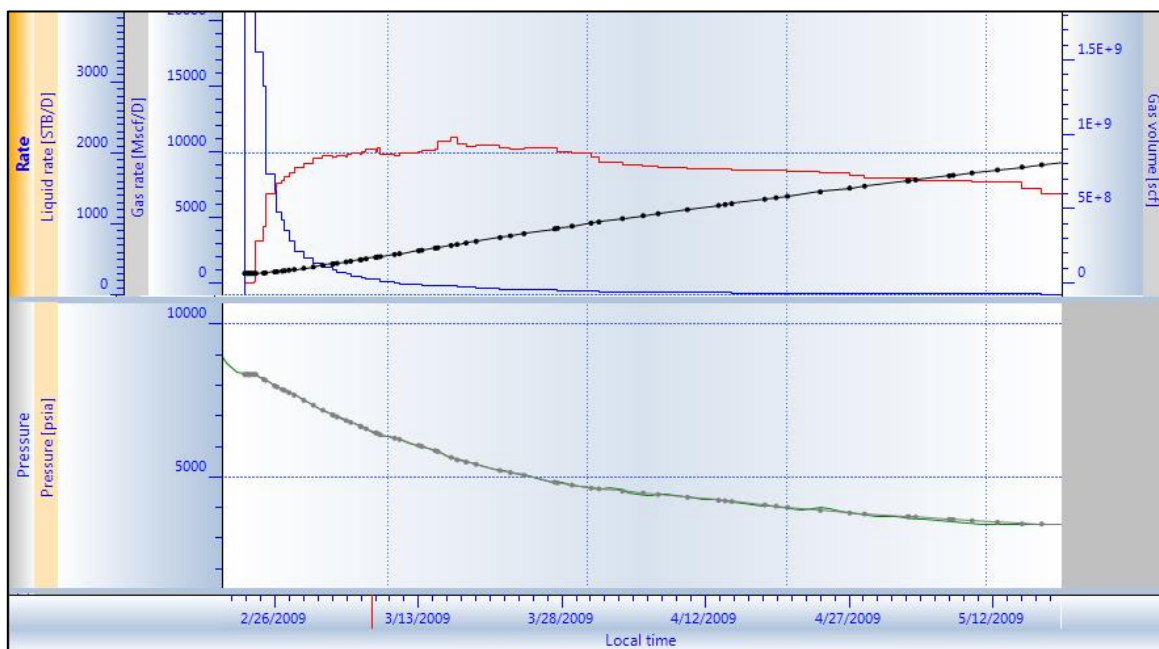


Fig. 1.H.16 – Example of simulated water and gas production.

This approach also captures some of the water trapping in the matrix. In a given cell, the volume of water added to represent the initial 'flood' is:

$$V_{wi}^{added} = V_i \cdot \phi_i \cdot (S_w^{max} - S_{wi})$$

As a consequence, if the original initial water saturation is lower than the residual water saturation,  $S_{wi} < S_{wr}$ , some water will be capillary trapped in this cell after some production time. The volume of trapped 'injection water' in the cell will be:

$$V_{wi}^{trapped} = V_i \cdot \phi_i \cdot (S_{wr} - S_{wi})$$

This allows us to take into account capillary trapping and representing lost volumes without strictly modeling injection and KrPc hysteresis. Gravity trapping within the fractures can be simulated with vertical subdivisions of the simulation grid.

For the DFN model, the procedure is almost the same:

- A fast run (steady state) is conducted to identify the parts of the DFN that are effectively connected to the hydraulic fractures
- The total system is initialized at  $S_{wi}$
- Water is added inside the hydraulic fractures ( $S_{wmax}^{HF}$ )
- Water is added inside the connected part of the DFN ( $S_{wmax}^{DFN}$ )
- The remaining water is added in the matrix ( $S_{wmax}^{matrix}$ ), so that the total volume flooded honors the total amount of injected water

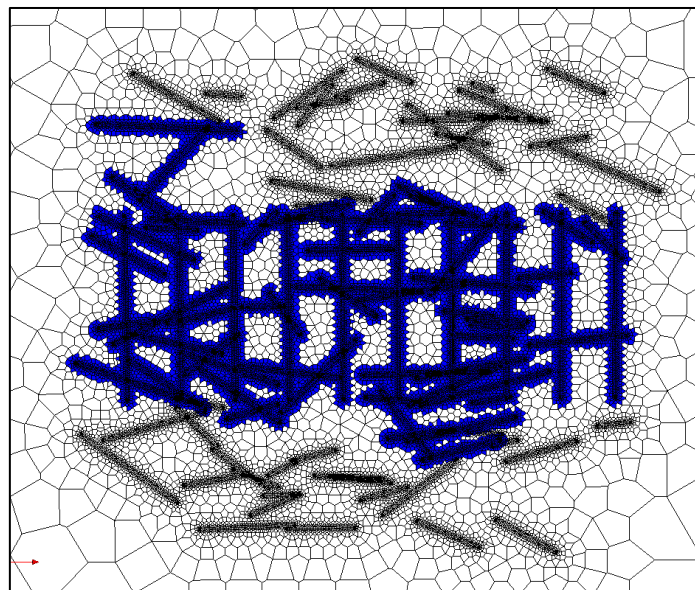


Fig. 1.H.17 – Initial water saturation profile in a DFN.

### 1.H.3.b Dynamic initialization

In the "Dynamic method" initialization, we simulate the injection in the hydraulic/natural fractured system.

The resulting water distribution is more rigorous because it corresponds to the ability of the various fractures and matrix to store water. It results also a non-uniform pressure field which corresponds to a realistic consequence of an injection.

It requires a rather complex simulation and the exact injection history.

Even though this approach does not model the opening of the fractures nor the stress reorientations, using the  $k$  and  $\phi$  pressure dependent option, the volume of water stored in the fractures can be simulated.

The saturation distribution and the pressure map are realistic and synchronized:

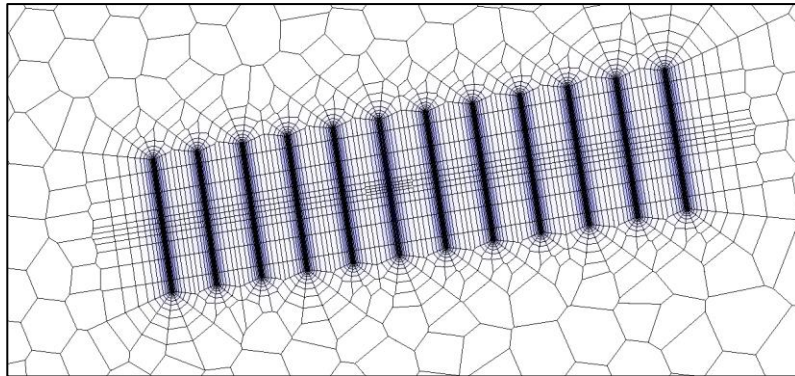


*Fig. 1.H.18 – Initial water saturation after dynamic initialization*

The static and the dynamic methods give rather different results. In particular, since the shape of the water bank is not very realistic with the static method (too much water at the tip of the fractures because of the assumed stadium shape), the static method predicts less gas being produced – since a lot of water remains trapped at the tip of the fractures and slightly impairs production.

NB - Spontaneous imbibition, osmosis phenomena, etc. that may participate in the trapping of injected water are still considered as research areas and are not covered in this chapter.

#### **1.H.4 Refrac jobs modeling**

Additional fracturing jobs can be performed after the well was put on production, either to create new fractures or to increase the existing fracture performances.

This option is only available for fractured horizontal wells with finite conductivity fractures. It is restricted to a delayed opening of fractures, limiting the input to a single time of opening.

The refrac possibility is compatible with special reservoir conditions like:

- Specific unconsolidation laws ( $k(p)$ ,  $\phi(p)$ ) in the fractures,
- Specific relative permeability laws in the fractures,
- Stimulated zones around fractures option.

The principle is to act on the transmissibility of the fractures and on the well index, starting with a matrix properties at start, then setting them to the high conductivity value at the “refrac time” mimicking the activation of the selected fractures.

### 1.H.4.a Features for simple fracture system

When the fractures properties are globally defined, two global parameters are required:

- The re-fracking time which corresponds to the time when the fracture system will be modified.
- The re-fracking ratio  $R_f$ , expressed as a positive number equal or greater than 1, is the ratio between the initial and the final number of fractures.

The number of fractures at time zero  $N_i$  is related to the number of fractures  $N_f$  after the refrac, that are evenly distributed along the well, with the formula:  $N_f = N_i + (N_f - 1) R_f$ .

When 'Infill' option is invoked, we consider that  $N_f = N_i$ , the whole well is an infill well and is entirely fractured at the refrac time.

In either case, the user interface does not distinct between the fractures opened at simulation start and the refrac ones.

For example, in case the re-fracking ratio  $R_f$  is set to 2 with an initial number of fractures  $N_i$  equal to 4, the final number of fractures  $N_f$  would be 10.

In this case, the initial grid includes all 10 fractures but only 4 'initial' fractures will be active, and 6 more will be activated at the re-fracking time, set in this example to 3,000 hours for a total simulation duration of 6,000 hours.

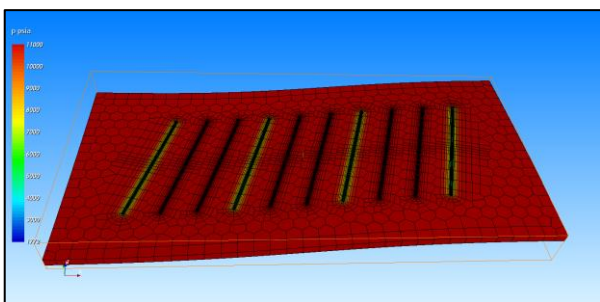


Fig. 1.H.19 - Pressure map before re-frac job

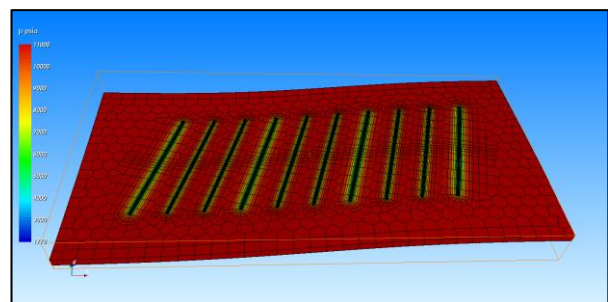


Fig. 1.H.20 - Pressure map after re-frac job

The effect of the refrac can be easily observed on the pressure and rate history plot at 3,000 hrs when 6 more fractures are activated in addition to the original 4 fractures:

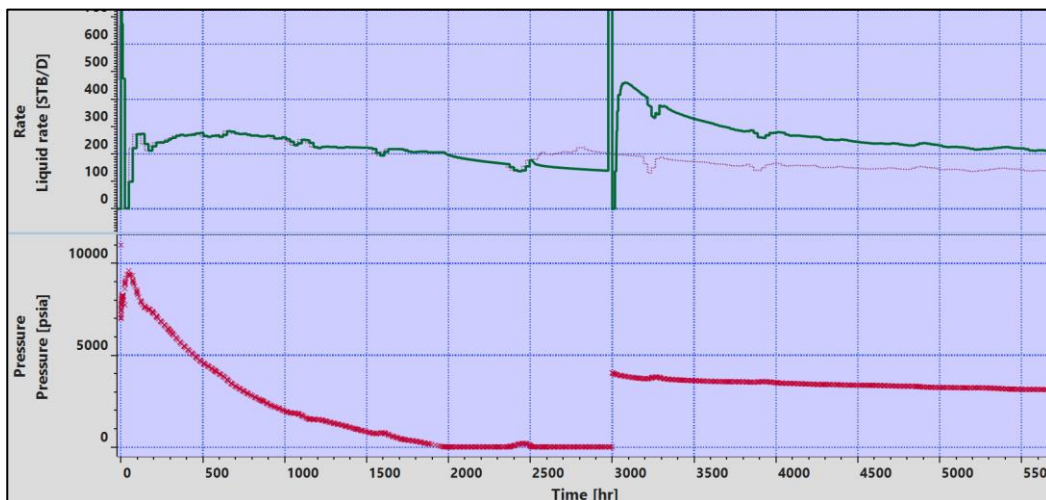


Fig. 1.H.21 - Pressure and rate history with a refrac job

### 1.H.4.b Features for complex fracture system

When the well fractures modelling type is set to “complex” and the “Individual properties” can be input, each fracture can be re-fracked at its individual “fracture opening time”.

In this case, the initial grid includes all the fractures and they are activated according to the “opening time” attributed to each one.

For instance in the following case the fracture 6 opens after 3,000 hours and the fracture 8 after 5,000 hours:

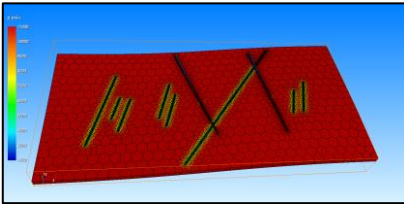


Fig. 1.H.22 - Pressure map before refracs

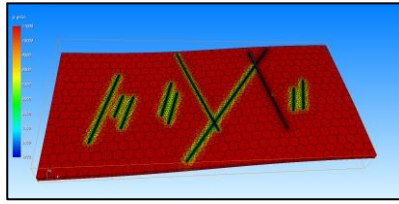


Fig. 1.H.23 - Pressure map after 3,000 hrs, refrac of "fracture 6"

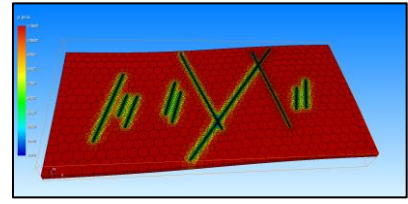


Fig. 1.H.24 - Pressure map after 5,000 hrs, refrac of "fracture 8"

The effect of the multiple refrac jobs can be observed on the pressure and rate history:

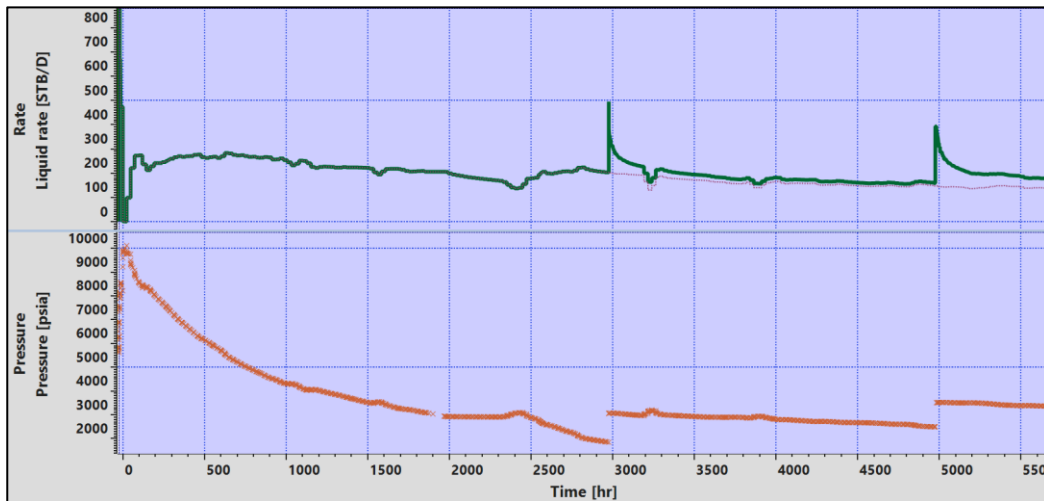


Fig. 1.H.25 - Pressure and rate history with two refrac jobs

## 1.H.5 Multi-Zone Fractional Dimension

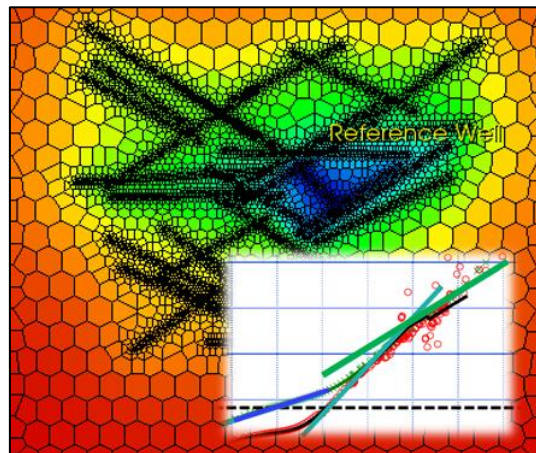


Fig. 1.H.5.26 - Multi-Zone Fractional model schematic

This approach presents a way to analytically model transient behavior of a complex fracture network.

The method presented by Acuña (2016) allows interpreting pressure and flow rate behaviors observed in unconventional wells that do not exhibit linear flow regime. The method suggests a way to diagnose multiple flow regimes (sub-linear, linear, sub-radial) on the standard loglog plot.

A multi-fractured horizontal well in a fractured formation can be compared to a fractured well (with the fracture length equal to the sum to all initially connected high conductivity fractures) that drains a reservoir with a flowing area  $A$ , that is perpendicular to the flow and changes with distance according to the power law:

$$A = X_f h r_D^{2\delta-1}$$

Where:

$X_f$  is the half flow area width,

$$r_D = \frac{r}{r^*}$$

$r$  is the distance and  $r^*$  is taken as the half fracture length.

$\delta$  is the half flow dimension

Note that in the case of  $\delta = 0.5$  the flow regime is linear and the flowing area becomes constant with respect to the distance to the fracture area, i.e. the case reduces to the channel geometry. Also the case of  $\delta = 1$  is a classical radial flow, and  $\delta = 0$  corresponds to the PSS.

This generalised model is versatile as it includes the cases with:

- The flow area  $A$  decreasing with the distance from the fracture (sub-linear flow, values of  $0 < \delta < 0.5$ , Fig. 1), and
- The flow area  $A$  increasing with the distance from the fracture (sub-radial flow, values of  $0.5 < \delta < 1$ , Fig. 2).

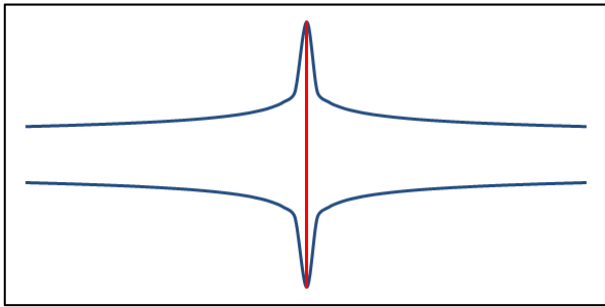


Fig. 1.H.5.27 - Sub-linear flow

with  $\delta = 0.375$

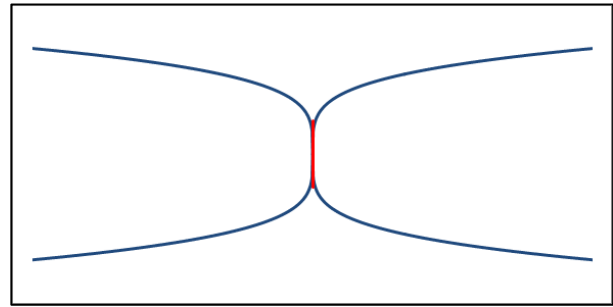


Fig. 1.H.5.28 - Sub-radial flow

with  $\delta = 0.75$

The dimensionless pressure is shown to have the following form:

$$p_D = \frac{(4t_D)^{1-\delta}}{2\Gamma(\delta)(1-\delta)}$$

And its log pressure derivative can be written as follows:

$$t_D \frac{dp_D}{dt_D} = \frac{(4t_D)^{1-\delta}}{2\Gamma(\delta)}$$

Hence during this flow regime the pressure and the derivative are functions of the time raised to the power  $(1 - \delta)$ , which can be reliably diagnosed on a loglog plot by two parallel straight lines with a slope  $(1 - \delta)$ , which provides directly the fractional dimension value  $\delta$  and gives an insight into the nature of the fractures network geometry.

The production of a Discrete Fracture Network system with its complex geometry can lead to a sequence of different flow regimes, depending on the drained and investigated area.

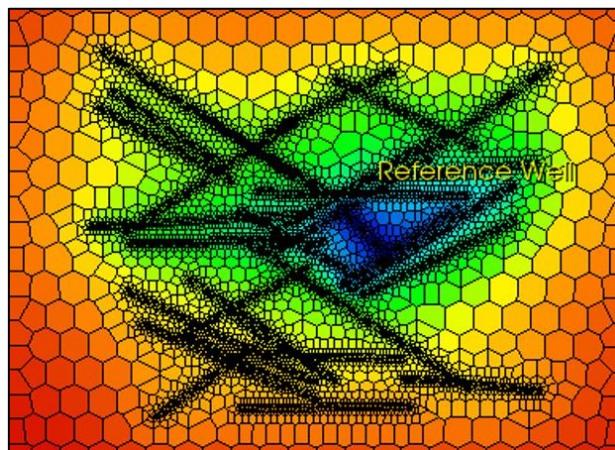
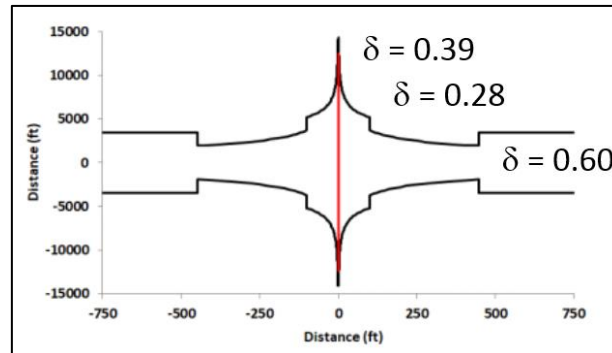


Fig. 1.H.5.29 - Investigation areas

The sub-linear case might represent a MFHW in a densely fractured reservoir, when the areas drained by each fracture reduce with distance because of fractures interference. On the other hand, the sub-radial case might correspond to a network of fractures of both high and low conductivity, the latter having drainage area that increases with distance in a more pronounced way.

Also the presence of fractures of different conductivity and their geometrical closeness can result in a system that exhibits a sequence of linear, sub-linear, radial, sub-radial flow regimes. This is illustrated below in terms of reservoir model geometry and corresponding  $\delta$  versus distance from the fractured area.



*Fig. 1.H.5.30 - Model flow area geometry*

This type of geometry gives a sequence of straight lines on the loglog plot.

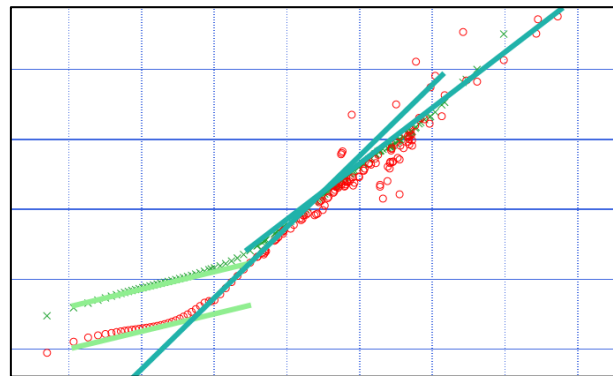


*Fig. 1.H.5.31 - Pressure and derivative loglog plot*

The multi-zone fractional dimensional model concept presents an extension of the described model to  $n$  zones characterized by their individual  $\delta$  parameters and sizes. The outer boundary of the last zone can be defined as infinite, no-flow or constant pressure.

## References

Analytical Pressure and Rate Transient Models for Analysis of Complex Fracture Networks in Tight Reservoirs. Jorge A. Acuña\*, SPE, Chevron U.S.A. Inc. URTEC: 2429710, 2016.

Pressure and Rate Transient Analysis in Fracture Networks in Tight Reservoirs Using Characteristic Flow Volume. Jorge A. Acuña\*, SPE, Chevron U.S.A. Inc. URTEC: 2667753, 2017.

Alternative Production Mechanisms in Unconventional Reservoirs. Jorge A. Acuña\*, Shugang Wang and David Forand, SPE, Chevron U.S.A. Inc. URTEC: 2896802, 2018.

Straightforward Representative Fluid Flow Models for Complex Fracture Networks in Unconventional Reservoirs. Jorge A. Acuña. SPE, Chevron U.S.A. Inc. URTEC: 2876208, 2018.

### 1.H.6 Anomalous Diffusion in a Tri-linear model

#### 1.H.6.a Description and assumptions

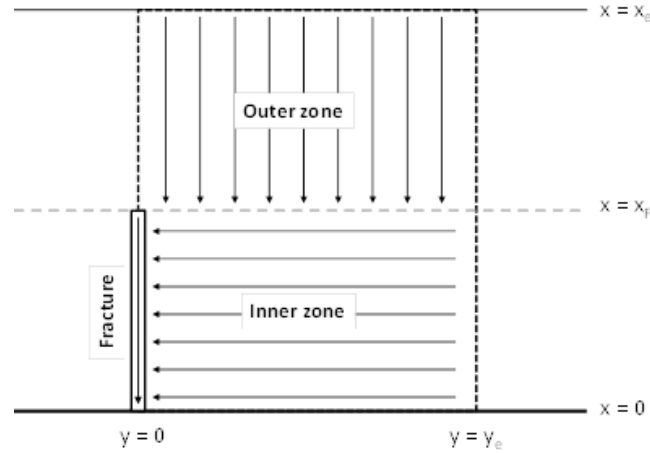


Fig. 1.H.6.32 - Tri-linear model basic component

This model considers transient flow under a possible anomalous diffusion (also called Space-Time Fractional Diffusion) toward a horizontal well that produces a reservoir through multiple fractures. The objective of this modelling approach is to address the effects of the magnitude of heterogeneities in both the fissure and matrix systems by considering non Gaussian distributions governing rock properties. This model, is a simplified composite 3-zone linear model that is normally called a trilinear model.

As mentioned in the chapter “Theory” paragraph 2.A.3, the “normal” diffusion equation for a linear flow is:

$$\lambda \frac{\partial^2 p(x,t)}{\partial x^2} = \phi c_i \frac{\partial p(x,t)}{\partial t}$$

We consider a diffusion as “Anomalous” when the relationship between the time and the displacement is governed by:

$$\frac{\partial}{\partial x} \left[ \lambda_{\alpha,\beta} \frac{\partial^\beta p(x,t)}{\partial x^\beta} \right] = \phi c_i \frac{\partial^\alpha p(x,t)}{\partial t^\alpha}$$

Where the diffusion exponents  $\alpha$  and  $\beta$  are  $\leq 1$ .

With  $\alpha = \beta = 1$  we get normal diffusion corresponding to Darcy’s Law with ordinary permeability

Note that if the super-diffusion exponent  $\beta = 1$  and the sub-diffusion exponent  $\alpha < 1$ , then, we have a case with pure sub-diffusion.

Among the anomalous diffusions, the sub-diffusion is an appropriate model for situations that reflect internal structure with numerous scales and existence of cracks, cervices & obstacles.

In the model used in this chapter, the reservoir can be either homogeneous or double porosity.

In case of Dual Porosity the sub-diffusion exponent are considered in both the fissures ( $\alpha_f$ ) and the matrix ( $\alpha_m$ ). Note that for classical diffusion,  $\alpha_f = 1$  and  $\alpha_m = 1$ .

When double porosity is considered, the flow from matrix to fissures can be either pseudo steady state or transient. For transient double porosity consideration, the configuration of matrix elements can be slab, sphere or cylinders. The reservoir can be infinite or a rectangular reservoir.

The hydraulic fractures can be either infinite conductivity, uniform flux or considering incompressible or compressible fluid in fractures.

The hydraulic fracture properties are assumed to be identical.

Note: in the reference papers, dealing more with sub-diffusion, the exponent  $\beta$  is considered equal to 1.

### 1.H.6.b Model features and parameters

The inner and the outer zone model can be either:

- homogeneous
- double porosity pseudo steady state
- double porosity transient, slabs matrix
- double porosity transient, sphere matrix
- double porosity transient, cylinder matrix

The fracture model can be: Uniform Flux, Infinite Conductivity, Finite Conductivity, Incompressible or Finite Conductivity Compressible.

The relative zone properties are defined by the composite ratio parameters:

The mobility ratio

$$M = (k/\mu)_{outer} / (k/\mu)_{inner}$$

and the diffusivity ratio

$$D = (k/\Phi\mu c_t)_{outer} / (k/\Phi\mu c_t)_{inner}$$

### 1.H.6.c General Anomalous Diffusion Behaviour

In a first step it is convenient to describe briefly and simply the physical meaning and consequences of the two diffusion exponents  $\alpha$  and  $\beta$ .

Globally, the sub-diffusion exponent  $\alpha < 1$  will induce a lower equivalent diffusivity, and the super-diffusion exponent  $\beta < 1$  will induce a higher equivalent mobility.

This can be illustrated by using a simple version of the model, where the well model in a 8000ft horizontal drain with 40 fractures of 200ft half-length and where the two regions of the reservoir are initially defined as identically homogeneous, with the sub-diffusion exponent  $\alpha$  and a super-diffusion exponent  $\beta$  are equal to 1 to simulated a normal diffusion.

It results a sequence of two linear flows corresponding to the flow from reservoir to the fractures, then from the reservoir to the SRV:

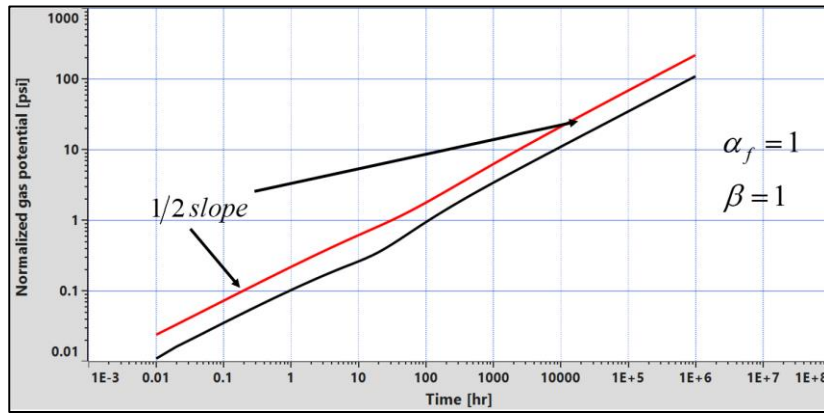


Fig. 1.H.6.33 - Reference case: 2 equal homogeneous regions, Infinite outer zone

Now, let's consider the influence of the exponents  $\alpha$  and  $\beta$  in the inner zone:

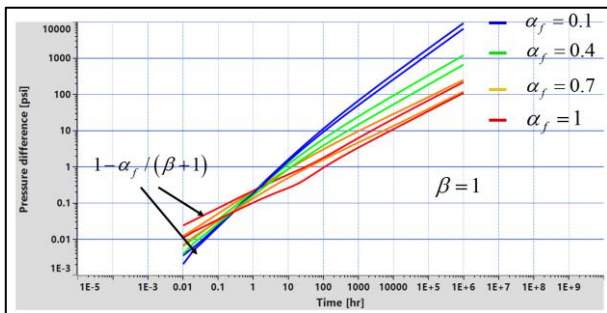


Fig. 1.H.6.34 - Influence of the inner zone  $\alpha$  (constant  $\beta=1$ )

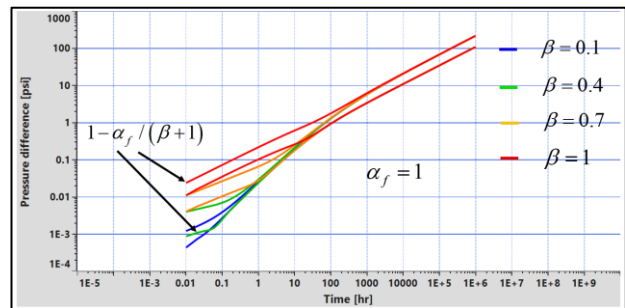


Fig. 1.H.6.35 - Influence of the inner zone  $\beta$  (constant  $\alpha=1$ )

An inner  $\alpha$  smaller than 1 leads to as lower diffusion in the inner zone, it decreases the fractures efficiency thus increases the early time behavior slope, as a "pseudo skin" it increases the pressure drop at late time.

An inner  $\beta$  smaller than 1 leads to as higher mobility in the inner zone, it imposes a very early time slope smaller than  $1/2$ , it has not impact on the late time behavior.

The influences of the exponents  $\alpha$  and  $\beta$  in the outer zone are even more characterized:

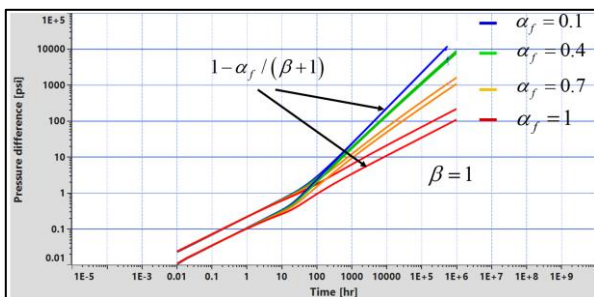


Fig. 1.H.6.36 - Influence of the outer zone  $\alpha$  (constant  $\beta=1$ )

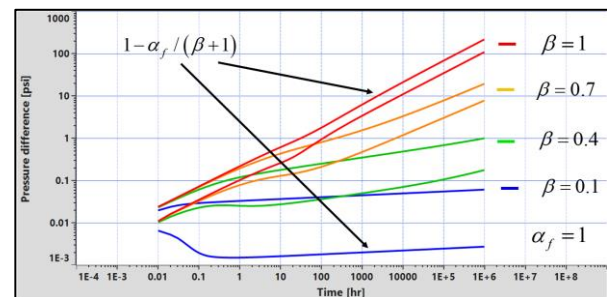


Fig. 1.H.6.37 - Influence of the outer zone  $\beta$  (constant  $\alpha=1$ )

An outer  $\alpha$  smaller than 1 leads to as lower diffusion in the outer zone, a small  $\alpha$  value can lead the model to show a slope close to the unit, close to Pseudo Steady State created by a very low diffusion surrounding area.

An outer  $\beta$  smaller than 1 leads to as higher mobility in the outer zone, a small  $\beta$  value reduces drastically the slope value.

Conjugated influences of the exponents  $\alpha$  and  $\beta$ : the  $\alpha$  effect on the behavior can vary according to the  $\beta$  value, it can almost hide the  $\alpha$  influence.

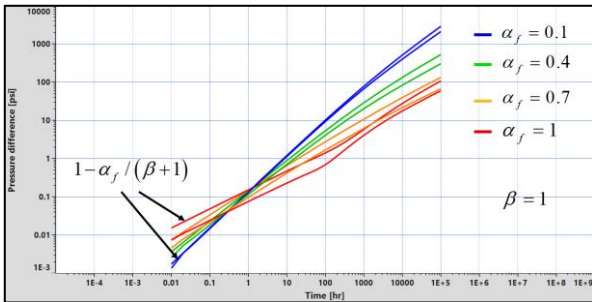


Fig. 1.H.6.38 - Influence of the inner zone  $\alpha$  (with  $\beta=1$ )

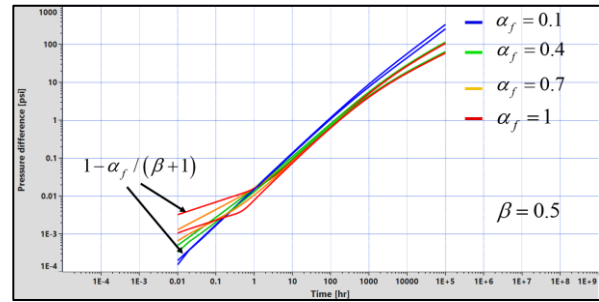


Fig. 1.H.6.39 - Influence of the inner zone  $\alpha$  (with  $\beta=0.5$ )

The two figures below show that the effect of the inner  $\alpha$  on the late time is extremely reduced by a value of  $\beta=0.5$ , all other parameters remaining equal.

In a similar way, the outer exponents  $\alpha$  and  $\beta$  interact one on each other:

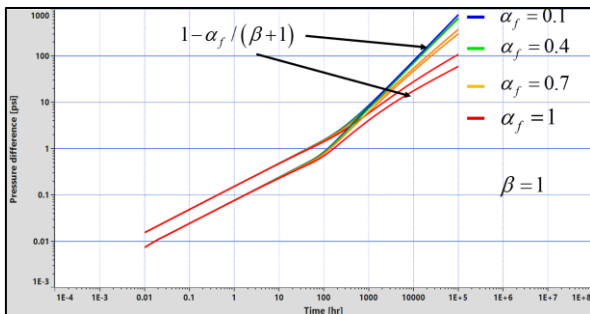


Fig. 1.H.6.40 - Influence of the outer zone  $\alpha$  (with  $\beta=1$ )

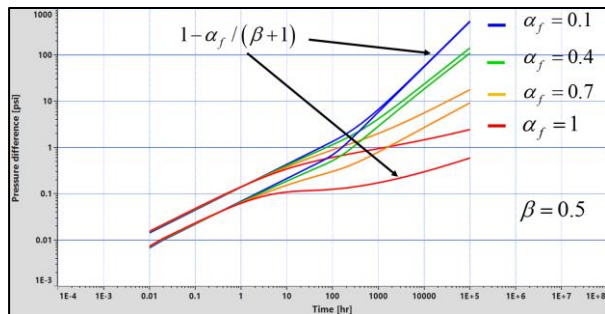


Fig. 1.H.6.41 - Influence of the outer zone  $\alpha$  (with  $\beta=0.5$ )

The two following figures show that while a small value of the outer  $\alpha$  (0.1) makes the model to tend to a P.S.S. effect, a value of  $\beta=0.5$  will leave the ( $\alpha=0.1$ ) effect identical but will modify the behavior for  $\alpha$  values close to 1, widening consequently the  $\alpha$  effect.

When the system is considered as closed, it will be mainly the outer zone  $\beta$  and  $\alpha$  diffusion exponents that will affect the pressure behavior.

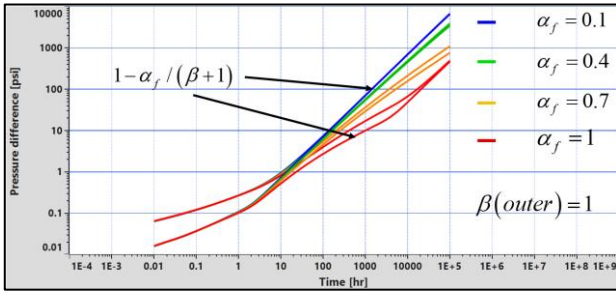


Fig. 1.H.6.42 - Closed outer zone, influence of  $\alpha$  (with  $\beta = 1$ )

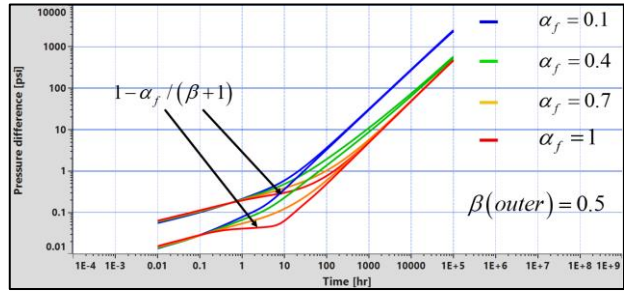


Fig. 1.H.6.43 - Closed outer zone, influence of  $\alpha$  (with  $\beta = 0.5$ )

The above figures show that the P.S.S. final unit slope is always observed, but smaller values of  $\alpha$  make the diffusivity smaller, therefore a latter P.S.S.. But values of  $\beta$  smaller than one increase the equivalent mobility and make the  $\alpha$  effect to appear earlier.

### 1.H.6.d The anomalous diffusion applied to a heterogeneous reservoir

#### Composite reservoirs parameter impact

The effects of the two composite ratios:

The mobility ratio

$$M = (k/\mu)_{outer} / (k/\mu)_{inner}$$

and the diffusivity ratio

$$D = (k/\Phi\mu c_t)_{outer} / (k/\Phi\mu c_t)_{inner}$$

Are classical and well known, as shown in the two following figures:

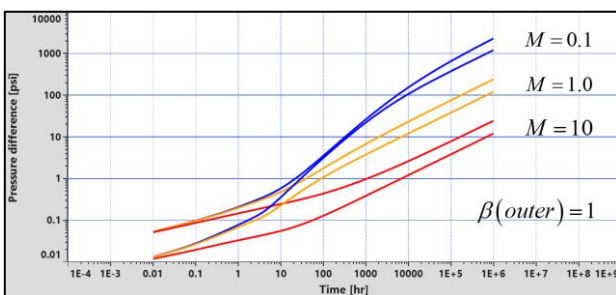


Fig. 1.H.6.44 - Infinite outer zone, influence of mobility ratio with  $\beta = 1$

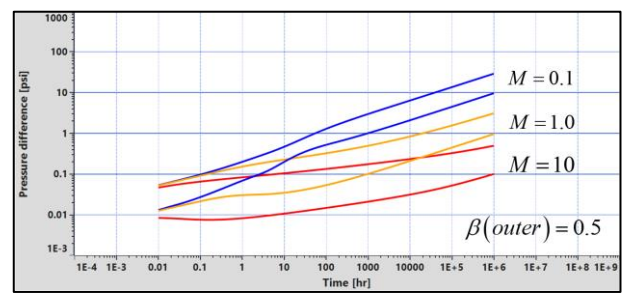


Fig. 1.H.6.45 - Infinite outer zone, influence of mobility ratio with  $\beta = 0.5$

The smaller the M, the smaller will be the external mobility therefore the higher will be final pressure response, but a  $\beta$  value smaller than one, will compensate this effect by increasing the outer resulting mobility.

In case of closed outer region, in addition to the observed final P.S.S. unit slope, the same M effect is observed:

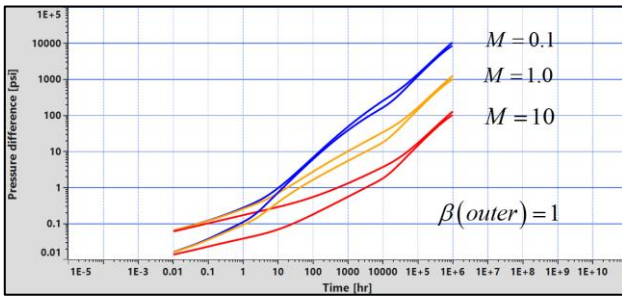


Fig. 1.H.6.46 - Closed outer zone, influence of mobility ratio with  $\beta=1$

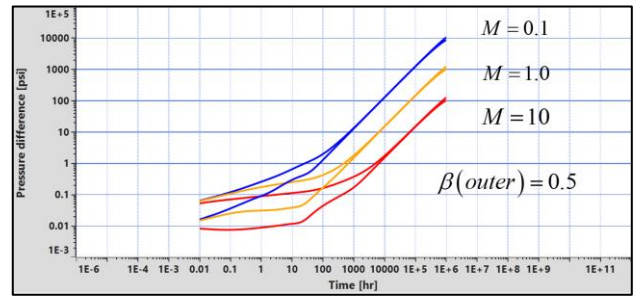


Fig. 1.H.6.47 - Closed outer zone, influence of mobility ratio with  $\beta=0.5$

Once more a  $\beta$  value smaller than 1 makes the external conditions to be observed earlier because of the increase equivalent mobility.

The diffusivity ratio  $D$  has a similar effect: for a constant  $M$  value, the smaller the  $D$  value, the larger is the storativity product  $\Phi C_r$ , then the latter the depletion effect:

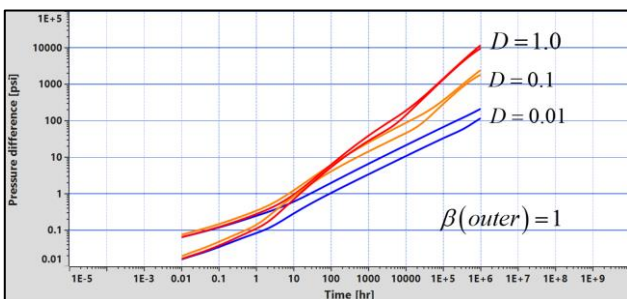


Fig. 1.H.6.48 - Closed outer zone, influence of diffusivity ratio with  $\beta=1$

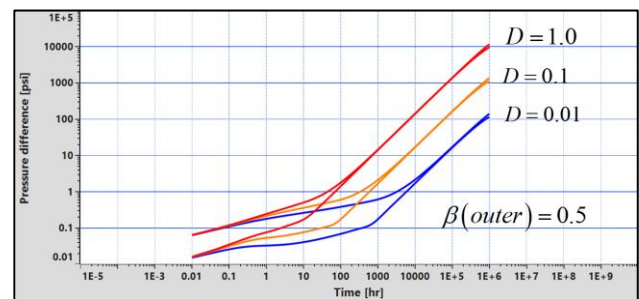


Fig. 1.H.6.49 - Closed outer zone, influence of diffusivity ratio with  $\beta=0.5$

In the same time, a  $\beta$  value smaller than 1 makes the P.S.S. to be observed earlier because of the increase equivalent mobility.

**The Sub-diffusion in a composite heterogeneous reservoir.**

In the following, we are going to consider only the case of sub-diffusion setting the  $\beta$  exponent equal to one and the  $\alpha$  exponent in both fracture system ( $\alpha_f$ ) and matrix system ( $\alpha_m$ ).

Even if the homogeneous reservoir or the pseudo steady state double porosity options are available, the transient double porosity option probably is the best model option to describe the unconventional plays.

For the transient-flow double porosity model, five types flow regimes could be considered:

Flow Regime	Fissure System	Matrix System
FR 1	Infinite-acting	No influence
FR 2	Infinite-acting	Infinite-acting
FR 3	Infinite-acting	Pseudosteady
FR 4	Pseudosteady	Infinite-acting
FR 5	Pseudosteady	Pseudosteady

Fig. 1.H.6.50 - Table 1 Flow regimes summary

In the current case, we have to go beyond the regimes noted above because of the need to consider fractured wells; many sub-flow-regimes may exist depending on fracture conductivity,  $k_F w_F$ , and length,  $x_F$ , (single or multiple fractures) and fracture spacing (multiple fractures).

**Flow Regimes of the model**

There are two major paths can happen depending on existence of flow regime 3.

Path A is from FR 1 → FR 2 → FR 4 → FR 5

Path B is FR1 → FR 3 → FR 5.

Note that flow regime 3 is the condition of the Warren and Root model. In reality, the path in unconventional most probably is Path A without FR 5, i.e. FR 1 → FR 2 → FR 4.

As the general behaviour of the subdiffusive consideration is the power-law behavior, the well responses in many cases may be represented by the expressions of the form

$$\frac{\Delta p(t)}{q} = At^a, \quad (1)$$

for production at a constant rate or by

$$\frac{\Delta p}{q(t)} = At^a \quad (2)$$

for production at a constant pressure.

The exponent  $a$  for many typical situations is noted in Table 2.

	Exponent
FR1, Linear Flow	$(2 - \alpha_f) / 2$
FR 1, Bilinear Flow	$(2 - \alpha_f) / 4$
FR 2, Linear Flow	$(4 - 2\alpha_f - \alpha_m) / 4$
FR 2, Bilinear Flow	$(4 - 2\alpha_f - \alpha_m) / 8$
FR 4	$(2 - \alpha_m) / 2$
FR 5, Constant Rate	1
FR 5, Const.Pressure	$1 / (1 + \alpha_f)$

Fig. 1.H.6.51 - Table 2: Exponents of the flow regimes

Flow Regime 3 is not listed in Table 1 as responses do not follow the form suggested in Eq. 1.

During flow regime 3, 
$$\Delta p(t) \sim \frac{1}{2} \frac{1}{\Gamma(2 - \alpha_f)} t^{(1 - \alpha_f)} * \ln t^{\frac{(\alpha_f - \alpha_m)}{2}}.$$

It is worth to note that the exponential decline only happens during pseudo steady state when the well is produced under constant rate production. It is power-law behavior during pseudo steady state when the well is produced under constant pressure production. It is also reasonable to expect that the late time performance would be flow regime 4 and the heterogeneity in the matrix system dominates the behavior as the exponent of flow regime 4 is  $(2 - \alpha_m) / 2$ .

The production rate,  $q$ , during hyperbolic decline, according to the Arps (1945) model is given

$$\text{by } \frac{q(t)}{q_i} = \frac{1}{(1 + bD_it)^{1/b}}, \quad (3)$$

where  $q_i$  is the rate at any point in time following the onset of the decline period,  $D_i$  is the corresponding loss ratio, and  $b$  ( $0 \leq b \leq 1$ ) is the exponent of the decline curve. During Flow Regime 4, the expression for  $b$  is  $2 / (2 - \alpha_m)$ . Again, this implies that the matrix heterogeneity dominates the late time performance.

It is also important to note that the permeability in the model input is the apparent fissure permeability instead of the intrinsic fissure permeability.

On the log-log plots in Saphir and Topaze, users can right click on the plot to choose the Chow Pressure Group to check the exponent on the plots directly. In the following two plots, the CPG curves are also displayed.

**Global pressure behaviour and parameters influence**

The double porosity parameters,  $\lambda$  interporosity flow coefficient and  $\omega$  storativity ratio can be specified for both inner and outer regions.

The inner interporosity flow coefficient has only and influence on the early time and acts on the time of the transition that can be observed on the derivative

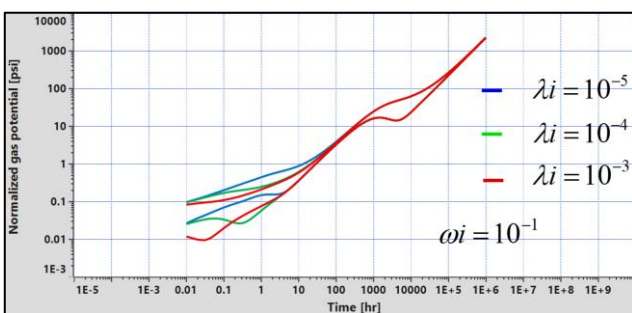


Fig. 1.H.6.52 - Closed outer zone, influence of interporosity flow coefficient with  $\omega = 0.1$

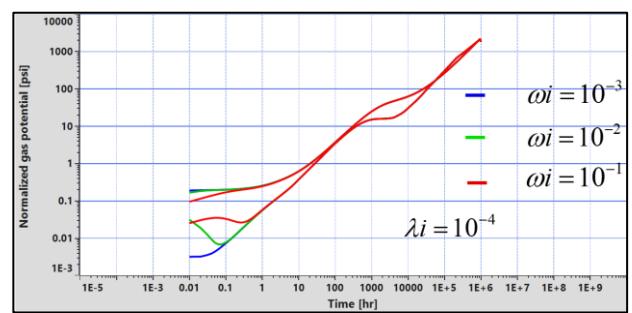


Fig. 1.H.6.53 - Closed outer zone, storativity ratio with  $\lambda = 0.0001$

The smaller is  $\lambda$ , the latter is the transition and the smaller is  $\omega$  the deeper the transition but this effect affects only the early time in the inner region.

Because it is acting in total system behaviour, the inner condition does not influence the outer region behaviour.

Conversely, the dual porosity outer parameters values affect only the late behaviour of the outer region.

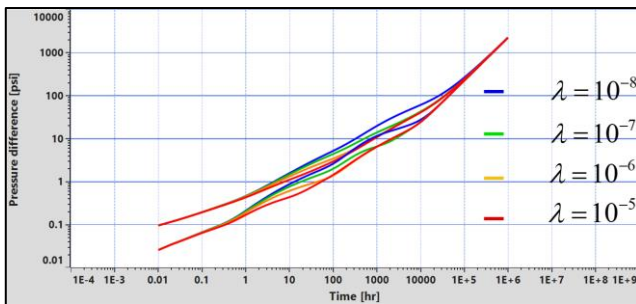


Fig. 1.H.6.54 - Closed outer zone, influence of interporosity flow coefficient with  $\omega = 0.1$

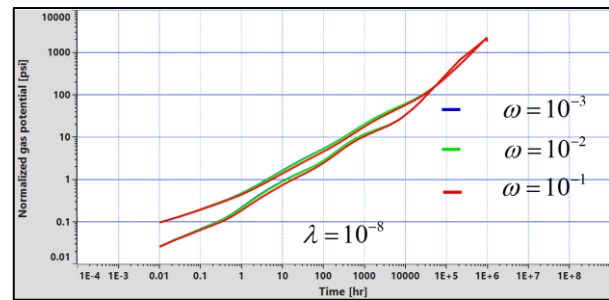


Fig. 1.H.6.55 - Closed outer zone, storativity ratio

While the effect of the outer lambda determines the time of transition, the effect of the omega is not significant because it occurs at intermediate time, masked by the multiple flow behaviours.

The late P.S.S. remains unchanged because it occurs after the transition, therefore during the global system behaviour.

We have seen that we can set specific sub-diffusion exponent in the fissure and in the matrix system. The result is not much different in the P.S.S. part since it acts mainly of the diffusion parameter.

## References

Raghavan and Chen, "Addressing the Influence of a Heterogeneous Matrix on Well Performance in Fractured Rocks", March 2017, Transport of Porous Media, Volume 117, No. 1

Raghavan and Chen, "A Conceptual Structure to Evaluate Wells Producing Fractured Rocks of the Permian Basin", SPE 191484, 2018

## 1.I KAPPA recommended workflow (2020)

In the early days of the production of unconventional plays the workflow seemed to be limited to decline curve analysis using Arps hyperbolic equations. Due to early time linear flow it was very likely to arrive at high 'b' values which would most likely overestimate reserves without proper constraints. Recently it became common to see the incorporation of analytical and numerical solutions into the workflows for well performance analysis and forecasting.

However, a lot of work has been completed in terms of understanding complex PVT and interference between wells we still have to go deeper with flow phenomena at the nanoscale, geomechanics, etc... For this reason the workflow recommended in this section is dated (2020) because it will be in continuous evolution and this is for several reasons:

- We are still on the learning curve for advanced technologies.
- The data available today is still poor, considering what is at stake. Metrology, although it improved, is still, on average, below what we could expect. These plays are strategic and complex, but despite that we seldom get proper rates and downhole pressures. The best case scenario is to get daily wellhead pressure and rate data for analysis.
- The processing software tools (from KAPPA and others) are still a work in progress.

So we position the workflow described in this section as the best, or least bad thing we can do today with the tools we have at hands. For KAPPA this means Citrine, Topaze and Rubis. Other technical groups will offer alternatives.

### 1.I.1 Accessing data

Production data are typically stored in public or proprietary databases and historians. One may sometimes have to dig and find the necessary information (e.g., well completion data) in flat files and printed reports. The retrieval of this data in a proper state is sometimes far from a trivial task and may involve a lot of wasted time.

Whenever there is a structured way to store this data, commercial software applications will typically provide flexible means to access and load the data, either built-in or using specific plug-ins that will allow this data to be loaded with a minimum effort from the engineer.

The amount and quality of data may be unequal from one play to the next and from one company to the next. The workflow presented in this section implies that sufficient quality data is available. This is in no way guaranteed. Public data sources generally lack key information (e.g. continuous pressure data, completion information) that would be required for proper processing. The main data used are listed below:

**Well information:** The basic request will be the position/location of the well and its trajectory, well completion data (i.e. number of fracture stages, number of perforation clusters, well length) and wellbore data which will be used to correct pressure to datum when needed. When the completion changes, or when the flow path changes (e.g. casing production followed by tubing production) such information related to those events will have to be known to the engineers. In addition, petrophysical data (e.g., formation thickness, initial water saturation, porosity) and PVT data are required for analysis. Public data sources generally do not include such completion and reservoir data.

**Production data (rate-time data):** This data we will always have and, unfortunately, sometimes it will be the only available data. In this case analysis will be reduced to standard decline techniques. Statistical analyses may be performed based on the results of decline curve analyses.

**Surface pressures:** The surface pressure data is generally measured at the wellhead continuously by most of the operators. However, public data sources do not provide this data. It is, however, critical to have at least surface pressure data to be able to perform rate transient analysis/model-based analysis for production forecasting. In particular, rate transient analysis is very useful for forecasting when there is no apparent decline behavior due to varying pressures/choke management.

**PDG data:** Unfortunately, PDG data are still rarely acquired in unconventional reservoirs, although having access to downhole pressure data can provide critical information.

Surface pressures require lift curve corrections i.e. converting surface pressure data to bottomhole pressures, which are a potential source of error, especially when the producing systems and the phases in the wellbore change. Having the bottomhole pressure data directly eliminates the problem.

PDG data also record incidental shut-ins. Shut-in data may be very useful in some instances such as when, even with limited linear flow regime data, it might carry information on the well productivity ( $k$ ,  $x_f^2k$ ), skin and its evolution. Shut-ins are also ideal occasions to 'listen' to the reservoir, sometimes even detecting well to well interference.

**Microseismics:** Monitoring microseismic events during hydraulic fracturing is increasingly popular, though it still represents only a small percentage of fracturing operations in North America. Raw signals are recorded by the array of geophones. Interpreted data include, for each microseismic event: (1) the event time, (2) its location, and (3) some attributes, especially its magnitude and amplitude.

The distribution of events can help characterize the limits of the possible fracture network induced by the fracturing operations. The interpretation process is delicate and results should not be taken for granted. Since the microseismic events are not necessarily correlated with production, it is not trivial to insert the microseismic data in a flow model. At the very least the interpretation of microseismic can qualitatively give an idea about the possible drainage area.

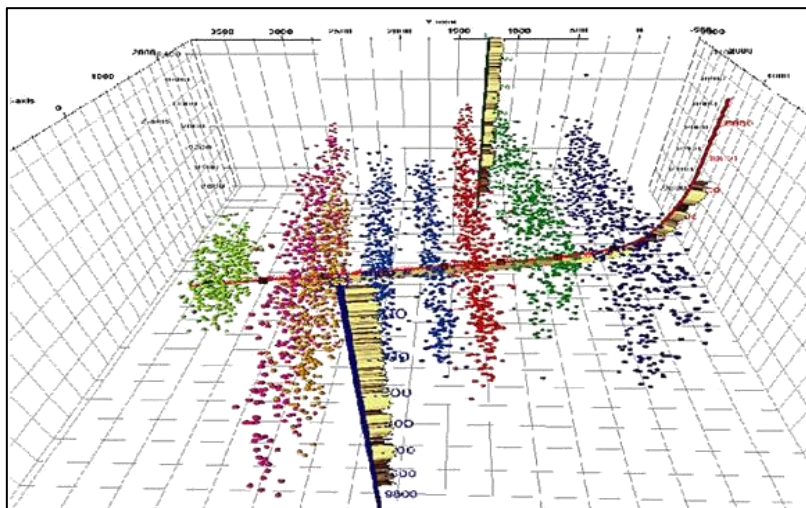


Fig. 1.1.1 – Microseismic events (Canada National Energy Board)

**Fracture related data:**

- Minifrac (also called DFIT: Diagnostic Fracture Injection Test) analyses can be conducted before the actual hydraulic fracturing operations to estimate a number of parameters such as permeability, formation pressure, leakoff coefficient, closure stress, providing critical information to design the hydraulic fracturing job. Results of DFIT data interpretation (particularly permeability, formation pressure) may help to calibrate production analysis, although the interpretation of DFIT data is oftentimes challenging.

**1.I.2 Quality control (Citrine)**

Quality control of data is critical to assess rate-time and pressure-rate-time data consistency and quality. It is generally preferable to start by reviewing available pressure-rate-time data for quality assurance and detection of correlations between pressure and rate data. Data without correlation will not provide any diagnostic value, and is thus meaningless for analysis. A diagnostic plot should highlight if there is something wrong with the data and identify the causes and deviations from the data plot.

One can also detect features or events which could be filtered or discarded prior to the analysis. For example, off-trend data can be removed from log-log plots used for flow regime diagnosis. A visual inspection may reveal obvious events or inconsistencies, such as well-completion changes, liquid loading, offset well fracture hits, etc. It is generally common to observe data inconsistencies and issues throughout the quality control process. Failure to identify and address these issues likely results in analysis of artefacts unrelated to actual well/reservoir behavior.

**1.I.3 Diagnostic analysis, well grouping and selecting representative wells (Citrine)**

It is usually not desirable to perform a diagnostic analysis on a very large group of wells. Many of the data features are difficult to distinguish and it is often difficult to establish characteristic performance trends due to differing completion practices and reservoir heterogeneities, to name a few. Using Citrine's well selection feature, working sets or groups may be defined.

These subsets of wells may be established according to differing fluid type, completion practice, completion horizon, start of production. The following order is preferred for grouping the wells: (1) similar location/geology, (2) similar fluid properties, (3) similar completion practices. In addition, metrics can be defined via normalizations and parameter plots which could indicate certain well groupings. A special plot referred to as Probit, which is used to plot the distribution of a well parameter across all wells, can also help in visual identification of well groups.

Once the groups are identified, production diagnostics can be performed. We can either perform diagnostics on a single well to identify characteristic flow regimes or on multiple wells to compare flow efficiencies, completion effectiveness, and characteristic reservoir signal. The identification of flow regimes is a primary objective of production diagnostics.

The Log-log plot is a particularly useful tool to detect these flow regimes. On the Y scale one will display the flow rate, preferably normalized by the pressure drop. On the X scale one can use standard time or, preferably, Material Balance Time, i.e. the instantaneous cumulative production divided by the instantaneous rate.

Such a plot is particularly useful to identify flow regimes. Some commonly used slope values are listed below:

- Quarter slope → bi-linear flow (finite conductivity fracture)
- Half slope → linear flow (infinite conductivity fracture)
- Unit slope → depletion type flow (or productivity loss) [material balance time plot]

The following figure illustrates an example of a single well plotted on a log-log rate and material balance time plot with a half slope (linear flow) identified by an annotation. This exercise is performed for the other wells of the group to make sure each well exhibits the same behavior.

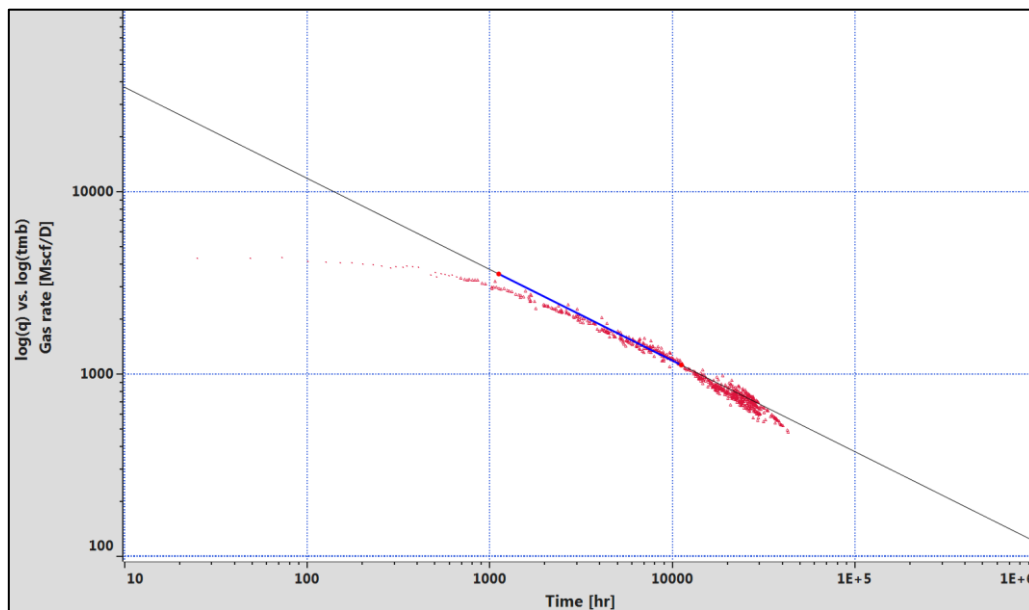


*Fig. 1.1.2 – Log-log plot of rate versus material balance time with a negative half slope*

In addition to analyzing individual well behavior, we will investigate the possibility of characterizing flow regimes for an entire group of wells. For instance, on the left hand side of the figure below all of the wells from the well group are plotted on the same rate versus material balance time plot as before.

It is immediately noted that while the well responses seem to exhibit a similar shape, there are marked differences between the wells in the vertical direction. These vertical separations can be thought of as differences in productivity due to reservoir heterogeneity, completion practices, or operational issues to name a few. Normalizations can be used to pinpoint the cause of the shifts.

For instance, the right hand side of the figure below shows each of the wells in the well group normalized by six month cumulative production for each well.

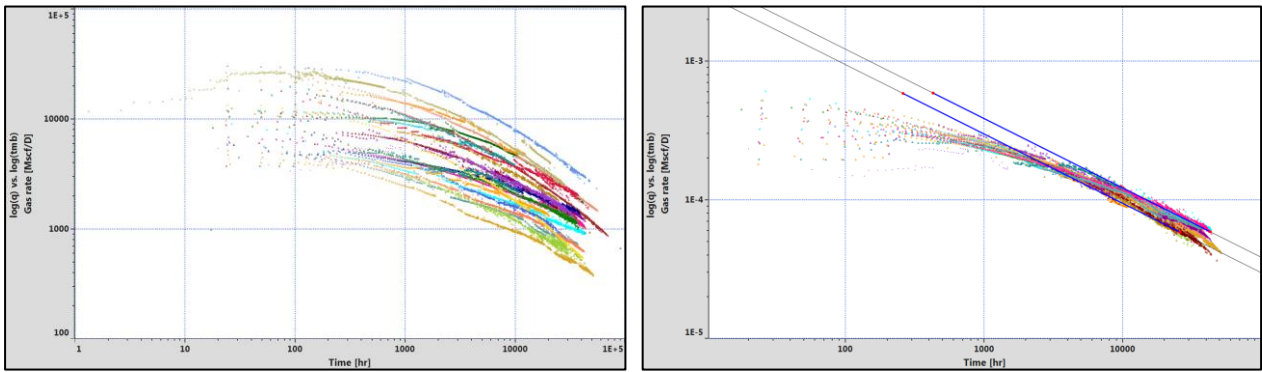


Fig. 1.I.3 – Normalization application for a group of wells

The six month cumulative production could serve as a ‘proxy parameter’ for local differences in reservoir quality and completions that might drive production behavior. With normalization, most wells exhibit linear flow at early times and then transition towards a unit slope at late times. This interpretation serves as a basis for choosing an appropriate model for the group of wells.

One may use qualitative and quantitative production metrics to compare wells within and across groups. For instance, the slope of the initial data trend on a reciprocal rate (or rate normalized pressure drop) versus the square root of time plot may serve as a proxy for a ‘lump parameter’ integrating the number of fractures, average effective fracture half-length and permeability (a.k.a. the linear flow parameter). This information can be used to handle non-uniqueness in model based production analysis, keeping different parameter combinations consistent with the diagnostic.

The following figure presents rate normalized pressure drop and square root of time plot and straight lines drawn to identify the slope values corresponding to each well. Note that it is possible in Citrine to attach a straight line to each of the wells in a particular well group, with individual line slopes found as a best fit to the data from an individual well.

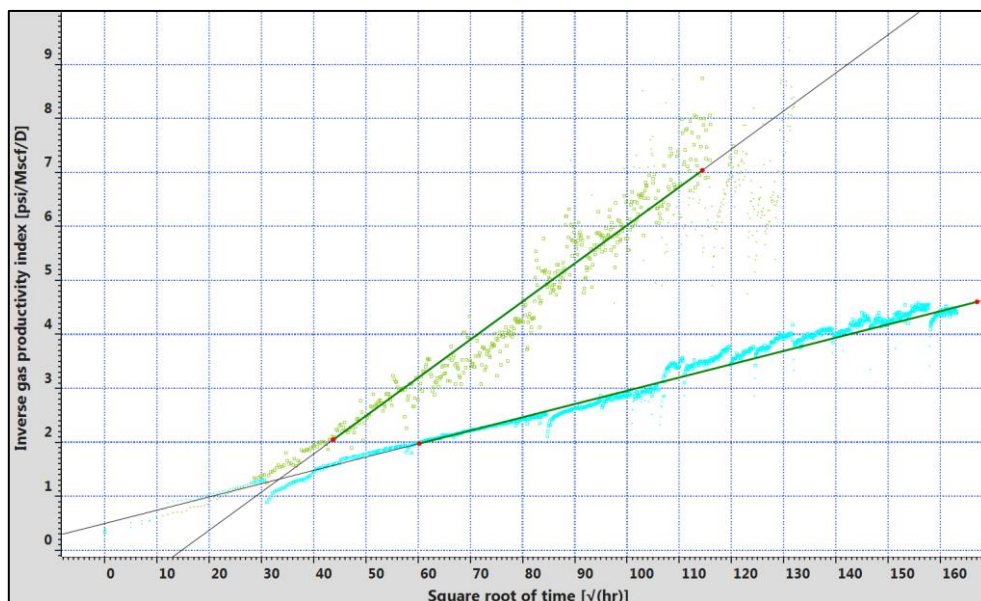


Fig. 1.I.4 – Rate normalized pressure drop versus square root of production time (Cartesian scale for linear flow)

Recalling the simple linear flow equation,  $m_{sqrt}$  is a lump parameter, which is inversely related to the slope of the straight line drawn on data. The lump parameter term contains the product of cross sectional area perpendicular to the flow (effective fracture half-length times fracture (or formation) height and the square root of permeability.

The slope values can be used as a guide for the rate transient analysis of the wells. For example, if one assumes the same permeability for these two wells, slope values may yield effective fracture half-length. The well with the shallower slope may indicate a better completion efficiency compared to the well with the steeper slope. This type of observation can be used to filter well groupings more accurately and/or compare completion types between similarly drilled and fractured wells in the same reservoir.

The Y-intercept on this plot is an indication of fracture conductivity. A well with a slope directly through the origin is said to be flowing into an infinitely conductive fracture from the well's stimulated or matrix regions. Wells with positive intercepts may have an associated skin around their fractures due to non-darcy flow, proppant embedment, or fracture fluid not breaking down properly. It should be mentioned that negative intercepts may be an indication of a well being supercharged by the high pressures during fracturing and flowback. These pressures may need to be filtered prior to rate transient modeling.

Other plots can be used to identify additional performance metrics. For example, straight line extrapolations on a semi-log rate or pressure drop normalized rate vs. cumulative production might give a rudimentary estimation of total recovery, or the stimulated region volume. These values may serve as a performance metric for the recovery of each well.

Similarly, these values can be mapped on a cross-plot versus another parameters like completion properties to identify high and low productive areas.

To conclude, various diagnostic plots will be useful to serve for the purposes mentioned earlier. The following four plots are found to be applicable and relevant in many cases and are recommended to start diagnostic interpretation:

1. [Log-log] rate (or pressure drop normalized rate) and time for flow regime identification
2. [Log-log] rate (or pressure drop normalized rate) and material balance time for flow regime identification (Blasingame plot)
3. [Cartesian] reciprocal rate (or rate normalized pressure drop) and square root of time for well productivity assessment (metrics)
4. [Semilog] rate (or pressure drop normalized rate) and cumulative production for production

More diagnostic plots, which the analyst may find useful, can be created and used to accomplish diagnostic interpretation. These additional plots may be different for each play or field. However, it is strongly recommended that the four plots above are created for diagnostic interpretation.

### 1.I.4 Selection of representative wells (Citrine/Topaze)

Following production diagnostics, the next step is to carry out rigorous modeling for one or more wells within a group. These wells are called the 'representative wells' and show the characteristic behavior of the group. When choosing a representative well it is critical that the chosen well has consistent rate and pressure data. The additional data required for analysis and modeling, namely PVT and well/reservoir properties along with completion data must also be considered. Once the representative well is selected, it can be sent to Topaze (RTA) for analysis and forecast.

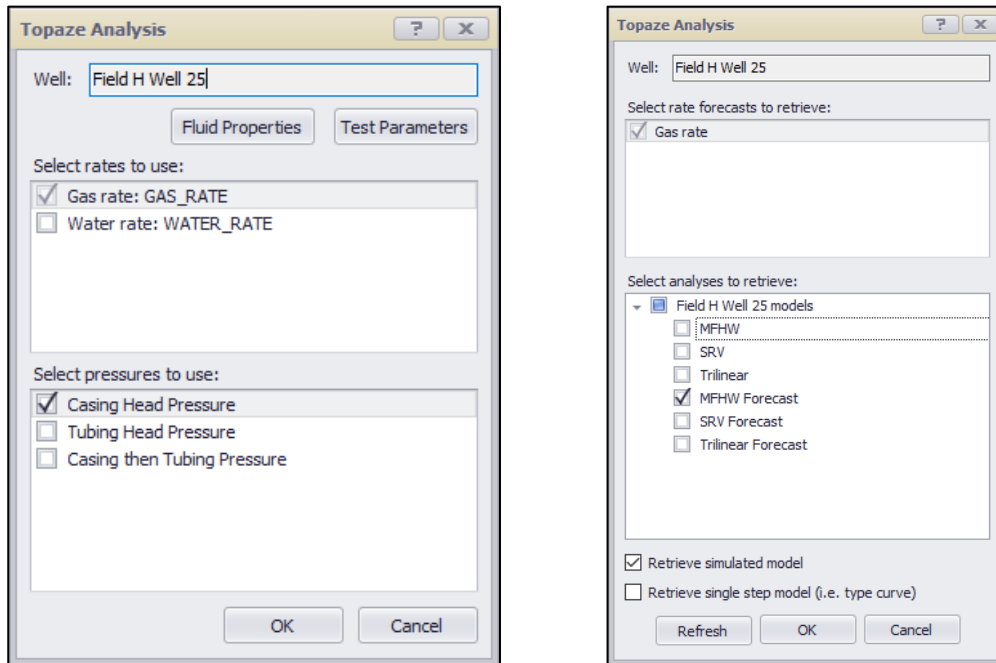


Fig. 1.I.5 – Import/export dialog of connection between Citrine and Topaze

### 1.I.5 Single well Rate Transient Analysis (Topaze)

Single well rate transient analysis of the representative well is performed using the workflow described earlier in the document. For this example uncertainties were considered on the contacted drainage area and three almost identical history matches were obtained using SRV bounded, trilinear, and infinite-acting multi-frac horizontal well models.

Other uncertainties (e.g., contribution from fracture stages, contacted drainage area, formation properties, etc.) can also be considered for history matching. Eventually, this process will transform into a probabilistic forecast through experimental design / Monte Carlo simulation.

Each of the cases provides virtually the same match of the historic well production; however, each of the models has different assumptions, and therefore each history match was obtained with different model parameters (e.g., effective fracture half-length). Therefore, using the model parameters obtained from three different history matches will translate into a range of production forecasts.

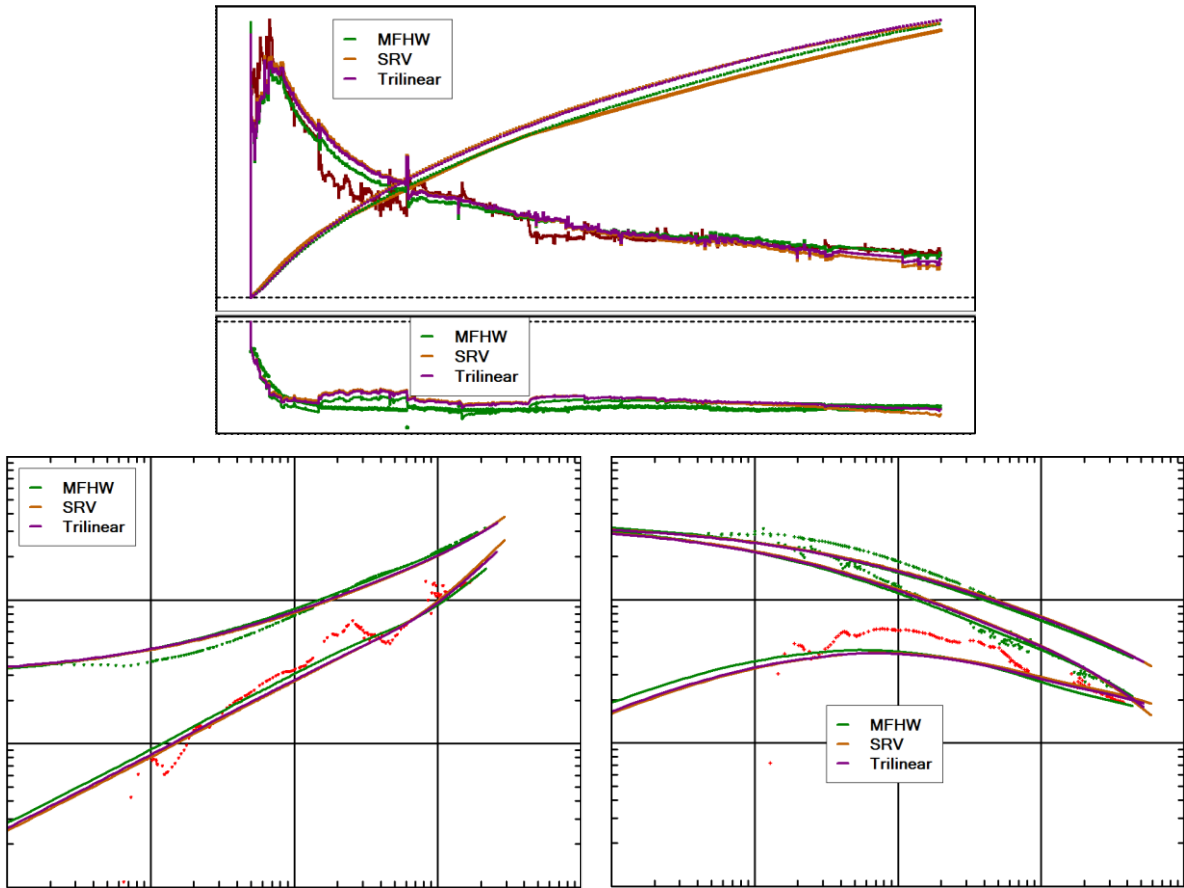


Fig. 1.I.6 – Comparison of three different rate, pressure, and diagnostic matches for the representative well

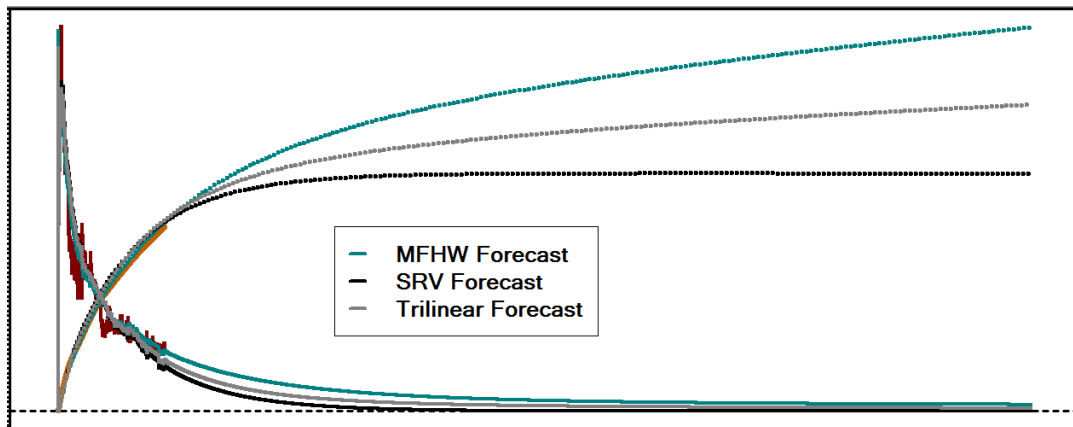
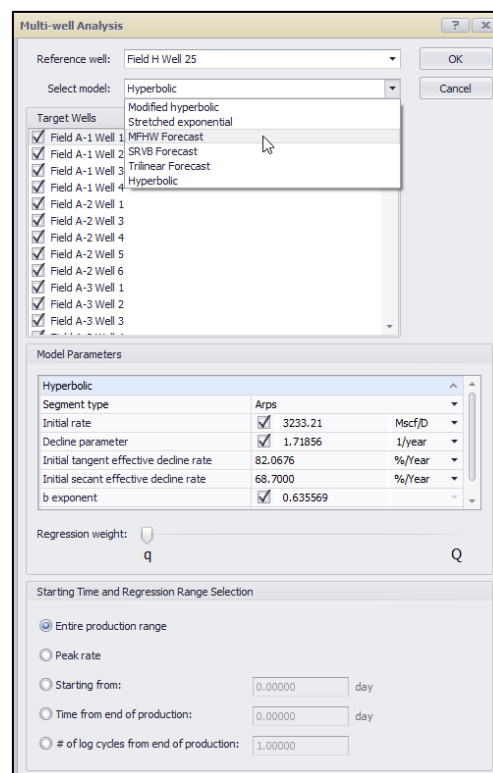


Fig. 1.I.7 – Production forecasts of the representative well based on three different models

### 1.I.6 Extension of the representative well model forecast to other wells

Once the history match of the representative well is established, production can be forecast based on a future pressure constraint. Uncertainties on model parameters can be considered to yield probabilistic forecasts. The main question at this point becomes how to extend these forecasts to other wells. In order to answer this question, it is critical to make sure that well groups consisting of similarly performing wells are established correctly.

Model forecasts in Topaze are retrieved in Citrine and can be extended to other wells in Citrine's Analysis mode using the n-Well (a.k.a. Multi-well) option. As different wells might have different early clean-up times, it is possible to fit the reference model to the other wells' data starting after their corresponding peak rates, or select a particular time interval for fitting the trend.



*Fig. 1.I.8 – Initialization of Topaze type curve for other wells analysis in Citrine*

In Citrine, '(Sim)' is added to the Topaze model forecast for the representative well and can only be applied to the well which was chosen to be modeled in Topaze. Once this forecast is imported into Citrine, the model match can be visualized across all selected plots.

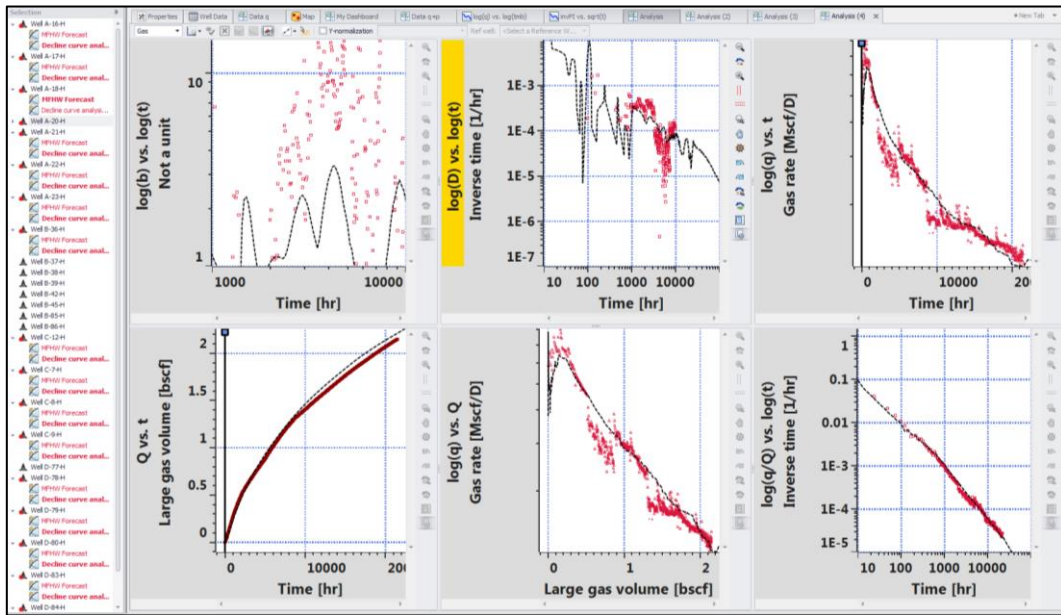


Fig. 1.I.9 – Imported Topaze model response for the representative well

A response of the same model to a single step response is also simulated in Topaze and is brought into Citrine as a Type Curve, hence an addition '(TC)' to its name, and it can be transferred to other wells through X and Y factors found automatically to history match and forecast well performance for each well in the group.

If the working sets, or groups of similar wells, were chosen correctly, we might find that some of the wells that were not modelled will almost behave like the representative well. Other times, however, we will find that there is a degree of separation between the model matches and the other wells in the group. This separation that was discussed earlier could be due to the differences in completion and reservoir characteristics. If the well groups are properly chosen, then utilizing X and Y factors as 'shifting' parameters on the  $\log(q)$  vs.  $\log(t)$  plot could be used for extending Topaze models to other wells within a particular working set.

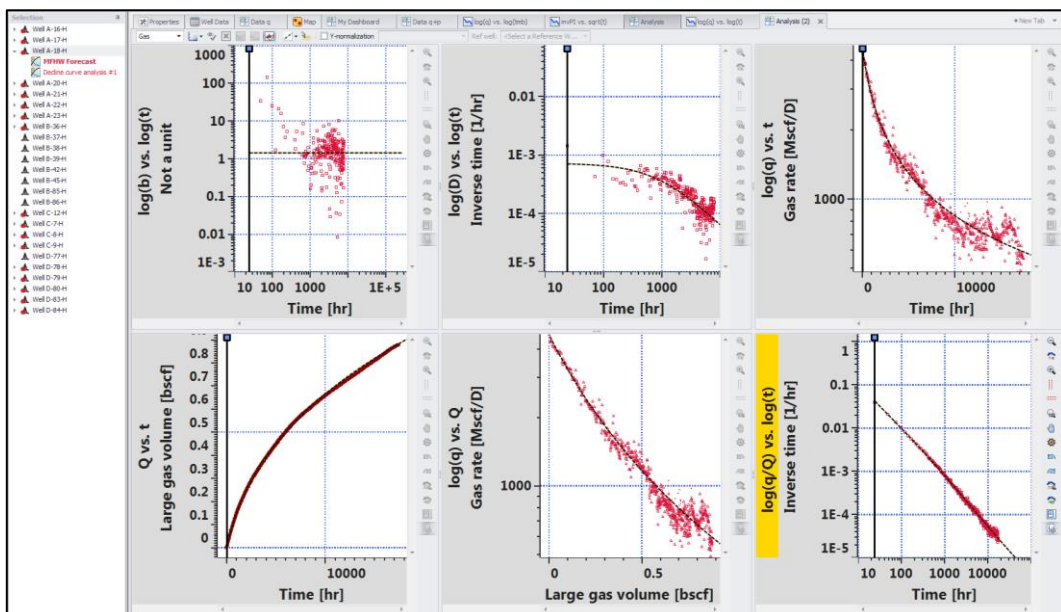


Fig. 1.I.10 – Type curve from Topaze adjusted for the other well in the working set

Once each of the wells in a group has a forecast associated with it, statistical curves can be applied to the model values to show the average/percentile forecast curves. Note that these would be different from fitting a model to the percentile wells that were created based on wells’ data only, so it might prove an interesting exercise to compare the two.

In case when multiple single step curves are imported from Topaze, it is possible to forecast wells production as a combination of these forecasts using machine learning algorithms. The essential idea behind the workflow is that the single-step models represent and encompass the important physical processes that occur during production, and by combining them one can match other wells behaviour and perform forecasting. Iterating over each well, Model Mining first employs superposition to condition the type curves to the individual well pressures, and then employs regression to match the superposed type curves to the well production. The advantage of using this method is that the Model Mining procedure automatically creates a data-driven, physics-based forecast. The diagram below provides a visual description of the workflow.

**For the detailed description and information on how to use this option please refer to additional documentation on the Citrine section of KAPPA website. Please note that the Model Mining option is provided as an Experimental module.**

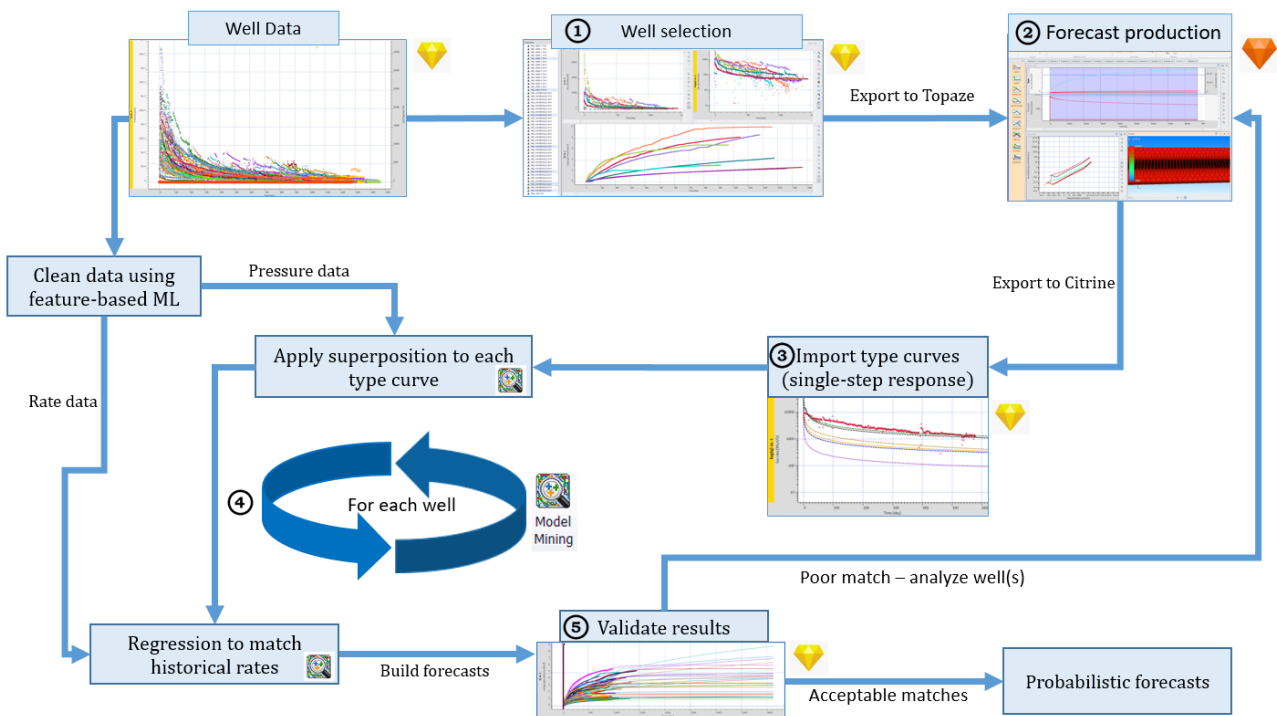


Fig. 1.I.11 – Diagram of the Model Mining workflow

Once all the forecasts are calculated, being the result of DCA, Topaze modeling, or Model Mining, a consolidated forecast for the group of well or the entire field can be calculated in Citrine, so that the historical (data) and future (forecast) production are rolled up into a channel of the total production for the selected wells. The reference forecasts for all the wells can also be exported in bulk in a spreadsheet for further reporting purposes, or converted into a required format to be re-imported into third party economical evaluation and planning packages.



# TABLE OF CONTENTS



<b>UNCONVENTIONAL RESOURCES .....</b>	<b>1</b>
1.A INTRODUCTION AND DEFINITIONS .....	1
1.A.1 <i>Shale gas</i> .....	2
1.A.2 <i>Shale oil</i> .....	3
1.A.3 <i>Coal seam gas (not covered in this chapter)</i> .....	5
1.A.4 <i>Oil shale (not covered in this chapter)</i> .....	5
1.A.5 <i>Hydrates (not covered in this chapter)</i> .....	6
1.B SPECIFICS OF SHALE PLAYS .....	7
1.B.1 <i>Impact of the low permeability</i> .....	9
1.B.2 <i>Diffusion equations</i> .....	10
1.B.2.a Desorption .....	11
1.B.2.b Molecular diffusion and diffusion between micropores .....	13
1.B.2.c Fracture diffusion .....	14
1.B.2.d Stress and pressure-dependent properties .....	16
1.B.2.e PVT issues.....	16
1.B.2.e.i Confined PVT solution.....	17
1.B.3 <i>Fractured horizontal wells</i> .....	19
1.B.4 <i>Initial state of the system</i> .....	20
1.B.5 <i>Heterogeneities and DFN</i> .....	21
1.B.6 <i>Lack of quality data</i> .....	22
1.C BASIC PRODUCTION BEHAVIOUR OF A SHALE WELL.....	23
1.C.1 <i>'Early' linear flow</i> .....	23
1.C.2 <i>Transition from linear flow to SRV flow</i> .....	24
1.C.3 <i>SRV flow</i> .....	25
1.C.4 <i>Beyond SRV</i> .....	26
1.D DECLINE CURVE ANALYSIS (DCA) OF UNCONVENTIONAL PLAYS .....	29
1.D.1 <i>Main plots used in Decline Curve Analysis</i> .....	29
1.D.2 <i>The Arps equations</i> .....	32
1.D.3 <i>Power-law exponential</i> .....	34
1.D.4 <i>Stretched exponential function</i> .....	36
1.D.5 <i>The Duong model</i> .....	38
1.D.6 <i>Logistic growth</i> .....	40
1.D.7 <i>Stimulated Reservoir Volume Bounded decline curve</i> .....	42
1.D.8 <i>Segmented DCA models</i> .....	43
1.D.8.a Segmented Power Law Model .....	43
1.D.8.b Segmented Hyperbolic DCA model .....	44
1.D.9 <i>Conclusions</i> .....	45
1.E RATE TRANSIENT ANALYSIS (RTA) FOR UNCONVENTIONAL PLAYS.....	46
1.E.1 <i>Linear flow diagnostics</i> .....	46
1.E.2 <i>Diagnostic of the SRV flow</i> .....	48
1.E.3 <i>Simultaneous diagnostic of several flow regimes</i> .....	49

1.E.4	<i>Matching data with a model</i>	51
1.E.5	<i>History matching</i>	53
1.E.6	<i>Production forecasting and EUR</i>	55
1.E.7	<i>EUR statistics</i>	55
1.F	<b>SIMPLE MODELS</b>	58
1.F.1	<i>'Classic' Multi-Fractured Horizontal Well (MFHW)</i>	58
1.F.2	<i>SRV bounded model</i>	60
1.F.3	<i>Trilinear model</i>	62
1.G	<b>FIELD EXAMPLE – DEMONSTRATION OF SIMPLE MODELS</b>	64
1.G.1	<i>First eight months of production</i>	64
1.G.2	<i>Linear flow model</i>	65
1.G.3	<i>Analytical Multi Fractures Horizontal Well (MFHW)</i>	66
1.G.4	<i>Numerical MFHW</i>	66
1.G.5	<i>Comparing production forecasts</i>	67
1.G.6	<i>Receiving ten more months of production data</i>	69
1.G.7	<i>Discussion</i>	71
1.H	<b>ADVANCED MODELS</b>	72
1.H.1	<i>Complex geometries (analytical + numerical)</i>	72
1.H.2	<i>DFN models (numerical + analytical)</i>	74
1.H.2.a	<i>Numerical DFN</i>	74
1.H.2.b	<i>Stochastic DFN</i>	76
1.H.2.c	<i>Analytical DFN</i>	78
1.H.3	<i>Modeling water flowback (numerical)</i>	78
1.H.3.a	<i>Static initialization</i>	78
1.H.3.b	<i>Dynamic initialization</i>	80
1.H.4	<i>Refrac jobs modeling</i>	81
1.H.4.a	<i>Features for simple fracture system</i>	82
1.H.4.b	<i>Features for complex fracture system</i>	83
1.H.5	<i>Multi-Zone Fractional Dimension</i>	84
1.H.6	<i>Anomalous Diffusion in a Tri-linear model</i>	87
1.H.6.a	<i>Description and assumptions</i>	87
1.H.6.b	<i>Model features and parameters</i>	88
1.H.6.c	<i>General Anomalous Diffusion Behaviour</i>	88
1.H.6.d	<i>The anomalous diffusion applied to a heterogeneous reservoir</i>	91
1.I	<b>KAPPA RECOMMENDED WORKFLOW (2020)</b>	96
1.I.1	<i>Accessing data</i>	96
1.I.2	<i>Quality control (Citrine)</i>	98
1.I.3	<i>Diagnostic analysis, well grouping and selecting representative wells (Citrine)</i>	98
1.I.4	<i>Selection of representative wells (Citrine/Topaze)</i>	102
1.I.5	<i>Single well Rate Transient Analysis (Topaze)</i>	102
1.I.6	<i>Extension of the representative well model forecast to other wells</i>	104